Deutsches Zentrum für Neurodegenerative Erkrankungen in der Helmholtz-Gemeinschaft

Herr Prof. Dr. med. Gerd Kempermann

Investigating the role of cell-autonomous ROS status in the regulation of hippocampal neural precursor cells in adult mice

Dissertationsschrift

zur Erlangung des akademischen Grades

Doctor of Philosophy (Ph.D.)

vorgelegt

der Medizinischen Fakultät Carl Gustav Carus

der Technischen Universität Dresden

von

Vijaya Subba Rao Adusumilli, MSc

aus

Hyderabad, India

Dresden, 28.02.2020

1. Gutachter: Prof. Dr. Gerd Kempermann, CRTD/ DZNE Dresden

2. Gutachter: Dr. Mike O. Karl, DZNE Dresden

Tag der mündlichen Prüfung:

gez.: _____

Vorsitzender der Promotionskommission

Zusammenfassung

Die adulte hippocampale Neurogenese beinhaltet die fortgesetzte Rekrutierung neuraler Vorläuferzellen (neural precursor cells, NPCs) in den aktiven Zellzyklus und deren fortschreitenden Übergang in postmitotische Körnerzellen. Diese im Erwachsenenalter geborenen Neurone integrieren sich in das bestehende Netzwerk und ermöglichen eine strukturelle Plastizität, die wichtige Funktionen des Hippocampus unterstützt. Für eine anhaltende Neurogenese muss der Eintritt in den Zellzyklus der NPCs genau kontrolliert werden.

Umweltfaktoren regulieren diesen Kontrollpunkt stark und differenziell. Freiwillige körperliche Aktivität stellt einen etablierten Stimulus dar, der zu einer verstärkten Proliferation in der neurogenen Nische führt. Mechanistische Einblicke in die Aufrechterhaltung und Regulierung des Ruhezustands (Quieszenz) von NPCs und deren Reaktion auf akute körperliche Aktivität als eine Form der adaptiven Neurogenese sind jedoch noch nicht hinreichend vorhanden.

In meiner Doktorarbeit haben wir die Redoxregulation als einen Schlüsselweg zur Regulierung des zellulären Zustandsgleichgewichts identifiziert. Weiterhin habe ich die Rolle von zellulärem oxidativem Stress im neurogenen Verlauf und bei der adaptiven neurogenen Antwort untersucht. Unsere Ergebnisse zeigen, dass nicht-proliferative Vorläufer des hippocampalen Gyrus dentatus, im Gegensatz zu anderen Stammzellsystemen, durch einen hohen Gehalt an zellulären reaktiven Sauerstoffspezies (ROS) gekennzeichnet sind. Mithilfe von cytometrischen Methoden, Ex-vivo-Bioassays und Transkriptionsprofilen konnten wir nachweisen, dass die Klassifizierung von Zellen anhand des intrazellulären ROS-Gehalts funktionell definierte Subpopulationen von adulte NPCs identifiziert. Wir gehen davon aus, dass ein Abfall des intrazellulären ROS-Gehalts dem Übergang der Zellzustände vorausgeht, insbesondere von der Quieszenz zur aktiven Proliferation. Akute körperliche Aktivität führt zu einer Aktivierung nicht proliferierender Zellen durch einen transienten Nox2-abhängigen ROS-Anstieg in ruhenden NPCs mit hohem ROS. In Abwesenheit von Nox2 war die basale Neurogenese nicht beeinträchtigt, die aktivitätsabhängige Antwort war jedoch aufgehoben. Diese Ergebnisse werfen ein neues Licht auf die diskreten zellulären Ereignisse, welche die Homöostase zwischen verschiedenen zellulären Zuständen von NPCs im adulten Hippocampus der Maus aufrechterhalten.

Summary

Adult hippocampal neurogenesis entails a continued recruitment of neural precursor cells (NPCs) into active cell cycle and their progressive transition into post-mitotic granule cells. These adult born neurons integrate into the existing circuitry and confer structural plasticity, which aids in key hippocampal functions. For sustained neurogenesis, the cell cycle entry of the NPCs has to be tightly controlled.

Environmental cues strongly, and differentially, regulate this checkpoint. Voluntary physical activity represents such an established strong stimulus that results in enhanced proliferation within the neurogenic niche. However, mechanistic insights into the maintenance and regulation of quiescence and the responsiveness of the NPCs to acute physical activity, as a form of adaptive neurogenesis, are yet to be elucidated.

In my doctoral studies, we identified redox regulation as a key pathway regulating the cellular state equilibrium. I further explored the role of cellular oxidative stress in the neurogenic course and in adaptive neurogenic responses. Our results show that non-proliferative precursors within the hippocampal dentate gyrus, unlike in other stem cell systems, are marked by high levels of cellular reactive oxygen species (ROS). Using cytometric methodologies, ex vivo bioassays and transcriptional profiling, we revealed that classifying cells based on intracellular ROS content identified functionally defined sub-populations of adult NPCs. We propose that a drop in intracellular ROS content precedes the transition of cellular states, specifically from quiescence to active proliferation. Acute physical activity involves the activation of non-proliferating cells through a transient Nox2-dependent ROS surge in high-ROS, quiescent NPCs. In the absence of Nox2, baseline neurogenesis was unaffected, but the activity-dependent response was abolished. These findings shed new light on the discrete cellular events, which maintain the homeostasis between distinct cellular states of NPCs within the adult murine hippocampus.

Acknowledgements

Some words in the English language have dichotomous meanings. One such word is “chance”. Prof. Dr. Gerd Kempermann took a chance by having me as a doctoral student. This chance, in many ways, led me to discover myself. Gerd, you have been a mentor, a guidepost, a friend and a father. You gave me direction, motivation and space to discover myself as a scientist. Your support truly went beyond the lab or science. You danced with me, you consoled me, you stood by me against all odds, personal and professional. You took the time and effort to make sure I have a position to pursue science, even beyond our lab. Now, at the end of the first phase of our journey together, all I can do is to thank you and words do fail in expressing the reverence I have for you. I will always be indebted to you and all my science will be an ode to your mentorship.

If takes a village to raise a child, it definitely requires a township to do a successful project. The chieftain of my township was (and always will be) Dr. Annette Rünker. Annette, when I joined the lab I had no idea of neurogenesis. You took me under your wing and taught me everything I know. You have always been helpful and I do know, you went above and beyond for me. If not for you, I would never have come out the depressive hole I got stuck in. You gave me the confidence and never said no to experiments. You took my rants and still could say it was okay, which is, frankly, superhuman. You opened your home to me, made me like your kin. You, Marius, Ella, Fionn and Kiera will always be family and if not for you I would have never achieved anything. Thank you!

During my initial years Muhammed, Zeina taught me the day-to-day workings of the lab and the project and always were there to help me out I would like to acknowledge their help. The foundation of my work comes from the discussions with Dr. Tara Walker who really streamlined the initial ideas and provided the critical thinking required to undertake a tricky project. The absolute linchpin in address the aims I set out to answer was Dr. Rupert Overall. I would like to acknowledge the many hours he spent with me, for the project. He has truly been a brother in arms and without him, I would have never personally and professionally able be sane. Thank you Rupert. Thank you brother!

Dr. Sara Zocher’s friendship and support is the single greatest gift the Kempermann gave me. She critically analyzed my ideas, supported me through countless experiments and was by my side selflessly through and through. Acknowledging her support would be akin thanking the eyes for vision.

I have truly made great friends during my stay in the Kempermann lab, some really special such as Dr. Diane Engel, Monika and Anna Grzyb. Anna, you inspired me through our many discussions to think more critically and getting you to see the point of my interpretations was a true joy! Monika was truly a great friend who literally was the air behind my wings, when I needed it the most. I would like to further acknowledge the support rendered by the present the past members of the Kempermann Lab- Steffi, Daniel, Fanny, Richard, Stefan Vogel, Christopher, Odette, Alisa, Alex, Jadna, Nuning, Angela and everyone else. I know I am could never do justice in expressing my gratitude for you love and support! If I missed someone that is just a slip of the mid and not loss of fondness.

The heart of my project was to deal with mice. The true unsung hero for me is Anne Karasinsky and Sina. Anne literally worked night and day for the project and her help in designing the breeding, organizing the perfusions and injections is unquantifiable. Anna's smile meant everything was going to be okay. I truly cannot imagine animal work without you! Sina organized the chaos and made work possible. I would also want to mention the camaraderie we developed and thank you and Mike for all your support.

The soul of the Kempermann lab is Kristin. You are a true champion and without you I would have lost my Job on a daily basis! Thanks Kristin.

All the technicians, Christina, Nicole, Sandra, Dani were always helpful and shouldered a lot of responsibilities. I would like to acknowledge the support offered by Jana and Antje with the administrative responsibilities.

Although my work did not overlap with the expertise of Dr. Klaus Fabel and Dr. Alex Garthe, they were always willing to offer help and support. Thanks guys!

I would like to thank the FACS facility at CRTD, specifically Katja and Anne Gompf who made me an expert at cytometric techniques. Thank you for your patience and support. I would further like to acknowledge the help and support offered by the Deep-Sequencing facility of the CRTD, specifically Dr. Andreas Dahl and Susanne Reinhardt who were very support and instrumental for the RNA sequencing experiments performed.

I would like to thank the administrative staff of the CRTD and DZNE (both in Dresden and Bonn), Medical faculty of the Carl Gustav University and the TUD for their timely help and great support.

I would also like to thank Dr. Tomohisa Toda for all his help and mentorship. I would like to acknowledge the support of all the research group leaders at the CRTD and DZNE, specially

Dr. Natalia Rodriguez-Muela and Dr Jörg Mansfeld for the collaborative support. I further thank the larger scientific community of CMCB for their support and help.
I am privileged to have had the opportunity to train some of the best students imaginable and would like to acknowledge the help and efforts of Gesa Klatt, Salma, Merve and Konstantinos. You guys have a great scientific career ahead and I really enjoyed my time with you guys.
There are just 3 people left to acknowledge. These three people make little sacrifices every day for me, my Grandma in India, who literally is the superhero in my life. My little sister Anu who made me feel loved. And my Dad, my identity.
I truly believe in the presence and power of a spiritual source. I am thankful for all the blessings You have showered on me. Thank you for benevolence and omnipresence in my life!

Index

List of figures

List of tables

List of abbreviations

abGC	adult born granule cell neuron
Akt	serine/threonine protein kinase
ANOVA	Analysis of variance
Ascl1	Achaete-scute family BHLH transcription factor 1
BHLH	basic helix-loop-helix transcription factor
BMP4	Bone morphogenic protein 4
BrdU	5-Bromo-2'-deoxyuridine
CA1	Cornu Ammonis, region of hippocampus major efforent connections to cortex
CA3	Cornu Ammonis, region of hippocampus receive inputs from DG
CldU	5-Chloro-2'-deoxyuridine
CNS	Central nervous system
CPM	Counts per million
Dcx	Doublecortin
DG	Dentate gyrus
DHE	Dihydroethidium
EC	Entorhinal cortex
EdU	5-ethynyl-2'-deoxyuridine
EGF	Epidermal growth factor
EGFR	Epidermal growth factor receptor
FACS	Fluorescent Associated Cell Sorting
FAO	Fatty Acid Oxidation
FGF	Fibriblast growth factor
Foxo	Forkhead box transcription family member O
FSC	Forward scatter (size)
GC	granule cell neuron
GF	Growth factor
Gfap	Glial fibrillary acidic protein
GFP	Green fluorescent protein
GO	Gene Ontology
HICAP	Hilar commissural-associated pathway-associated cells
Hif	hypoxia inducible factors
HIPP	Hilar perforant path associated neurons

HSC	Hematopoietic stem cell
ID	Inhibitor of differentiation family of transcription factors
IdU	5-Iodo-2'-deoxyuridine
Igf-1	Insulin growth factor 1
IPC	Intermediate progenitor cell
iPSC	induced Pluripotent stem cell
KCl	Potassium chloride
Klf4	Kruppel-like factor 4
lEC	lateral entorhinal cortex
LPP	Lateral perforant path
MCM	minichromosome maintenance proteins (marks proliferating cells)
mEC	medial entorhinal cortex
mitoROS	mitochondrially generated ROS
MOPP	molecular layer perforant path associated neurons
MPP	medial perforant path
MSC	Mesenchymal stem cell
n	sample size
Nes-GFP	EGFP expressed under Nestin promoter
Nox	NADPH oxidising enzyme
NPC	Neural Precursor Cell
NSC	Neural Stem Cell
OB	Olfactory bulb
PCA	Principal Component Analysis
PCNA	proliferating cell nuclear antigen
Pten	phosphotase and tensin homolog
qRT-PCR	quantitative real-time Polymerase chain reaction
REST	RE-1 silencing transcription factor
RGL	Radial glial-like cell
RMS	Rostral migratory scheme
ROS	Reactive Oxygen species
SEM	standard error of mean
Sox2	SRY-Box transcription factor 2
SSC	sideward scatter (granularity)
Std.	standard housed animals
SVZ	subventricular zone
TAP	transient amplifying progenitors
TF	transcription factor

v-SVZ	ventral- subventricular zone
Vegf	Vascular endothelial growth factor

Publications (only primary author papers)

Vijay S Adusumilli [1,2*], Tara L Walker [1,2,6*], Rupert W Overall [1,2*], Gesa M Klatt [1,2], Salma A Zeiden [1,2,4], Tim J Fischer [1,2], Sara Zocher [1,2], Alex M Sykes [5], Susanne Reinhardt [3], Andreas Dahl [3], Dilyana G Kirova [4], Jörg Mansfeld [4], Annette E Rünker [1,2], and Gerd Kempermann [1,2 #] (2019) Redox potential defines functional states of adult hippocampal stem cells. *Under re-consideration in Cell Stem Cell*

Introduction

Neurogenesis is the phenomenon of generating a neuron. It involves multipotent neural stem cells (NSCs) entering a canonical proliferation paradigm leading to intermediate transient amplifying cell types, which progressively undergo a lineage restriction leading to formation of many distinct terminally differentiated excitatory and inhibitory neurons of the central nervous system (CNS; beside other non-neuronal cells termed glia, their generation is referred to as gliogenesis), which, synergistically, form connections.

In the embryonic neurogenic phase, neuronal generation and synaptic connectivity correlates with the formation of brain structures, beginning with the specification of NSCs (E9.5 in mice) and progressive neuronal production continuing through the early stages of post-natal life, which leads to the formation of the mammalian brain (Gilbert 2000). Embryonic NSCs are continually exhausted, and as textbook knowledge from a few decades ago noted, with the formation of brain structures, neurogenesis rapidly seizes resulting in a rather static organ for sustained neuronal production (Götz et al., 2016; Rakic, 2009). All experiences of an animal's life are therefore coded for, stored and remodeled within these stable neuronal elements by altering their synaptic strength and connections at the network level, which is referred to as synaptic plasticity. However, pioneering work by Altman and Das (Altman and Das, 1965), which was later confirmed by seminal work in the 1990s (Alvarez-Buylla et al., 1990; Barnea and Nottebohm, 1994; Gage et al., 1995; Kuhn et al., 1996; Nottebohm, 1985), helped in the discovery of the adult neurogenic process, wherein neurons are generated and integrated into the existing circuitry post structural consolidation of brain regions, thus representing a specific type of structural plasticity (Deng et al., 2010). Adult neurogenesis is highly restricted to a few brain regions wherein it continues throughout the animal's life, albeit with progressive restriction in adult born neuronal numbers with age (Kalamakis et al., 2019). The lateral walls, or the subventricular zone (SVZ), of the lateral cerebral ventricles and the subgrangular zone of the dentate gyrus (DG) within the hippocampus are two such restricted neurogenic niches within the adult mammalian brain, wherein resident multipotent adult NSCs continuously generate adult born neurons and the ensuing structural plasticity enables key functions and

behavior adaptabilities (Zhao et al., 2008; Garthe et al., 2009, 2014). The process of adult neurogenesis, particularly hippocampal neurogenesis, is conserved through mammalian evolution and retained in primates, including humans (Kempermann, 2015; Spalding et al., 2013). The dysregulation of adult neurogenesis has been implicated in a wide range of diseases, ranging from neurodegenerative diseases, such as Alzheimer's disease, to depression to post-traumatic stress disorder (PTSD) to epilepsy, among a list of others (Besnard and Sahay, 2015; DeCarolis and Eisch, 2010; Kheirbek et al., 2012).

Superficially, adult neurogenesis is similar in the two neurogenic niches, NSCs with an elaborate radial glial morphology sporadically enter proliferation, and based on the symmetry of their division, undergo either self-renewal or generate transiently amplifying precursor cells (neural precursor cells; NPCs), which are progressively lineage restricted (neuroblasts) and terminally differentiate to yield postmitotic neurons that over weeks integrate into the local circuit (Kempermann et al., 2004). This phenomenon is incessant, with a snapshot at any time identifying a homeostatic distribution of cellular states with distinct transcriptional profiles, marker expression, proliferative potential and neuronal commitment. The hardwired mechanics of adult neurogenesis, at different checkpoints, is further subject to environmental regulation, which differentially regulate the process in the SVZ and DG (Kempermann, 2011). Hence, for continued neurogenesis it is paramount to regulate the cell cycle entry and exit of the NSCs, the *terminus a quo* neurogenic population.

In my doctoral work, my inspiration was to identify cellular parameters which identify, and causally regulate, the transitions of the cellular states of the early hippocampal neurogenic trajectory. Further, I wanted to understand how differentially regulated pathways confer a unique specificity to NPCs within the adult DG to respond to the most elementary environmental stimulation, physical activity.

In this introductory section, I will detail the current understanding about the origin, distinct stages and functions of the neurogenic cells of the adult DG, give a brief overview of neurogenesis in the SVZ and would highlight the different methodologies to study the processes. I will present environmental stimulation paradigms that specifically regulate adult hippocampal neurogenesis and end with a clear list of aims, which I pursued over the course of my study.

Adult hippocampal neurogenesis

The dentate gyrus serves as a gateway to the hippocampus, wherein different sensory modalities are merged leading to initial representations of the animal's environment and,

thus, is critically involved in learning and memory formation (Dengler and Coulter, 2016). Glutamatergic granule cells (GCs) are the principal neuronal subtype within the DG and are continuously generated (and integrated) through adult neurogenesis (Aimone et al., 2014). Different stages of adult neurogenesis can be identified based primarily on marker expression and morphology. A true start point are NSCs (Bonaguidi et al., 2011), which have an elaborate bipolar radial glial morphology with an oval cell body located in the subgranular zone and a basal process extending through the granule cell layer into the molecular layer terminating in branched endpoints on synapses and vasculature (Palmer et al., 2000). They are often termed as type-1 cells or RGL cells (radial glia like cells). These cells are astrocytic, expressing key genes such as Gfap (glial fibrillary acidic protein; intermediate filament), Fabp7 (also referred to as BLBP; lipid binding); sparse expression of Glast (amino acid transporter) and yet retain the ability to enter cell cycle, which is marked by the expression of Sox2, Klf4 (Moon et al., 2018) and receptors for morphogens, such as Gli1 (Yao et al., 2016) and EGFR (epidermal growth factor receptor; Katsimpardi and Lledo, 2018; Kempermann et al., 2015; Zhang and Jiao, 2015) . The type-1 cells are multipotent (capable to terminally differentiate astrocytes and neurons), quiescent and only sporadically enter proliferation (Bonaguidi et al., 2011; Pilz et al., 2018). Cell cycle inhibitors such as Pten, Cdkn1b (p27kip); transcriptional suppressors such as REST and the expression of genes such as Hes1, Id1/3/4 and Btg1/2 have been implicated in regulating the cell cycle entry of type-1 cells (Boareto et al., 2017; Gao et al., 2011; Hatakeyama et al., 2004; Yan et al., 2018; Hörster et al., 2017). The events leading to NSC entry into active growth cycle are still an active area of investigation, but once activated, the progression through the growth cycle is mediated by TFs such as Ascl1 (Kim et al., 2011; Raposo et al., 2015) and can be marked by the expression of proliferation markers such as Ki67, PCNA and MCM2. Activated type-1 cells can either undergo symmetric divisions leading to more type-1 cells or asymmetrically divide to generate type-2a cells. It is unclear if the type-1 cells have an unlimited ability to self-renew and a few reports suggest a tipping activation point, where type-1 cells, once activated, go through a “neurogenic burst” before exhausting their stemness and converting into an astrocyte (Encinas et al., 2011; Pilz et al., 2018). This hypothesis is, however, controversial as long-term population studies do suggest a capability of type-1 cells to re-enter a protracted period of quiescence (Kempermann, 2011a).

Type-2a cells lack the elaborate morphology of type-1 cells and are horizontal (bipolarity is retained). These cells continue to express Sox2 but have limited capacity of self-renewal. They rapidly and transiently amplify their numbers before becoming committed to a neuronal lineage. These cells are marked not just by morphology, but also the continued expression of Nestin and expression of the transcription factor (TF) Tbr2 (Eomes; Hodge et al., 2008; 2012). It is unclear whether type-2 cells also are multipotent but they do not express markers of the neuronal lineage. This prompts terming type-1 and type-2 cells together as neural precursor cells (NPCs). The downregulation of Nestin leads to a decrease in proliferative ability and these Nestin -negative horizontal cells are referred to as the type-2b cells, which have limited proliferation potential and are lineage committed. Longitudinal imaging shows that these cells undergo an average of 2.3 divisions in a short window of time. Type-2 cells, based on their morphology and proliferative characteristics, are grouped together as intermediate progenitor cells (IPCs) or transient amplifying cells (TAPs). Type-2b cells start to develop a more elaborate bipolar morphology whilst downregulating Sox2 expression. This change in morphology leads to the committed type-3 cells, which are essentially neuroblasts. The type-2b and type-3 cells are together often referred to as progenitor cells. Type-3 cells exit cell cycle, start expressing proneuronal genes like Calb2 (Calretinin), NeuroD1, NeuN (Rbfox3; among others) and undergo a high degree of pruning through apoptosis (Ryu et al., 2016), depending on the neuronal demand. The surviving cells are immature neurons. Discrete sequential steps mark the maturation process of adult born neurons: establishment of neuronal polarity, GABAergic synapses to the apical dendrites and soma, glutamatergic synaptogenesis and circuit integration (Toni and Schinder, 2016). Mature GCs feedback onto parvalbumin (PV) interneurons, which develop connections to the young adult born granule cells (abGCs) followed by glutamatergic innervation from the medial and lateral entorhinal cortex (m/lEC) through the medial and lateral perforant path (MPP/LPP in middle and outer molecular layer, M/OML), respectively, and from hilar mossy cells through the commissural/associational pathway (inner molecular layer, IML). Further on, GABAergic input derives from diverse interneurons including HICAP (hilar cell bodies, targeting the commissural/ associational pathway in IML), HIPP (hilar cells bodies, targeting the perforant path in M/OML), MOPP (cell body in the molecular layer, project to the performant path in M/OML), perisomatic-targeting, or CR (calretinin-expressing hilar cells) cells (Alvarez et al., 2016; Bergami et al., 2015; Deshpande et al., 2013). Recent reports suggest that abGCs spiking could differ based on

the quality of the input, thereby suggesting a role in mood regulation. AbGCs spike more in response to MPP than to LPP and excitation through LPP leads to a direct inhibitory activity on mature GCs through glutamate receptors (if the input is from lEC) and while excitation through the MPP leads to direct activation of mature GCs through NMDA receptors (input from mEC; Luna et al., 2019). These adult born neurons further project to CA3 excitatory neurons and inhibitory interneurons (with different synaptic strength) and finally, CA3 projects to CA1 excitatory neurons thereby completing the "hippocampal loop" (Aimone et al., 2014; Rangel et al., 2013). This maturation takes about four weeks in an young adult.

Immature neurons are hyper-excitable (combination of high input resistance, response to tonic GABA and lack of inhibitory innervation), a property that makes them instrumental in responding to sub-optimal novel cues (Trinchero et al., 2017). The firing of these young cells leads to the activation of inhibitory interneurons, which, in turn, silence mature GCs. This leads to sparcified firing of the network in the context of a novel environment that enables the animal to separate overlapping yet distinct patterns, which is referred to as pattern separation (Sahay et al., 2011a; 2011b). This property leads to increased adaptive spatial learning with the flexible integration of novel information into pre-existing contexts (Garthe et al., 2009; 2014) and simulation reveals the importance of this structural plasticity conferred by the abGC (Kempermann, 2012; Wiskott et al., 2006). Furthermore, adult born neurons play a key role in mood stabilization and the generalization of aversive memories (Kheirbek et al., 2012). It has to be noted that the events leading to maturation of abGCs is a simplified overview.

An important limitation of defining the cellular states within neurogenic cells by marker expression or morphology is that it does not capture transcriptomic changes which correlate with, or casually regulate the transition events. To this end cytometric identification of NPCs, specially marked by Nestin (the broadest marker of type-1 and type-2a stages) or a combination of other early stage markers, followed by singly cell transcriptomics has been invaluable to understand molecular events regulating the entry of NSCs into proliferation, neurogenic commitment (Shin et al., 2015; Walker et al., 2016). It has also enabled the identification of key markers for different stages such as Hopx, Aldoc and Statmin (stmn). Aligning the $Nestin^{+}$ cells along a developmental or a "pseudotime" trajectory, Shin and coworkers have identified that quiescent cells have markedly high cell to cell communication along with the expression of molecules, which help in regulating cell-autonomous behavior by extracellular factors. Further, lipid and glutathione metabolism is particularly high in these

quiescent cells, with low dependency on oxidative phosphorylation (oxphos). As cells enter active cycling, key cell-autonomous pathways change, relative to quiescent cells. The mitochondrial activity and dependency on oxphos increases; enhanced Pol2 mediated transcription and alternative splicing; and increased de novo lipogenesis (Knobloch et al., 2012). This transcriptomic analysis, however, does not identify key metabolic changes preceding the cell cycle entry of quiescent NSCs. Thus, using transcriptional profiling it has been possible to identify correlative changes with cellular states, metabolic changes causally driving these cellular state transitions (such changes would precede a change in expression profile) are yet to be identified.

Two theories could potentially explain the origin of the resident adult NSC within the DG, a "set-aside" theory, wherein a certain subpopulation of embryonic NSCs that are slowly cycling or have entered dormancy, migrate and home into the subgranular zone. A second hypothesis argues that embryonic NSCs are patterned early in development to form the DG and progressively transition into adult NSCs with marked quiescence. Recent work from Berg and colleagues (Berg et al., 2019) provides evidence for the latter "sequential" theory. Using Hopx-CreER^{T2} mice, they demonstrate that NSCs, which form the prospective adult hippocampus and cortical regions, can be marked in the neuroepithelium at embryonic day E10.5. These NSCs quickly become patterned for their regional specificity by E15.5, i.e. cells which give rise to DG, CA and cortical regions. By E18.5 a dentate migratory scheme is established wherein proliferating cells lose their contacts to the ventricle and start to migrate to the prospective DG region. These cells are highly proliferative at this embryonic timepoint and their progeny generates the cell types, which would populate the adult DG. Interestingly, no slow dividing NSCs could be identified. Embryonic NSCs undergo a transition in expression profile by postnatal day (P) 3, with the first marks of quiescence and loss of proliferative marks setting in. An important metabolic shift pertaining lipid metabolism is correlated with the transition from lipogenesis to fatty acid oxidation (FAO). This shift in metabolism is conserved in adult NSCs, with quiescent cells primarily relying on FAO and a shift in lipid metabolism precedes a NSC's commitment to active cycling (Knobloch et al., 2014; 2017). Coupled with transcriptomic transitions, postnatal NSCs migrate and by P14, thus before adulthood, are localized to the adult neurogenic niche with proliferative kinetics, which are retained with age (Nicola et al., 2015).

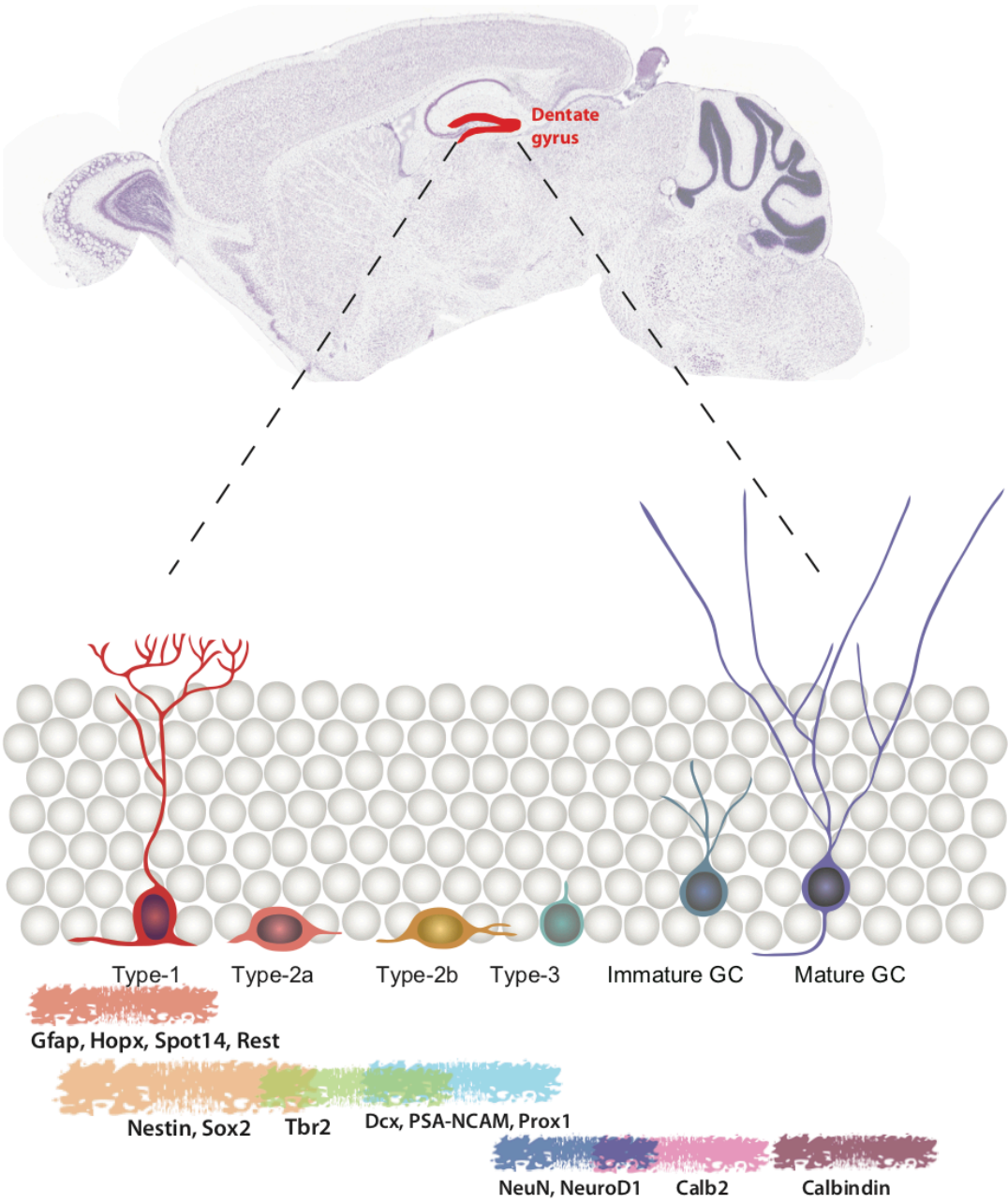

Figure 1: Adult hippocampal neurogenesis. The adult dentate gyrus houses NSCs (type-1) which can be retained in quiescence for long periods of time. Type-1 cells sporadically enter proliferation and progressively transition through multiple stages with defined marker expression to yield post-mitotic immature neurons. These immature neurons over the course of 4 weeks integrate into existing circuitry.

Adult neurogenesis in the subventricular zone

The largest neurogenic zone in the adult mammalian brain is the ventral subventricular zone (V-SVZ), which is located adjacent to the walls of the lateral ventricles and runs along the

septal wall. Both sides of the wall harbor radial glial stem cells, which are termed as B1 cells. B1 cells are GFAP, GLAST, BLBP and Sox2 positive and only upon activation express Nestin (Codega et al., 2014; Doetsch et al., 1997; 1999; Silva-Vargas et al., 2013). These cells are in direct contact with cerebrospinal fluid (CSF) through processes between the ependymal cell layer of the ventricle and have end feet which contact the blood vessels. B1 cells are multipotent and apart from neurogenesis can give rise to oligodendrocytes for the corpus callosum (Menn et al., 2006) and to astrocytes (Chaker et al., 2016). These adult V-SVZ (ventral subventricular zone) NSCs, unlike the adult NSCs of the DG, are set aside during embryogenesis, remaining quiescent till adulthood (Fuentealba et al., 2015; Furutachi et al., 2015) .

The largely quiescent B1 cells, like the type-1 cells within DG, upon activation and asymmetric division give rise to transient amplifying cells, type C cells that are Ascl1 and DLX2 positive. The type C cells amplify (~3 times) and generate neuroblasts which are DCX and PSA-NCAM positive and are referred to as the type A cells (Lim and Alvarez-Buylla, 2016). These type A cells, unlike Dcx-positive type-3 cells of the DG, are capable of migrating over long distances. Type A cells are ensheathed by GFAP-positive cells and migrate within a network of interconnecting paths that converge to form a rostral migratory scheme (RMS) into the olfactory bulb (OB; Lois and Alvarez-Buylla, 1994). During the RMS, type A cells further divide one to two times. In the anterior SVZ, the neuroblasts migrate radially and differentiate into multiple types of interneurons (unlike the DG wherein neurogenesis results in only one type of terminally differentiated neuron, the abGC; Ponti et al., 2013). I will not further discuss the function of these adult born interneurons since this is beyond the scope of my doctoral work.

Unbiased transcriptional profiling of cells within the SVZ identifies cells along the developmental trajectory, ranging from quiescence to neuronal commitment (Linnarsson, 2015; Llorens-Bobadilla et al., 2015; Mizrak et al., 2019). Interestingly, non-proliferating NPCs within the SVZ can be further classified into distinct cellular states. Similar to the DG, quiescent cells are shown to exist in a dormant state with a high glycolytic and lipid metabolism which can transit into a discrete quiescence-primed state that is marked by upregulation of protein translation and downregulation of Notch and Bmp signaling. Transcriptomic profiling further elucidated regional biases and sex differences in the neuronal and oligodendrocyte lineages, with the NSCs of the lateral wall disposed towards

a neurogenic lineage whereas those of the septal wall are biased to an oligodendrocytic lineage.

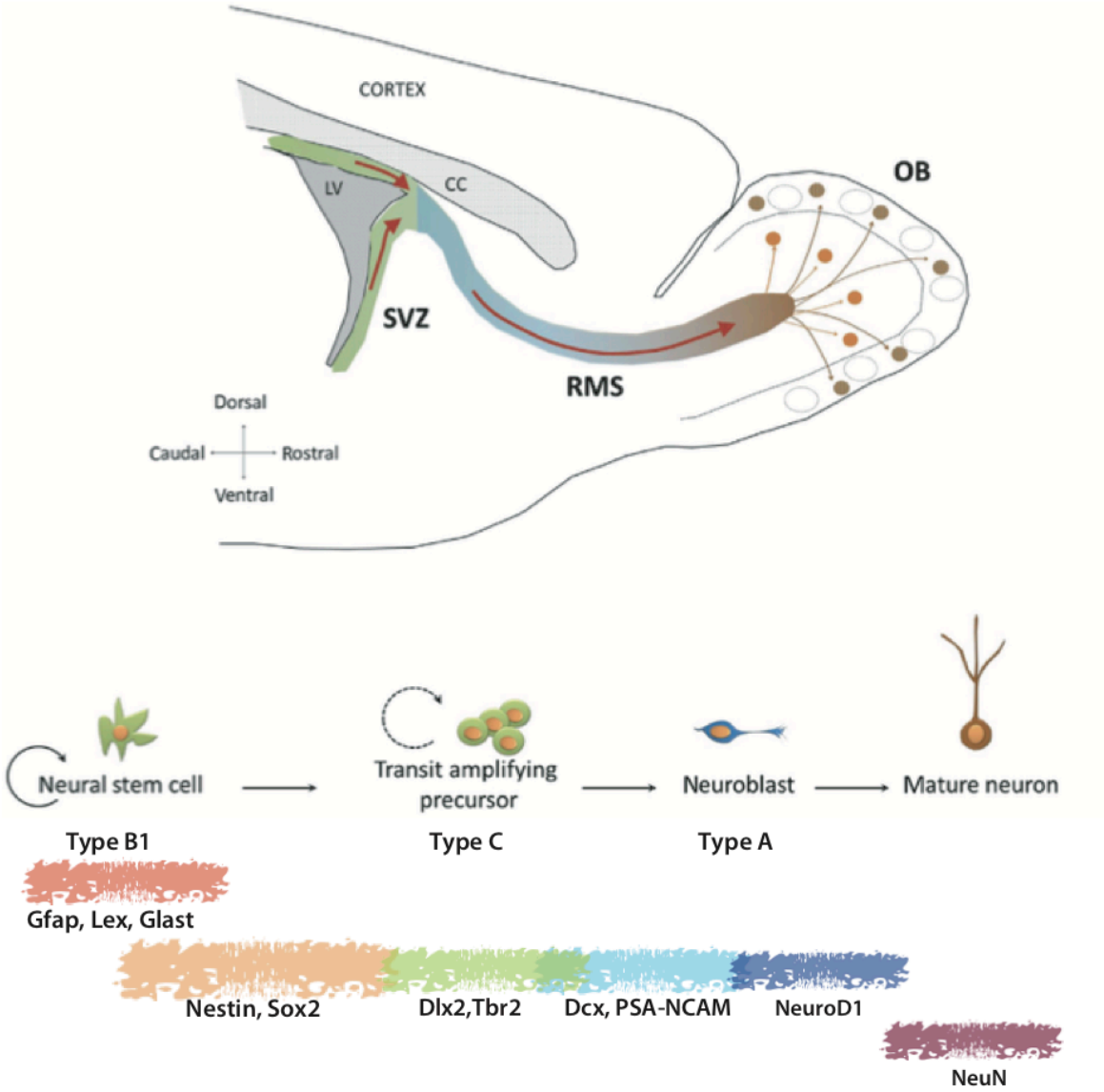

Figure 2: Adult subventricular neurogenesis. The adult ventral subventricular zone (V-SVZ) houses NSCs (type-B1) which can be retained in quiescence for long periods of time. Type-B1 cells sporadically enter proliferation and progressively transition through multiple stages with defined marker expression to yield neuroblasts (type A) which migrate via the RMS to enter and radial migrate within the olfactory bulb. These immature neurons give rise to diverse type of interneurons which progressively integrate into existing circuitry. (image modified from Toenillei, 2017)

Methods to study adult neurogenesis

In this section thus far, I have described the organization of the adult neurogenic niches. It is pertinent going forward to list the different methodologies to study neurogenesis, both in

vivo and in vitro. Immunohistological staining has been the conventional methodology employed to identify the neurogenic stages and their abundance. As the crux of defining a neurogenic zone is the presence of proliferating cells, going on to become mature integrated neurons, the earliest of studies involved using the 3H-thymidine labelling to identify proliferating cells (Kuhn et al., 2018). This method progressively made way for thymidine analogs such as BrdU, which replaces thymidine during DNA replication and with the advent of immunofluorescence against halogenated thymidine analogs it is now possible to identify successive rounds of proliferation cycles (Podgorny et al., 2018). Another commonly used method to identify cell division is to stain for markers of active growth cycle or distinct stages of cell cycle such as the S-phase and the M-phase such as Ki67, PCNA, MCM2 among others. This staining, combined with the identification of cell stage using restricted markers such as GFAP, Sox2, Tbr2, DCX, NeuN, Calb2 (Calretinin) and Calb1 (Calbindin) represents an indispensable element of queries of neurogenesis. Furthermore, transgenic mice with fluorescent proteins such as green fluorescent protein (EGFP) under the promoters of stage restricted markers such as Nestin (Yamaguchi et al., 2000) to mark the early phases of neurogenesis, Gfap to mark astrocytes and type-1 cells (Nolte et al., 2001; Steiner et al., 2006), Lpar1 (Walker et al., 2016), Dcx (Walker et al., 2007), Hopx (quiescent cells; Li et al., 2015) are routinely employed. To birthdate cells at a certain stage and for following the cellular events in their progeny, inducible transgenic animals are invaluable and some of the examples, among many others, include Ascl1-CreER^{T2} (Kim et al., 2011) Nes-CreER^{T2} (Dranovsky et al., 2011), Hopx-CreER^{T2} (Berg et al., 2019), Spot14-CreER^{T2} (Knobloch et al., 2012). In addition to these strategies, stereotactic injection of different virus particles, coupled with restricted markers' promoters driving the expression of different genes (such as Cre, EGFP, optogenetic and chemogenetic proteins such as DREDDS, among others) can label different cellular stages - retroviruses label proliferating cells (Artegiani and Calegari, 2013; Lange et al., 2009). Lentiviruses and adenoviruses target all cells within the injected area, pseudotyped retroviral labeling help in highlighting the input cells to a specific starter pool of cells (Enikolopov et al., 2015; Semerci and Maletic-Savatic, 2016; Suh et al., 2007), These methodologies, along with electrophysiology on acute slices, have been remarkably useful in detailing the functions and properties of abGCs (Berdugo-Vega et al., 2020) and NPCs (Song et al., 2016).

Apart from in vivo strategies, ex vivo and in vitro strategies to probe mechanisms and molecular cues of neurogenic regulation are important to mention. It was discovered, very

early on, that NPCs from neurogenic regions and other brain areas can be isolated from embryonic and adult animals and cultured in vitro in the presence of specific growth factors (GFs) such as FGF2 and EGF (Morshead et al., 1994; Palmer et al., 2001). Depending on the substrate these precursors can be cultured in distinct ways. When adult NPCs are plated on uncoated surfaces, it precludes cell-substrate contacts. These cells are triggered into proliferation by the mitogens and only the precursors self-renew and form spheres of proliferating cells referred to as neurospheres (Reynolds and Weiss, 1992). The number and size of the neurosphere does indicate the stemness of the NPCs and is a great start point of comparative studies. Furthermore, stimulants such as KCl or Norepinephrine selectively trigger latent precursors from the DG to enter proliferation (Jhaveri et al., 2010; Walker et al., 2008). The neurosphere assay, however, is a “mixed bag” experiment as it does not recapitulate the in vivo regulation or proliferative dynamics of NPCs and, thus, should rather be viewed as a test of total cellular stemness. After dissociation of neurospheres, cells can be further plated on different surfaces, in the absence of GFs to induce differentiation into neurons and glial cell types (Walker and Kempermann, 2014). In addition to the neurosphere assay, our lab has established that by plating cells on surfaces coated with poly-d-lysine and laminin, which enables cell-substrate contacts, a 2-dimensional adherent monolayer culture of homogeneous Nestin- and Sox2-positive NPCs can be obtained that is capable of indefinite self-renewal in the presence of GFs (Babu et al., 2007; 2011). This is a bona fide culture system of multipotent (at least bipotent) NPCs, as upon the withdrawal of growth factors cells differentiate to yield astrocytes and neurons. Monolayer culture is a valuable tool for studying specific mechanisms, which regulate many cellular parameters including, but not limited to, proliferation and differentiation potential. The advantage of this model system lies in the robustness of the readouts, a practically unlimited supply of cells, ability to temporally resolve processes at a high resolution and a high degree of homogeneity in the control conditions. This culture model, thus, was successfully used to identify processes regulating different cellular states which were subsequently shown to have in vivo relevance (Knobloch et al., 2017; Martynoga et al., 2013).

The major caveat of the monolayer culture is the fact that it is a 2-dimensional culture system, which means a morphological classification of different neurogenic stages is not possible. The homogeneity for Nestin and Sox2; with no expression of Dcx, hints that the monolayer culture is predominantly analogous to type- 2a cells in vivo. Another major hurdle

in direct comparison between the monolayer culture and in vivo cells is that the culture system does not completely recapitulate the in vivo neurogenic trajectory, and specifically the timing of various stages before yielding terminal cellular states including the expression of key markers that identify these intermediary stages (such as Calb2, Dcx).

Environmental regulation of neurogenesis

Pioneering work from Kempermann and colleagues has shown that different stages of hippocampal neurogenesis can be intensely regulated by environmental cues (Akers et al., 2014; Kempermann et al., 1997; van Praag et al., 1999). Different experiences such as voluntary physical activity; housing in a socially and cognitively complex environment (together referred to as enriched environment); stress; diet; sleep effect hippocampal neurogenesis (Gould et al., 1999; Snyder et al., 2009; Steiner et al., 2008; Torres-Pérez et al., 2015) whereas housing animals in a enriched olfactory environments promotes SVZ neurogenesis (Bovetti et al., 2009). Interestingly, different cues effect different processes or checkpoints along the neurogenic trajectory. While physical activity leads to a pro-proliferative response in the adult DG resulting in a progressive increase in net neurogenesis (Kronenberg et al., 2003; Steiner et al., 2008), housing in enriched environments primarily leads to increased survival of post-mitotic immature neurons and their network connectivity (Kempermann et al., 1997). In addition to these effects, different cues might function additively, further regulating the process of neurogenesis (Fabel et al., 2009). These interventions are important to consider, as it has been shown that environment mediated neurogenic regulation is maintained through adulthood and, thus, might alleviate the age mediated decline in abGC production, connectivity and the function of the DG as a whole (Akers et al., 2014; Garthe et al., 2016).

Regulation by environmental cues differentially affects the neurogenic niches, with voluntary physical activity, the most elementary environmental cue, seemingly having no effect on the SVZ neurogenesis (Brown et al., 2003). The responsiveness of adult hippocampal neurogenesis to physical activity, poses particular challenges to the regulation of the NSC's cell cycle entry, which needs to be tightly controlled yet sensitive to a wide range of distant cues. Many studies have identified the role of mediators such as Igf1 (Trejo et al., 2001), VEGF (Fabel et al., 2003), endocannabinoids (Hill et al., 2010), serotonin (Klempin et al., 2013), T cells (Walker et al., 2018) as critical or even essential mediators of adult hippocampal neurogenesis but manipulating these factors does not, in isolation, regulate activity-dependent neurogenic response. The exact mechanisms of how physical

activity regulates proliferation in the adult DG remain unelucidated. Furthermore, it is unclear if there are subsets of responsive cells within the known precursor cell subpopulations unique to the DG, which might explain the differential effect of physical activity on the two niches, and whether such differences in functional states might in fact indicate how the actual activation takes place and if the response to running is different from the baseline recruitment at the most fundamental level of neurogenesis, the NSCs themselves. These questions are the key inspiration and focus of my doctoral thesis, the results which are presented in the following sections.

To understand the mechanisms through which acute de novo physical activity effects the cells within the neurogenic niche, the first question to tackle is the temporal resolution of the process.

In numerous studies the physical activity paradigm is used as a black box, with access to running wheel given for anytime between 4 and 28 days to observe the pro-neurogenic response (Akers et al., 2014; van Praag et al., 1999; Vivar and van Praag, 2017). This foundational temporal breakdown of response to cumulative running (and to enquire if physical activity is required as a cumulative stimulus) was one of the first questions I tried to answer, in a collaborated manner with colleagues in the Kempermann lab. In a previous study, our lab showed that continuous running for 4 nights robustly caused an increase in proliferation (Overall et al., 2013). Dr. Tim Fischer, along with Dr. Tara Walker and Dr. Rupert Overall investigated the preceding dynamics of the activation by studying effects of different bouts of physical activity (1, 2, 3, or 4 nights). By comparing the number of BrdU positive cells within the adult DG (6-8 weeks old animals), relative to the standard housed animals, they reported that the minimum time of sustained physical activity that is required to detect a statistically significant increase in the number of BrdU labeled cells was 3 days and at day 4, the proliferative pool had further increased to 183% of control values (unpublished data). This corroborates previously published results (Akers et al., 2014). This finding does not, however, resolve which of the following mechanisms in isolation or synergistically result in a pro-proliferative response. Theoretically, an extrinsic stimulus such as physical activity (arguably the most elementary known pro-neurogenic behavioral stimulus) might act at different checkpoints. The stimulus might (1) increase the recruitment of previously quiescent cells, which, post an “incubation” time before resulting in more proliferative cells within the niche, (2) increase the number of proliferative cycles by delaying cell cycle exit, (3) protect proliferating cell from cell death, or (4) shorten the cell cycle length

(Overall et al., 2016). Understanding which of these mechanisms underlies the increased number of proliferating cells is one of the key questions I pursued within my doctoral work. Identification of key responsive cells does not, in itself, answer the underlying molecular pathways responsible. To address this facet with NPCs of the DG, I relied on transcriptional profiling of Nes-GFP cells from the two neurogenic regions, conducted by Dr. Tara Walker and Dr. Rupert Overall in the Kempermann lab (unpublished data). Although Nestin marks NPCs with differential activation status or commitment to cell cycle, it is the single broadest marker of adult NPCs of the two niches, making it a valuable query population to identify differentially enriched pathways within the NPCs of the two niches. Nes-GFP expressing cells from the two niches (using Nes-GFP reporter mice; Yamaguchi et al., 2000) were FACSorted and profiled for their transcriptome and as shown in the figure below, a principal component analysis (PCA) shows that the NPCs of the two niches distinctly cluster. Differentially expressed transcripts were classified as 'signature' if they were expressed significantly higher than in the other group. Gene Ontology enrichment analysis of the signature genes showed that in the SVZ the top enriched pathways were related to 'cell division', 'transcriptional regulation', and 'cell cycle', which reflects their commitment to active growth cycle. The enriched pathways of the DG, in contrast, did not show this association but were related to cellular responses to environmental modulations, and of these 'redox regulation' showed the greatest enrichment ($p = 4^{e-9}$). I chose to focus on understanding the regulation of cellular redox levels within the NPCs, and the ensuing neurogenic trajectory, within the DG. Additionally, I investigated if intracellular redox status resolves the pool of NPCs responsive to physical activity and the key question – is adaptive neurogenesis just enhanced baseline neurogenesis?

To address this question, it is pertinent to understand the relation between cellular redox status and a stem cell's biology.

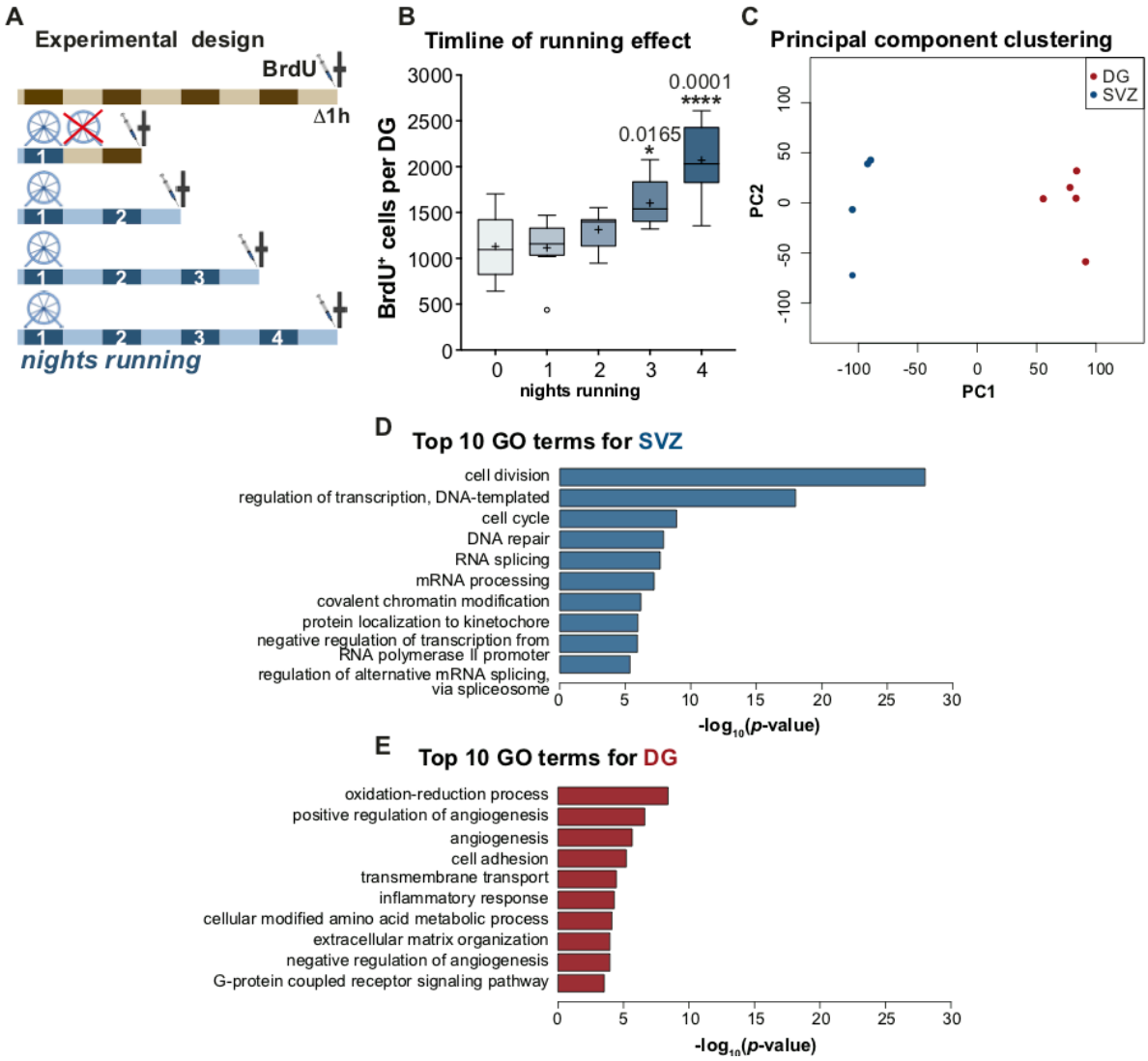

Figure 3: Regulation of adult hippocampal neurogenesis by acute de novo physical activity. (A) Experimental scheme to assay the minimum time of cumulative running required to result in pro-proliferative enhancement. (B) Plot showing that significant increase in proliferation can be observed on day 3 and at day 4 the effect is robust. (C) PCA of Nes-GFP cells from the two neurogenic niches shows distinct clustering. (D) Top 10 GO terms enriched within the signatures of SVZ. (E) Top 10 GO terms enriched within the signatures of DG.

Redox regulation in a stem cell

A cell's redox potential is determined by the balance between generation and scavenging reactive oxygen/nitrogen species (ROS/RNS). Cell redox status, often referred to cellular oxidative stress, affects the stability and function of a plethora of macromolecules and has been suggested to function as a "rheostat" coordinating multi-level cellular processes (Bigarella et al., 2014; Holmström and Finkel, 2014). ROS is a product of incomplete reduction of molecular oxygen and intracellular ROS primarily exists as the highly reactive

superoxide anion (O^{-}_{2}), which is marked by low half-life and highly localized reactivity. Superoxide anions are enzymatically reduced to hydrogen peroxides (H_2O_2), which are a more stable form of ROS, and/or further to hydroxyl radicals (OH^{-}) by the enzyme catalase (Phaniendra et al., 2015). Intracellular oxidative stress has been shown to act as physiological secondary messenger integrating cell-autonomous signaling and environmental cues. Different sub-cellular compartments, including the mitochondria, endoplasmic reticulum, lysosomes and the plasma membrane, can generate ROS as a by-product of metabolic activity and/or as a result of enzymatic functions contingent to the expression of proteins such as the NOX homologs, xanthine oxidase, cyclooxygenase etc.(Ye et al., 2015).

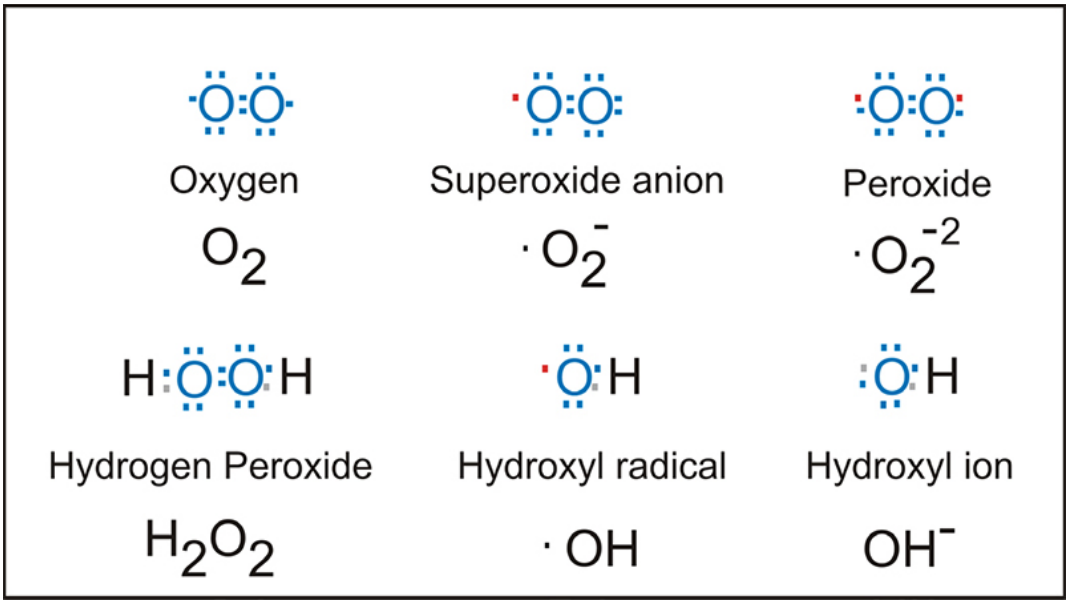

Figure 4: Electron structures of reactive oxygen species (ROS) [image from Biotek instruments]

This ROS primarily targets redox sensitive molecules or redox sensors, including AKT kinases (Murata et al., 2003), mTOR (Yoshida et al., 2011), Sirtuins (Salminen et al., 2013), p53 (Abbas et al., 2010) and others, which are post-translationally modified at specific amino acid residues which critically affects their availability and activation status. Certain key redox-sensitive transcription factors (including Nrf2, Hochmuth et al., 2011; FOXOs, Ferber et al., 2011; Hifs, Simsek et al., 2010) regulate the levels of oxidative stress in various cellular systems. These observations, in conjunction with many others, have further shown a specific and critical role for ROS fluctuations and oxidative stress in regulating

stem cell fate of practically all know stem cell systems, including bone marrow cells, iPSCs and cardiac cells (Armstrong et al., 2010; Gurusamy et al., 2009; Ludin et al., 2014; Smith et al., 2000). It has been shown in these systems that lower cellular ROS, as a result of heightened antioxidant defense, marks quiescent long-term retained multipotent cells and as cells enter proliferation and become lineage restricted they increase their cellular ROS content significantly, which is further required for the cellular state transitions. Although a central role of redox status as key functional determinant of "stemness" has been discussed in neural stem cell biology for many years (Noble et al., 2003; Noble et al., 2005) including intriguing findings for the SVZ (Belle et al., 2011), to date redox regulation has never been well studied for the DG in any detail.

Working hypothesis

Given that redox regulation is distinctly upregulated within the NPCs of the adult DG compared to the SVZ and the established ROS gradient with cellular state transitions in other stem cell systems, the working hypothesis is that cell intrinsic redox state and intracellular ROS content delineates specific and potentially unique functional states of the hippocampal precursor cells.

Specific aims

In order to test the above working hypothesis I had the following specific aims:

1. Corroborate that redox regulation and cellular ROS content is indeed different between the NPCs of the DG and SVZ.
2. Describe the correlation between stemness and cellular ROS levels. Further identify and characterize the cellular state heterogeneity (if any) marked by different ROS content using different model systems. Resolve the temporal relation between ROS changes and neurogenic trajectory.
3. Provide a temporal resolution of the pro-neurogenic effects of acute de novo physical activity. Characterize how physical activity results in enhanced proliferation of NPCs.
4. Identify if redox fluctuations in NPCs as a whole or within a subset of NPCs drive the pro-neurogenic response observed post running.

Based on the above specific aims, I can answer the key question mentioned above: Are the events leading to adaptive neurogenesis just enhanced baseline neurogenic processes?

Materials and methods

Table 1: List of all reagents, resources, animal genotypes and software

REAGENT or RESOURCE	SOURCE	IDENTIFIER
Antibodies		
Mouse monoclonal anti-IdU	BD Bioscience	Cat#347580
Goat polycolonal anti-doublecortin (DCX)	Santa Cruz	Cat# sc-8066
Rat monoclonal anti-BrdU (CldU/BrdU)	AbD Serotec	Cat#OBT0030
Rabbit polyclonal anti-Ki67	Novocastra	Cat#NCL-Ki67p
Goat polyclonal anti-Sox2	Santa Cruz	Cat# sc-17320
Rabbit polyclonal anti-Tbr2	Abcam	Cat# ab23345
Mouse monoclonal anti- Nestin	Abcam	Cat# ab22035
Chemicals, Peptides, and Recombinant Proteins		
Accutase	Sigma-Aldrich	Cat# A6964
B27 supplement	Thermo Fisher Scientific	Cat# 17504044
Bone morphogenic protein 4 (recombinant human BMP4)	R & D systems	Cat# 314-BP-050
CellROX Deep Red reagent	Thermo Fisher Scientific	Cat# C10422
5-Chloro-2'deoxyuridine (CldU)	Sigma-Aldrich	Cat# C6891
diaminobenzidine (DAB)	Sigma-Aldrich	Cat#D5905
Dihydroethidium (DHE)	Thermo Fisher Scientific	Cat# D1168
EdU- Click-iT™ EdU Alexa Fluor™ 647 Flow Cytometry Assay Kit	Thermo Fisher Scientific	Cat# C10424
Epidermal growth factor (EGF)	Peprotech	Cat# AF-100-15
Basic fibroblast growth factor (FGF)	Peprotech	Cat# AF-100-18B
GlutaMAX supplement	Thermo Fisher Scientific	Cat# 35050061
Heparin	MP Biomedicals	Cat# 0210193125
5-Iodo-2'-deoxyuridine (IdU)	Sigma-Aldrich	Cat# I7125
Laminin	Sigma-Aldrich (Roche)	Cat# 11 243 217 001

Neurobasal medium	Thermo Fisher Scientific	Cat# 21103049
L (-) norepinephrine	Sigma-Aldrich	Cat# A7257
MitoSOX	Thermo Fisher Scientific	Cat# M36008
eBioscience™ Fixable Viability Dye eFluor™780	Thermo Fisher Scientific	Cat# 65-0865-14
Parafomaldehyde (PFA)	Sigma-Aldrich	
Propidium Iodide	Thermo Fisher Scientific	Cat# P3566
Poly-D-lysine (PDL)	Sigma-Aldrich	Cat# P7280
Potassium Chloride (KCl)	Sigma-Aldrich	Cat# P9333
Critical Commercial Assays		
Neural Tissue Dissociation Kit (P)	Miltenyi Biotec	Cat# 130-092-628
RNeasy Micro Kit	Qiagen	Cat# 74004
VECTASTAIN ABC-HRP Kit	Vector Laboratories	Cat#PK-4000
Deposited Data		
Raw Sequence data		GSE124095
Experimental Models: Organisms/ Strains/ cell lines		
B6.129S-Cybb^{tm1Din}/J	The Jackson Laboratory	#002365
C57BL/6JRj	Janvier	
Tg(Nes-EGFP)1Yamm	Yamaguchi et al., 2000	RBRC06355
Tg(GFAP-EGFP)1Hket	Nolte et al., 2001	MGI:6188855 Frank Kirchhoff (University of Saarland, Germany)
Tg(Dcx-EGFP)BJ224Gsat/Mmmh	Gensat	MMRRC:000244-MU
Nox2$^{-/-}$ (B6.129S-Cybb^{tm1Din}/J)	Pollock et al., 1995	
NPC monolayer culture; C57BL/6JRj	Janvier	
Oligonucleotides		

Actb_ q_fw (forward) Actb_ q_rev (reverse)	ACCCGCGAGCACAGCTTC ACATGCCGGAGCCGTTGTC	Product_ size: 112 bp Annealing temperature: 58-60˚C
Ascl1_ q_fw Ascl1_ q_rev	GGAACAAGAGCTGCTGGACT TCGTTGGCGAGAAACACTAA	Product_ size: 119 bp Annealing temperature: 59˚C
Calb2_ q_fw Calb2_ q_rev	TGGAAATCTGGAAGCACTTTGA CATGCCAGAACCCTTCCTTG	Product_ size: 107 bp Annealing temperature: 59˚C
Rbfox3_ q_fw Rbfox3_ q_rev	CGGCATGACCCTCTACACAC TGCTGGTTGTCTGTCTGTGC	Product_ size: 126 bp Annealing temperature: 59˚C
Software and Algorithms		
Prism	GraphPad	V7
Flowjo	Flowjo, LLC	V7
Diva	BD Biosciences	V10

Mice

Mice were maintained on a 12-/12-h light/dark cycle with access to standard mouse chow (Sniff) and water ad libitum. Animals were aged between 6-8 weeks old at the time of the experiment. C57BL/6JRj female mice were purchased from Janvier Labs. Nox2 knockout mice (B6.129S-Cybb^{tm1Din}/J (Pollock et al., 1995) were initially purchased from The Jackson Laboratory and maintained as a homozygous breeding colonies, Nes-GFP mice (Yamaguchi et al., 2000), were obtained from Yamaguchi and colleagues and maintained as a homozygous colony. Dcx-GFP mice (Stock Tg(Dcx-EGFP)BJ224Gsat/Mmmh)were purchased from Mutant Mouse Resource and Research center and maintained as a homozygous colony (Gong et al., 2003). Gfap-GFP mice were acquired from the lab of Frank Kirchhoff (university of Saarland) and maintained as a homozygous colony (Nolte et al., 2001). Mice were housed in groups of at least two in standard polycarbonate cages (Type III, Techniplast, Germany), under baseline conditions. All experiments were conducted in accordance with the applicable European regulations and approved by the responsible authority (Landesdirektion Sachsen).

Physical activity paradigm

Animals were singularly housed in either standard cages or those containing a running wheel (150 mm diameter, TSE Systems, Germany) for 4days/ 2days/ 10days. The average distance run was monitored and recorded.

Thymidine labelling and tissue preparation

To label proliferating cells, animals were injected intraperitoneally with CldU (42.5 mg/kg), IdU (57.5 mg/kg). Mice were transcardially perfused with NaCl (0.9 % w/v) and brains removed and post-fixed in 4 % paraformaldehyde (PFA) at 4°C overnight. The next day, brains were transferred to a 30 % sucrose solution for 2–3 days. Coronal sections with a thickness of 40 µm were cut using a sliding microtome (Leica SM2010) cooled with dry ice. Sections were collected and stored as floating sections in cryoprotection solution (CPS; 25 % ethyleneglycol, 25 % glycerol in 0.1 M phosphate buffer pH 7.4) at -20°C. Every sixth section of each brain was pooled in one series for immunohistochemistry.

Fluorescence immunohistochemistry

Two combinations of antibodies were used to phenotype the proliferating cells (Sox2/Tbr2/IdU/CldU) which we termed as “early” phase neurogenic markers or (Tbr2/DCX/IdU/CldU) which we termed as “late” phase neurogenic markers. Sections were first washed with PBS and treated with 0.9 % NaCl, before DNA denaturation was performed in 2 N HCl for 30 min at 37 °C. The sections were then thoroughly washed with PBS and blocked for 1 h in PBS supplemented with 10 % donkey serum (Jackson ImmunoResearch Laboratories Inc) and 0.1 % Triton X-100. Primary antibodies (Sox2, Tbr2, DCX, rat anti-BrdU, or mouse anti-BrdU) were diluted in PBS supplemented with 3 % donkey serum and 0.1 % Triton X-100. Incubation was performed overnight at 4 °C. After several rinses in PBS, the sections were incubated with secondary antibodies diluted in PBS supplemented with 3 % donkey serum and 0.1 % Triton X-100 at room temperature for 4 hours. They were then washed in PBS, after which 4´,6-diamidino-2-phenylindole (DAPI, 1:2000) staining was performed for 10 min. After a final wash with PBS, the sections were mounted on glass slides and coverslipped with Aqua-Poly/Mount (Polysciences Europe GmbH). $CldU^+$ and IdU^+ cells in every sixth section (240 µm apart) were counted along the complete ventral dorsal extent of the DG at 40x magnification using a Zeiss Apotome microscope. Results were multiplied by 6 in order to obtain the total number of positive cells within the DG region of each brain. 100 randomly-selected $CldU^+$ and IdU^+ cells per DG were photographed using the apotome function and phenotyped for the co-

expression of Sox2 -Tbr2 and Tbr2 - DCX.

DG and SVZ dissection and dissociation

Mice were sacrificed, their brains immediately isolated, and the dentate gyrus (DG) and SVZ micro-dissected (Hagihara et al., 2009; Walker and Kempermann, 2014). The tissue was enzymatically digested using the Neural Tissue Dissociation Kit (Miltenyi) according to the manufacturer's instructions. Following a final wash in Hank's balanced salt solution (HBSS) (PAA; GE Healthcare) the pellet was resuspended in 1 ml of growth medium or HBSS, based on the succeeding procedure, and filtered through a 40 μm cell sieve (Falcon; BD Biosciences).

Flow cytometry

Dissociated SVZ or DG cells were analyzed using a FACS Aria III cell sorter (BD Biosciences) using a 85 μm nozzle or sorted with a 100 μm nozzle. Events were first gated based on the forward and side scatter (FSC and SSC) to identify the main cell population and exclude debris. Dead cells were excluded using the live/dead dye (vitality dye eFlour™ 780 in conjugation with DHE and Mitosox, PI in conjugation with CellROX DeepRed) and doublets were excluded based on the height and width of the cells. Cells were then gated based on their ROS content, irrespective of the genotype. For intracellular ROS measurements, either CellROX DeepRed Reagent (5 μM, Thermo Fisher Scientific, for the neurosphere assays) or dihydroethidium (DHE; 5 μM, Thermo Fisher Scientific, for all other ROS analyses) was added to the specimen before sorting and incubated for 30 min at 37 °C. Extended DHE exposure was found to be toxic to cells, and hence I had to Cellrox Deepred for neurosphere assays. For mitochondrial ROS measurements MitoSOX Red Mitochondrial Superoxide indicator (5 μM, Thermo Fisher Scientific) was added and incubated for 30 mins. The cells were transferred to a falcon tube and washed with 5ml of PBS. Following centrifugation, the supernatant was removed, the cells were resuspended in 500 μl PBS and transferred to a FACS tube for sorting. Cell populations were sorted, either into medium (for neurosphere experiments), RLT buffer (for RNA isolation).

Gating for ROS classes

The cells of the DG and SVZ yielded very stereotypical ROS profiles and were manually clustered, based on the contour of the ROS profile. An initial 2-gate strategy was employed and later, for all experiments, I used a four gating strategy to identify non-overlapping ROS classes with significant differences in the median ROS content, using Flojo (V10) for analysis and DIVA (BD Biosciences) for sorting the populations. The gates obtained from

control housed DG were used as the “master gates” which were applied to runner DG cells’ profiles or to the SVZ cells.

Neurosphere culture

For neurosphere culture, cells were resuspended in 10 ml neurosphere growth medium consisting of Neurobasal medium (Gibco, Life Technologies), supplemented with 2% B27 (Invitrogen), 1X GlutaMAX (Life Technologies) and 50 units/ml penicillin/ streptomycin (Life Technologies). The following growth factors were also included: 20 ng/ml EGF, 20 ng/ml FGF-2 and 20ng/ml Heparin. DG and SVZ are isolated from adult mice, dissociated using the neural dissociation kit and cells are spun down. These cells are passed through a 40 µm filter, plated into 96 well plates without any coating and incubated at 37 °C with 5 % CO2. I plated cells from 1 DG/ SVZ in one 96-well plate as at this density one NPC is present in one well, which is referred to as clonal density. The resulting neurospheres counted using an inverted light microscope after either 7 days for SVZ cultures or 14 days for DG cultures. The cut-off for a neurosphere is 40 µm. Although neurospheres can be classified based on size, I have not performed this analysis during my thesis. I used 15 mM KCl or L-(−)-noradrenaline (+)-bitartrate salt monohydrate (norepinephrine; 10 µM) as a stimulant to trigger latent DG NPCs into forming neurospheres in vitro (Jhaveri et al., 2010; Reynolds and Weiss, 1992; Rietze and Reynolds, 2006; Walker et al., 2008).

Generation of monolayer culture

To generate a monolayer culture, the critical step was to establish cell-substrate contacts. To this end, cells are isolated in a procedure similar to the above protocol described for neurospheres. But, instead of plating cells on plastic, which precludes any cell-substrate contacts, cells are plated on surfaces coated with poly-D-lysine (overnight coating with 50µM dissolved in water) and laminin (overnight coating with 50µM dissolved in PBS/ DMEM incomplete medium). The monolayer cultures are maintained in the presence of growth factors: 20 ng/ml EGF, 20 ng/ml FGF-2 and incubated at 37 °C with 5 % CO_2 and 21% O_2. Many of the cell types, including astrocytes, endothelial cells, neurons and NPCs, form stable divalent cation dependent connections with the substrate upon plating, but only the NPCs can proliferate and self-renew under these conditions. In 7-10 days proliferating islands within the dish can be identified. The culture is washed with PBS, the contacts are broken by treatment with accutase, counted and re-plated at a density which leads to 100% surface occupancy (confluency) in 3-4 days. This process is referred to as splitting/ passaging and after every accutase treatment the culture is referred to have progressed a

passage. Upon passaging, the dividing NPCs are selected for and by passage 5-6 a homogenous culture of Nestin, Sox2 double positive cells can be established. These cells can be differentiated by culturing them in medium without growth factors for 4-7 days, wherein GFAP expressing astrocytes and MAP2AB expressing neurons can be identified. This culture can be frozen and stored for extended periods of time in Liq. $N_{2.}$ The freezing medium has 1 million cells in proliferation medium with 10% DMSO. This procedure is described in detailed in (Babu et al., 2007; 2011)

Inducing quiescence through BMP4 treatment

Cells were plated at different confluences to achieve 60-70% at different days in either T25 or 6-well plates. 3 different durations of BMP4 treatment were employed- 1 day of BMP4 treatment which included 3 days of proliferation to yield 60-70% confluency and 1 day of EGF withdrawal and BMP4 treatment; 2 days of BMP4 treatment which included 2 days of proliferation to yield 60-70% confluency and 2 days of EGF withdrawal and BMP4 treatment; 3 days of BMP4 treatment which included 1 day of proliferation to yield 60-70% confluency and 3 days of EGF withdrawal and BMP4 treatment. Previous work showed that treating cells with 50 ng/ml BMP4 induces quiescence (Knobloch et al., 2017; Martynoga et al., 2013) , I have used 20 ng/ml BMP4 to show that quiescence can be also be induced at lower concentrations. Cells cultured for 4 days in the presence of growth factors was used as the proliferation control for the BMP4 experiment. To recover cells into proliferation post BMP4 treatment, it was paramount to split the cells and re-plate them in the presence of growth factors. Cells were given 1/ 2/ 3 days to recover and proliferate. Two different experiments were conducted at the end of each of the above treatments. First, ROS dyes were added to cells 30 minutes prior to accutasing them and the cellular ROS content was analyzed using the LSR2 cell analyzer (BD Biosciences). Secondly, to assay proliferation a Click-IT assay was performed, which involves labeling proliferating cells with 3-hour exposure to EdU. Post the exposure, cells were accutased, fixed with 4% PFA, the Click-IT reaction was performed as per manufacturer's protocol and cells were cytometrically analyzed.

Next Generation sequencing (NGS)

RNA extraction

Nes-GFP positive cells from the DG were gated into ROS classes, based on their intracellular ROS content. 400 GFP positive cells from each ROS class were FACsorted

into a PCR tube containing 8.5 µl of a hypotonic reaction buffer and RNA was prepared using the SMARTer Ultra Low RNA HV Kit (Takara Bio) according to the manufacturer's protocol. For both experiments, cDNA of polyadenylated mRNA was synthesized from RNA of the lysed cells using SmartScribe reverse transcriptase, a universally tailed poly-dT primer and a template switching oligonucleotide (Takara Bio). This was followed by 12 cycles of amplification of the purified cDNA with the Advantage 2 DNA Polymerase (Takara Bio). After ultrasonic shearing of the amplified cDNA (Covaris S2), samples were subjected to standard Illumina fragment library preparation using the NEBnext Ultra DNA library preparation chemistry (New England Biolabs). In brief, after physical fragmentation by ultrasonication (Covaris LE 220) cDNA fragments were end-repaired, A-tailed and ligated to indexed Illumina Truseq adapters. Resulting libraries were PCR-amplified for 15 cycles using universal primers, purified using XP beads (Beckman Coulter) and then quantified with the Fragment Analyzer (Advanced Analytics/Agilent). Final libraries were equimolarly pooled and subjected to 75-bp-single-end sequencing on the Illumina HiSeq2500 platform, providing ~35 (24–60) million reads per sample. Reads were mapped to the latest mouse genome build (mm10) using the STAR algorithm (Dobin et al., 2013) and counts per *ENSEMBL* gene model prepared using the RSubread package (Liao et al., 2013) or R/BioConductor.

Quality control and differential expression

RNASeq counts were filtered to have at least 1 count per million reads (CPM) in a minimum of 75% of the samples from at least one cell population. CPM were calculated using the function *cpm* from the *edgeR* package in R/BioConductor (Robinson et al., 2010). Samples were clustered by plotting the first two principal components and by unsupervised hierarchical clustering. One sample from each of the two experiments showed reduced sequencing depth and complexity and did not cluster with replicates. In both cases, these samples came from preparations with very low input RNA so we decided to remove them from further analyses. A filter for differential expression was then performed using the edgeR functions lmFit and topTags and only significantly (adjusted $p < 0.05$) differentially expressed transcripts were used for enrichment analyses. Transcripts were classified as 'enriched' in an experimental group if the mean expression in that group was significantly above the average expression over all groups. Enriched genes were further filtered by hierarchical clustering into two clusters based on inter-group *t*-statistics and those where only one group clustered separately were termed 'signature' genes.

Functional enrichment and expression profiles

Enrichment for Gene Ontology terms was performed using the R package *top*GO Expression profiles of curated gene lists were calculated by identifying all genes in the current data that corresponded to the genes in the gene list of interest and calculating the first principal component to collapse their expression into an 'eigengene'. The eigengene values were then used for plotting. A similar approach was used to reanalyze the Shin et al., dataset where the genes corresponding to the 'signature' genes for each ROS class were identified in the single-cell dataset and the first principal component of these used to create an eigengene. Smooth spline interpolation of the eigengene was then performed to produce the plotted values.

The curated gene lists used during the study are listed in the table below. I have divided the genes into functional groups regulating ROS (Table 2; blue); markers and regulators of cell cycle progression (Table 3; brown) and markers and regulators of neurogenic progression (Table 4; green). I have chosen key genes to mark the different stages of neurogenesis. Shin and colleagues ((Shin et al., 2015) have previously identified transcription factors (TFs) which are regulated along the progression of cellular states and divided the significantly altered TFs as either "Quiescent TFs" (Table 6; red), which are high in non-proliferative NPCs and downregulated with neurogenic progression, or as "activated TFs" (Table 6; black) which are upregulated with entry into cell cycle. I used these TF lists for corroborating some of my findings.

Table 2: Curated list of ROS regulators

3110043O21Rik	Epx	Jun	Nox4	Rnf7	Uba52
Alox12	Foxm1	Kcnk13	Nqo1	Rps27a	Ubb
Alox15	Fth1	Keap1	Nrf1	Rps27a	Ubb
Aox1	Fus	Krt1	Nudt1	Scara3	Ubc
Aox2	Gclc	Lpo	Oxr1	Sepp1	Ubc
Aox4	Gclm	Maf	Oxsr1	Sftpd	Ucp2
Apoe	Glyat	Mbl2	Pdlim1	Sirt2	Vimp
Atox1	Gm7866	Mgst3	Pnkp	Sod1	
Bnip3	Gpx1	Mmd	Pparg	Sod2	
Cat	Gpx2	Mpo	Ppargc1a	Sod3	
Ccl5	Gpx3	Mpv17	Prdx1	Sqstm1	
Ccs	Gpx4	Msra	Prdx2	Srxn1	
cyba	Gpx5	Mt3	Prdx3	Stk25	
Cybb	Gpx6	Nanos2	Prdx4	Surf1	
Cybb	Gpx7	Ncf1	Prdx5	Tardbp	
Cygb	Gpx7	Ncf2	Prdx5	Tpo	
Dbi	Gsr	Ncf4	Prdx6	Trpv6	
Dhcr24	Gss	Nfe2	Prex1	Ttn	
Duox1	Gstp1	Nfe2l1	Prnp	Txn1	
Duox1	Gstp2	Nfe2l1	Ptgs1	Txnrd1	
Duox2	Gstz1	Nfe2l2	Ptgs2	Txnrd2	
Dusp1	Gtf2i	Nos2	Pxdn	Txnrd3	
Dusp12	Hmox1	Nox1	Rac1	Uba52	
Ephx2	Hspa1a	Nox3	Rac2	Uba52	

Table 3: Curated list of cell cycle marker and key regulators of active cell cycle

Abl1	Cdk4	Mad2l1	Prm1
Ak1	Cdk5rap1	Mcm2	Psmg2
Apbb1	Cdk6	Mcm3	Pten
Ascl1	Cdkn1a	Mcm4	Rad17
Atm	Cdkn1b	Mcm5	Rad21
Aurka	Cdkn1c	Mcm6	Rad51
Brca1	Cdkn2a	Mdm2	Rad9a
Brca2	Cdkn2b	Mki67	Ran
Bub1	Cdkn2c	Mre11a	Rbl1
Camk2a	Chd5	Msh2	Rbl2
Camk2b	Chek1	Mtbp	Sesn2
Casp3	Cks1b	Myb	Sfn
Ccna1	Dnajc2	Mybl1	Shc1
Ccna2	Dst	Nek2	Skp2
Ccnb1	E2f1	Nfatc1	Slfn1
Ccnb2	E2f2	Notch2	Smc1a
Ccnc	E2f3	Npm2	Stag1
Ccnd1	E2f4	Pcna	Sumo1
Ccnd2	Gadd45a	Pes1	Taf10
Ccnd3	Gadd45g	Pkd1	Terf1
Ccne1	Gpr132	Plk1	Tfdp1
Ccnf	Hus1	Pmp22	Trp53
Cdc25a	Inha	Ppm1d	Trp63
Cdc7	Itgb1	Ppp2r3a	Tsg101
Cdk2	Macf1	Ppp3ca	Wee1

Table 4: Curated list of neurogenic marker and key regulators of neurogenic progression

Nes	Id1	Mcm6	Fzd1	Gfap
Sox2	Id2	Cdk4	Npy	Id1
Eomes	Id4	Cdk2	Lpar1	Nes
Pcna	Fabp7	Cdk6	Lrp6	Pax6
Mki67	Klf4	Ccnd1	Gsk3b	Fabp7
Hopx	Btg2	Ccnd2	Ncam1	Hes5
Dcx	Neurog2	Ccnd3	Yy1	Sox2
Calb2	Prom1	Atf3	Bmi1	Mki67
Rbfox2	Sox9	Atf4	Gad1	Ascl1
Gfap	Sox11	Calb1	Gad2	Eomes
Slc1a3	Runx1	Btg1	Bcl2	Neurod1
Ascl1	Fgf2	Cdkn1c	Mfn2	Dcx
Huwe1	Hes5	Id3	Nr2f1	Prox1
Thrsp	Trp53	Klf3	Yap1	Dpysl3
Cpt1a	Casp3	Hes1	Grin2a	Calb2
Fasn	Apbb1	Notch2	Grin2d	
Stmn1	Rbfox3	Sox1	Sox5	
Aldoc	Pax6	Sox21	Sox6	
S100b	Ldha	Sox14	Nfe2l2	
Gpx4	Neurod1	Jag1	Shh	
Selenop	Acaca	Gli1	Nrf1	
Cdkn1b	Nup153	Sirt1	Rest	
Cdkn1a	Mcm2	Sirt2	Tet1	
Pten	Mcm3	Nr2e1	Tet2	
Egfr	Mcm4	Wnt3	Sdha	

Table 5: Quiescent and activated TFs identified by Shin et al.

Id4	Sox2	Atf4	Foxg1
Zfp617	Dbx2	Hmgb2	Tcf12
Camta2	Zscan26	Hmgb1	Cebpg
Mxi1	Pou3f3	Sox11	Eomes
Thap7	Tcf7l2	Ybx1	Zmiz1
Lef1	Nr2e1	Nfib	Nfyc
Zfp869	Rfx4	Nfix	Zfp386
Zfpm2	Tsc22d3	Insm1	Zkscan1
Fezf2	Irf3	Hmgb3	Bcl11a
Mier1	Hes1	Ssrp1	Zfp763
Etv5	Id3	Smarcc1	Zfp944
Arx	Zfp65	Zfp367	Zbtb41
4932411N23	Bhlhe41	Smarce1	Trp53
Zbtb26	Npas3	Mxd3	Csde1
Klf15	Sox9	Zfp62	Zmiz2
Grhl1	Hopx	Zeb2	Zfp808
Zfp740		Nfia	Zbtb38
Nfx1		Sox4	
Ikzf2		Terf1	
Fos		Tcf4	
Bcl6		Tulp4	
Dmtf1		Emx1	
Tfe3		Hmga1b	
Zbtb4		Zfp637	
Nr3c1		Mycn	

RNA isolation and quantitative RTPCR (q-RTPCR)

DG of the Dcx-GFP animals was micro-dissected and cells were sorted into RLT buffer, similar to the sorting strategy described for neurosphere assays. Total RNA was isolated from sorted cells using the RNeasy Micro Kit (QIAGEN) according to the manufacturer's instructions. RNA was eluted at least four times from RNeasy columns and the volume reduced to 10 µl using a Speedvac (Eppendorf) at 37°C. RNA was reverse transcribed into complementary DNA (cDNA) using SuperScript^{TM} II Reverse Transcriptase (Thermo Fisher Scientific). Briefly, 0.5 - 1 µg of RNA was incubated with 500 ng Oligo(dT) primers and 1 µl dNTPs (10 mM; Thermo Fisher Scientific) for 5 min at 65°C and quickly chilled on

ice. For cDNA amplification, RNaseOut (Thermo Fisher Scientific) was added according to the recommendations in the manual and incubated at at 42°C for 2 hours.

Quantitative real-time polymerase chain reactions (qRT-PCRs) were performed using the QuantiFast SYBR Green PCR Kit (QIAGEN) and the CFX Connect^{TM} Real-Time PCR Detection System (Bio-Rad). Briefly, 20 µl reactions consisting of 10 µl SYBR Mix, 2 µl primers (10 mM) and 8 µl of undiluted cDNA were incubated using the PCR program. Gene specific, Exon-exon regions were identified using the online *ENSEMBL* tool. These regions were fed into the online tool Primer 3 version 0.4.0 (http://bioinfo.ut.ee/primer3-0.4.0/) to design primers. Specificity of primers and DNA contamination was checked in silico using the online tool Primer-BLAST (https://www.ncbi.nlm.nih.gov/tools/primer-blast/). Primer specificity was further ensured by validating single peak melting curves. Results of qRT-PCRs were analyzed using the delta Ct method. For normalization, gene-specific Ct values were subtracted from Ct values obtained for the housekeeping gene, beta-Actin (Actb).

Thermal cycling conditions for qrt-PCRs (denaturation to extension were repeated for 40 cycles).

Table 6: Cycling conditions for q-RTPCRs

Step	Temperature	Time
Initial denaturation	95°C	15 minutes
Denaturation	95°C	10 seconds
Annealing	59°C (see materials)	30 seconds
Extension	72°C	30 seconds
Final extension	72°C	10 minutes
Melting curve	Ramp down from 95°C to 60°C	

Ki67 immunohistochemistry and quantification of in vivo proliferation

Briefly, brain sections stored in CPS were transferred into PBS and washed. Endogenous peroxidase activity was blocked by adding 0.6 % hydrogen peroxide (H_2O_2; Merck Millipore) for 30 min and sections were then rinsed with 0.9 % NaCl. Protein-binding sites were blocked with a blocking solution (10 % donkey serum, 0.2 % Triton X-100 in PBS) for 1 h. Ki67 staining was performed with the Ki67 primary (rabbit anti-Ki67, 1:500; Novocastra) and donkey anti-rabbit-biotin secondary antibodies (1:1000; Jackson Immunoresearch Laboratories). Detection was performed using the Vectastain ABC-Elite reagent (Vector

Laboratories) with diaminobenzidine (Sigma-Aldrich) and 0.04 % NiCl as the chromogen. Sections were mounted onto gelatin-coated glass slides, dried, cleared with Neoclear (Merck) and coverslipped using Neo-mount (Merck). Every sixth section (240 µm apart) was counted in the complete ventral dorsal extent of the dentate gyrus, at 40x magnification using a standard brightfield microscope. Results were multiplied by 6 in order to obtain the total number of positive cells within the dentate gyrus region of each brain.

Quantification and statistical analysis

Data analysis (with the exception of the next-generation sequencing data) was performed using Prism software (Version 7, GraphPad Software, Inc). Flow cytometry data was analysed using the FlowJo software. Results were expressed as mean ± standard error of the mean (SEM). Statistical significance was determined using a Student's t-test when the experiment contained two groups, or an ANOVA when comparing more than two groups. Dunnett, Tukey's and Sidak post hoc tests applied, and mentioned in the text wherever applicable. The level of conventional statistical significance was set at $p < 0.05$ and displayed visually as * $p < 0.05$, ** $p < 0.01$, *** $p < 0.005$ and **** $p < 0.001$. The number of mice or repeat experiments performed per group is shown as a table below.

Table 7: list of experiments conducted with the replicate number

Experiment	Genotype	Age	Sex	No. of animals/ group	n
CldU-IdU dual labeling paradigm- 3 groups of 5S, 2R, 5R	C57BL/6JRj	8 weeks	female	8	8
ROS profiling of cells DG/ SVZ	C57BL/6JRj	6-8 weeks	female	1	5
Neurosphere post 2-way ROS gating	C57BL/6JRj	6-8 weeks	female	4-5/sample	5
Neurosphere post 4-way ROS gating	C57BL/6JRj	6-8 weeks	female	4-5/sample	5
Neurosphere post 4-way ROS gating to test the effect of stimulant (KCl)	C57BL/6JRj	6-8 weeks	female	4-5/sample	5

ROS profiling of Nes-GFP+ cells DG/ SVZ	C57BL/6-Tg(Nes-EGFP)	6-8 weeks	Mixed (matched)	4-5/sample	5
Expression profiling of Nes-GFP+ cells of different ROS classes	C57BL/6-Tg(Nes-EGFP)	6-8 weeks	Mixed (matched)	4-5/sample	5
1-day running paradigm followed by ROS profiling of Nes-GFP+ from DG	C57BL/6-Tg(Nes-EGFP)	6-8 weeks	Mixed (matched)	4-5/sample	5
1-day running paradigm followed by ROS profiling of Nes-GFP+ from SVZ	C57BL/6-Tg(Nes-EGFP)	6-8 weeks	Mixed (matched)	4-5/sample	5
4-day running paradigm followed by ROS profiling of Nes-GFP+ from DG 1-day running paradigm	C57BL/6-Tg(Nes-EGFP)	6-8 weeks	Mixed (matched)	4-5/sample	5
mitoROS profiling of Nes-GFP+ from DG of stnd. Housed and 1 day runners	C57BL/6-Tg(Nes-EGFP)	6-8 weeks	Mixed (matched)	4-5/sample	3
ROS profiling of Gfap-GFP+ cells DG, combined with EGF-647	C57BL/6-Tg(Gfap-EGFP)	6-8 weeks	Mixed (matched)	4-5/sample	4
ROS profiling of Dcx-GFP+ cells DG	C57BL/6-Tg(Dcx-EGFP)	6-8 weeks	Mixed (matched)	4-5/sample	7
ROS profiling of microglial cells, marked by Cd11b	C57BL/6JRj	6-8 weeks	Mixed (matched)	4-5/sample	3
ROS profiling of Nes-GFP+ cells DG in wildtype and Nox2 mutant animals	C57BL/6-Tg(Nes-EGFP)::B6.129S-Cybb^{tm1Din}/J	6-8 weeks	males	4-5/sample	5
1-day running and ROS profiling of Nes-GFP+ cells DG in Nox2 mutant animals	C57BL/6-Tg(Nes-EGFP)::B6.129S-Cybb^{tm1Din}/J	6-8 weeks	males	4-5/sample	5

4-day running and ROS profiling of Nes-GFP+ cells DG in Nox2 mutant animals	C57BL/6-Tg(Nes-EGFP)::B6.129S-Cybb^{tm1Din}/J	6-8 weeks	males	4-5/sample	5
Analysis of Ki67+ cells in wildtype and Nox2 mutants post 10 day running paradigm	B6.129S-Cybb^{tm1Din}/J	6-8 weeks	mixed	Wt: 12 stnd; 13 run; Nox2-/-: 12 stnd; 13 run	
Neurosphere assay with wildtype and Nox2 mutant; with and without KCl stimulation	B6.129S-Cybb^{tm1Din}/J	6-8 weeks	mixed	1/ genotype/ condition	4
ROS profiling of cells treated with BMP4	cell line from C57BL/6JRj (named MI6)	6-weeks	male	Technical rep. each passage = 1 replicate	4
ROS profiling of reverting cells post BMP4 withdrawal and EGF addition	cell line from C57BL/6JRj (named MI6)	6-weeks	male	Technical rep. each passage = 1 replicate	4
Proliferation of cells post BMP4 treatment	cell line from C57BL/6JRj (named MI6)	6-weeks	male	Technical rep. each passage = 1 replicate	4
proliferation of cells post BMP4 withdrawal and EGF addition	cell line from C57BL/6JRj (named MI6)	6-weeks	male	Technical rep. each passage = 1 replicate	4

Data and Software Availability

The raw sequence data for ROS experiments are deposited in GEO under the SuperSeries accession number GSE124095.

Results

Intracellular ROS content functionally delineates subpopulations of neural precursor cells

Identification of differentially enriched pathways between Nes-GFP$^+$ cells of the two adult neurogenic niches, the SVZ and the DG, provided a good starting point to test my working hypothesis that the DG houses unique subsets of neural precursors. Cell-autonomous redox regulation presented as the strongest candidate pathway, which could regulate or, at the least, resolve these subpopulations. As a first step, I wanted to further corroborate that genes integral for regulating cellular ROS content and redox regulation are differentially enriched in the DG precursors, I curated a list of 127 such genes including direct ROS producers, scavengers, sensors (Table 2; methods section), and together with Dr. Rupert Overall performed a hypergeometric comparison of their expression levels in the above described dataset (transcriptomic profiles of Nes-GFP$^+$ cells of the DG and SVZ). 51 of the queried genes are unique to DG Nes-GFP positive cells, which is significantly more than expected, while a significantly lower-than-expected 13 genes are enriched in SVZ cells (Fig. 5).

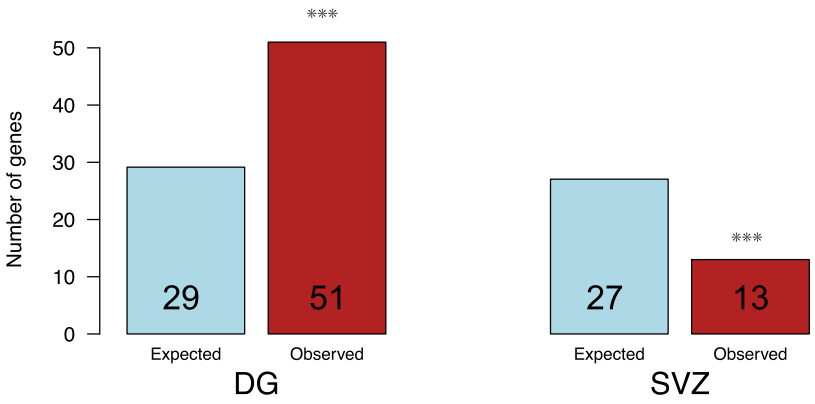

Figure 5: Redox genes are significantly enriched within the Nes-GFP$^+$ cells: A hypergeometric test shows, compared to an expected incidence, a significant enrichment of genes integral to ROS production in the DG's Nes-GFP$^+$ cells and significantly lesser expression of ROS genes in the SVZ Nes-GFP$^+$ cells' signatures.

Resolution of ROS profiles of DG and SVZ and neurosphere bioassay

Many approaches were considered to quantitatively measure the production and maintenance of cellular ROS levels. There are many commercial dyes, including Dihydroethidium (DHE; Dikalov and Harrison, 2012; Zhou et al., 2016; Zielonka et al., 2008), Cellrox dyes among others, which can be used as a snapshot measurement of cellular ROS

levels. To validate that cellular ROS content could be a discerning feature within the DG neurogenic niche, I optimized an ex vivo labeling protocol which is detailed in the methods section. Briefly, I freshly isolated cells from the entire DG/ SVZ from young adult (6-8 weeks old) C57Bl6 (wildtype) animals and used a viability dye (such as live/dead dye/ Propidium Iodide (PI)/ eflour780 viability dye; different fluorescent ranges for each of these vitality dyes) to identify and separate live cells. The concomitant staining of the ex vivo primary cells with the superoxide dye DHE proved to be the most reliable approach to assay cellular ROS levels. This approach demonstrated that DG and SVZ cells isolated from the same animals had distinct ROS profiles (Fig. 6). SVZ cells had a 5.3-fold higher overall ROS content than DG cells (two-way ANOVA, $p < 0.0001$, $F_{(1,16)} = 32.85$; Tukey: $p = .0045$).

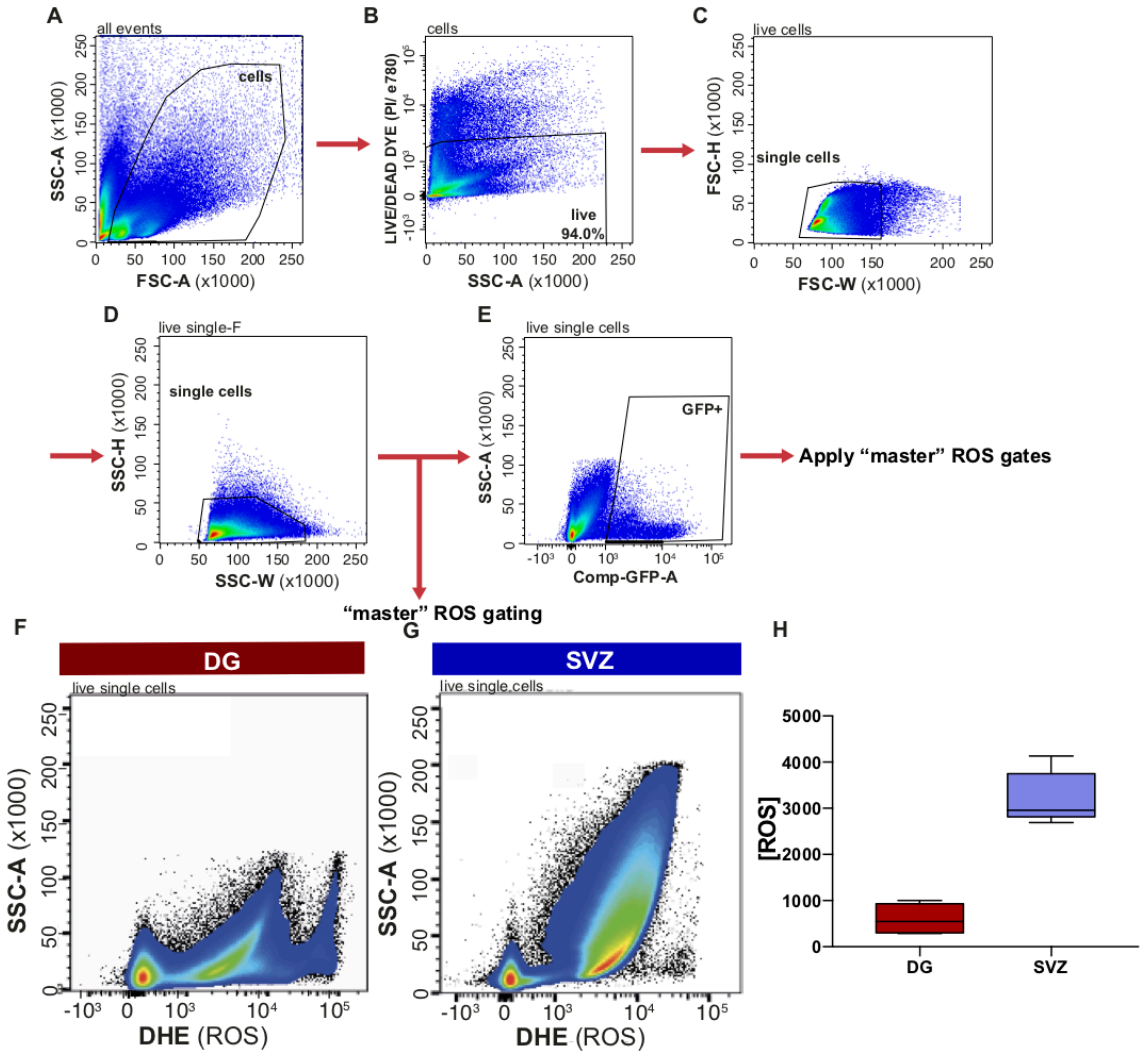

Figure 6: Pipeline for cytometric analyses and gating strategies and the comparison of ROS levels in the isolated cells of DG and SVZ. All events were gated for forward scatter (FSC-A, size of events) and sideward scatter (SSC-A, granularity of events) to exclude debris (A);

These events were gated to identify putative live cells by the exclusion of vitality dye and marked as live cells (B); The live cells were gated on size (C) and granularity (D) to identify singlets. The singlets were gated for ROS content and GFP content for subsequent analysis. This gating scheme resulted in the ROS profiles of DG (F) and SVZ (G), which are distinctly different. (H) Comparison of overall ROS content in single cells of DG and SVZ.

Interestingly, resolving the cells from the DG for cellular ROS content, either with DHE or Cellrox Deepred, revealed a stereotypic distribution, which enabled manual classification of cells into distinct “ROS classes” with significantly different median ROS content (Fig 7). I, together with Dr. Annette Rünker and Nicole Rund (technician), first classified the cells into ROS-Hi(gh) and ROS-Lo(w) classes, sorted cells and assayed them using the neurosphere bioassay, to determine whether cellular ROS content of DG cells could predict in vitro stemness (Reynolds and Weiss, 1992; Rietze and Reynolds, 2006). As long-term exposure to DHE is toxic, I used Cellrox deepred for this bioassay. Indeed, almost all of the of neurospheres (98.8%) were generated from the ROS-Hi class, which constitutes 17.8 ± 1.1% of FACS events with the highest ROS content. This corresponds to an 8.2 ± 1.5-fold ROS associated enrichment of neurosphere-forming cells relative to unsorted cells (one-sample t-test, vs. unstained, ROS-Hi: adj. p = .0156, ROS-low: adj. p < 0.0002; Fig. 7).

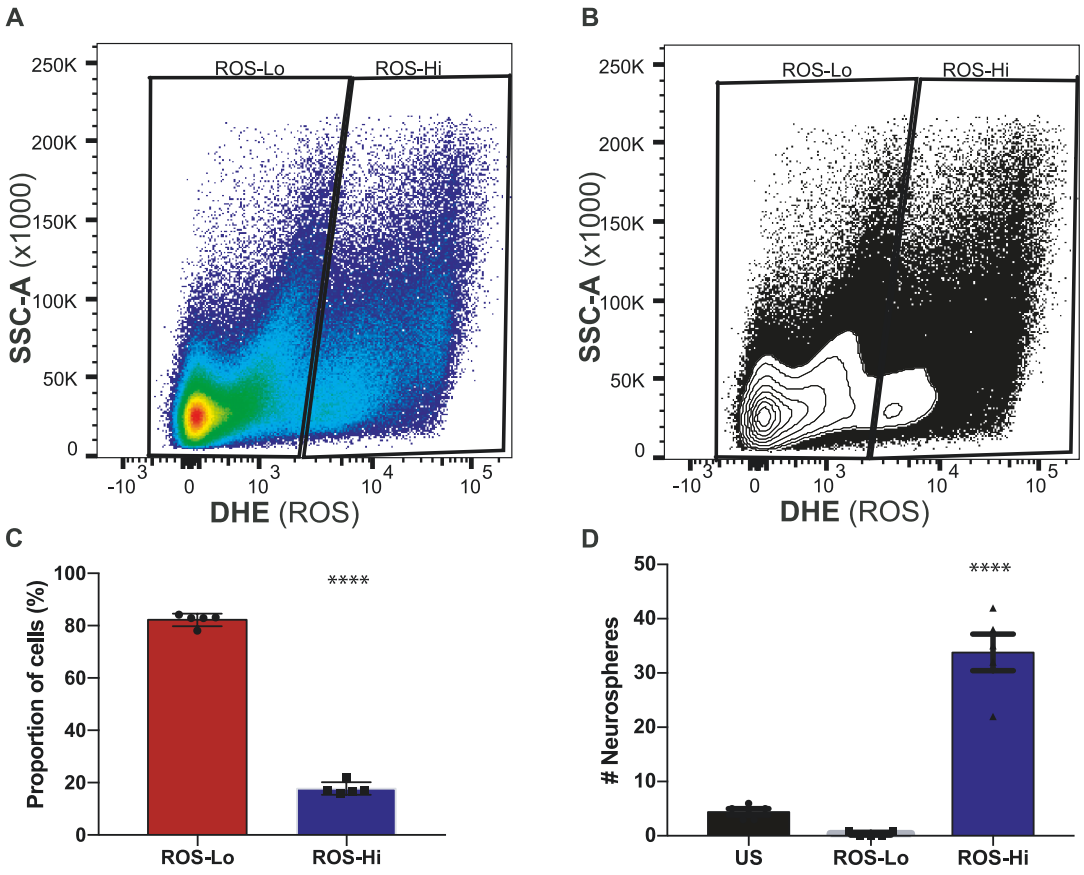

Figure 7: 2-gating strategy applied to DG cells and neurosphere bioassay. (A, B) All isolated cells of DG were gated into 2 ROS classes based on their contour and spread. (C) Proportion of cells in each of the ROS class. (D) The cells of the two ROS classes were sorted and plated for a neurosphere bioassay, resulting in no neurosphere from ROS-Lo class and significantly higher number of neurospheres from the ROS-Hi class. All data represent mean ± SEM. **** $p < 0.0001$.

To further resolve the correlation between ROS content and the potential for neurosphere formation, I defined four distinct, non-overlapping classes of ROS levels (Fig. 8A-C): hiROS (2.1 ± 0.3% events with highest ROS levels), midROS (next 9.5 ± 1.5% events), loROS (next 38.6 ± 4.7% events) and noROS (48.9 ± 5.8% events). When the same gating strategy was applied to the cells from the SVZ (Fig. 8D-F), I found that most of the SVZ cells were in the loROS (62.0 ± 6.2%) and midROS classes (25.7 ± 4.7%), with substantially fewer in the hiROS class (0.3 ± 0.0%). Interestingly from both the SVZ and DG, neurosphere-forming cells were restricted to the higher ROS classes (midROS and hiROS classes, which together constitute 26% and 11.6% of all sorted events from the SVZ and DG, respectively), with the highest density of neurosphere-forming cells in the hiROS class compared to unstained, sorted cells (one-sample t-test, DG: adj. $p = 0.002$, SVZ: adj. $p = 0.015$;Fig. 8G-H). Supplementing the growth medium with KCl or Norepinephrine, which are established stimulants for enhancing neurosphere formation (Jhaveri et al., 2010; Walker et al., 2008) augmented neurosphere formation only from hiROS and midROS cells, with significantly more neurospheres induced in the hiROS class after KCl treatment (2.4 ± 0.7 fold; two-way ANOVA, $p = 0.0029$, $F_{(6,36)} = 4.151$; Dunnett: $p < 0.0001$; Fig. 8I). Treatment with either of the stimulants did not lead to neurosphere formation from loROS and noROS classes. Our results, in corroboration with published results (Belle et al., 2011), suggest that cellular ROS content is an potent classifier of neurosphere-forming cells. Further, the total in vitro stemness of adult neural precursor cells from both niches is proportional to their steady state cellular ROS content.

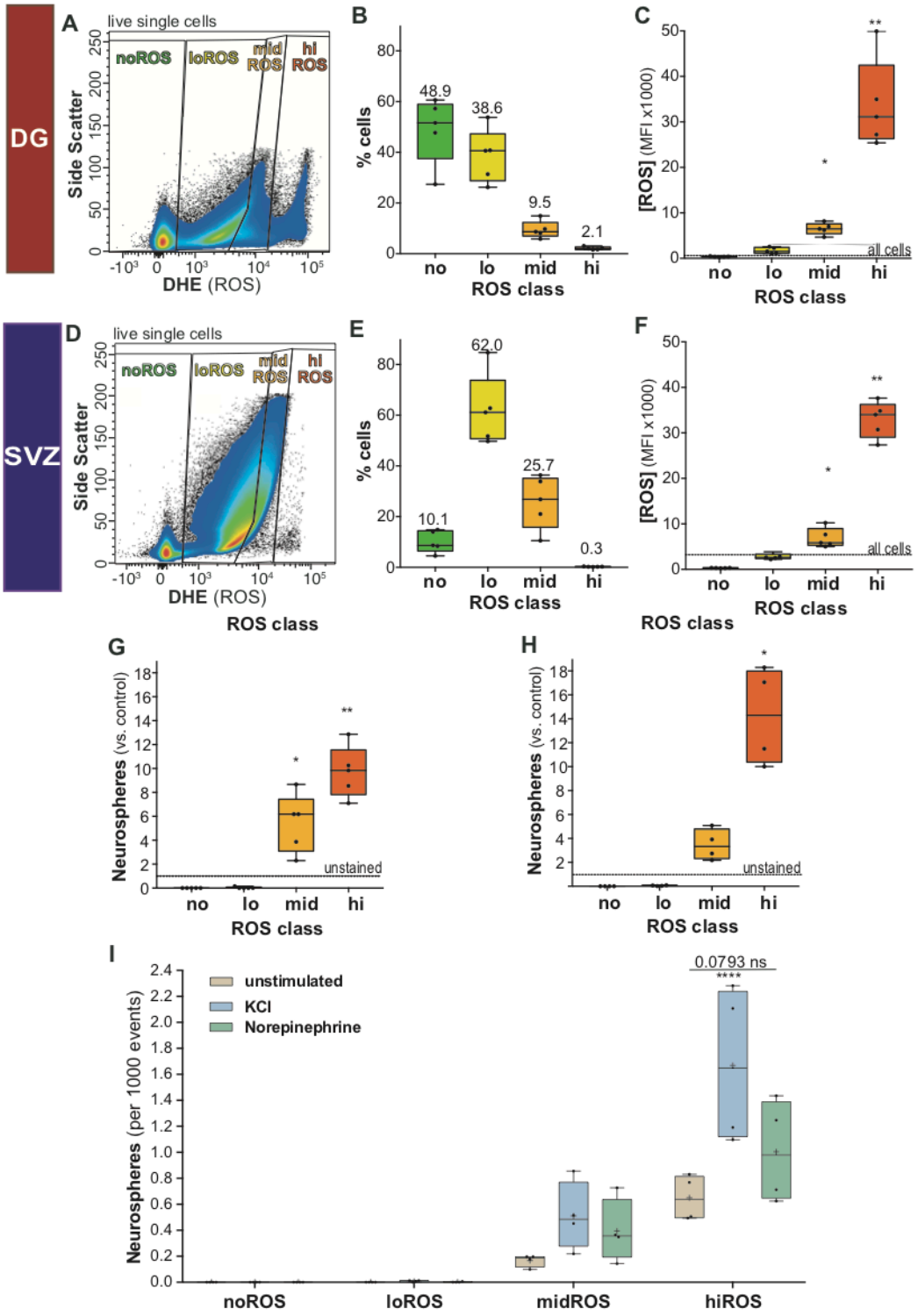

Figure 8: 4-gating strategy of DG and SVZ cells and neurosphere assay. (A) All cells of the DG were gated into 4 non-overlapping ROS classes – noROS, loROS, midROS and hiROS classes. (B) The resultant proportion of cells in each of the ROS class and their median cellular ROS content (C). (D) Gating of the SVZ cells into the ROS classes. (E) Proportion of SVZ cells in each of

the ROS class. (F) Median cellular ROS content in each of the SVZ ROS classes. (G) Neurosphere assay from each of the sorted DG ROS classes. (H) Neurosphere assay from each of the sorted SVZ ROS classes. (I) Neurosphere assay from each of the sorted DG ROS classes unstimulated and stimulated with KCl or norepinephrine. Note that neurosphere numbers post Norepinephrine are close to significance (p = 0.079). All data represent mean ± SEM. * $p < 0.05$, **** $p < 0.0001$.

Distribution of Nes-GFP cells into different ROS classes

A disproportionate segregation of stem and precursor cells into higher ROS classes could explain the finding that these classes harbor the neurosphere-forming cells. In order to test this hypothesis, I used Nes-GFP animals (Nes-GFP; Yamaguchi 2000), to cytometrically assay the ROS content in Nes-GFP$^+$ cells of the DG and SVZ. I found that the ROS content of Nes-GFP$^+$ cells of the DG was significantly greater than that of all isolated cells (3.7-fold; Tukey, $p = 0.001$; Fig. 9). In contrast to the DG, the Nes-GFP$^+$ cells of the SVZ had significantly lower absolute ROS levels than the entirety of cells isolated (Tukey, $p = 0.0047$; Fig. 9C). Further resolution of the entirety of the single cells from either niche into ROS classes and distribution analysis of Nes-GFP$^+$ cells of the DG revealed the following characteristic pattern: 50% of the Nes-GFP$^+$ cells were negative for or low in ROS (noROS: 5.3 ± 3.9% of all Nes-GFP$^+$ cells; loROS: 50.8 ± 3.7%; Fig. 9D, E), thus representing sub-populations that are not competent to form neurospheres. An additional 24.5 ± 5.1% of Nes-GFP$^+$ cells localized to the midROS and 19.4 ± 7.4% to the hiROS class, the classes which did yield neurospheres. In terms of their relative distribution among ROS classes, in the SVZ significantly more precursor cells segregated to the noROS class (35.3 ± 3.9%; two-way ANOVA, $p < 0.0001$, $F_{(3,32)} = 13.0$; Sidak, $p < 0.0001$), and significant fewer (1.22 ± 0.4%, p = 0.0151) were found in hiROS compared to the DG (Fig. 9D, E). Taken together, these results suggest that within the DG cellular ROS content classifies the precursor pool of cells into functional classes, based on their ability to form neurospheres. Further, compared to the SVZ, the Nes- GFP$^+$ hiROS population is substantially enriched in the DG.

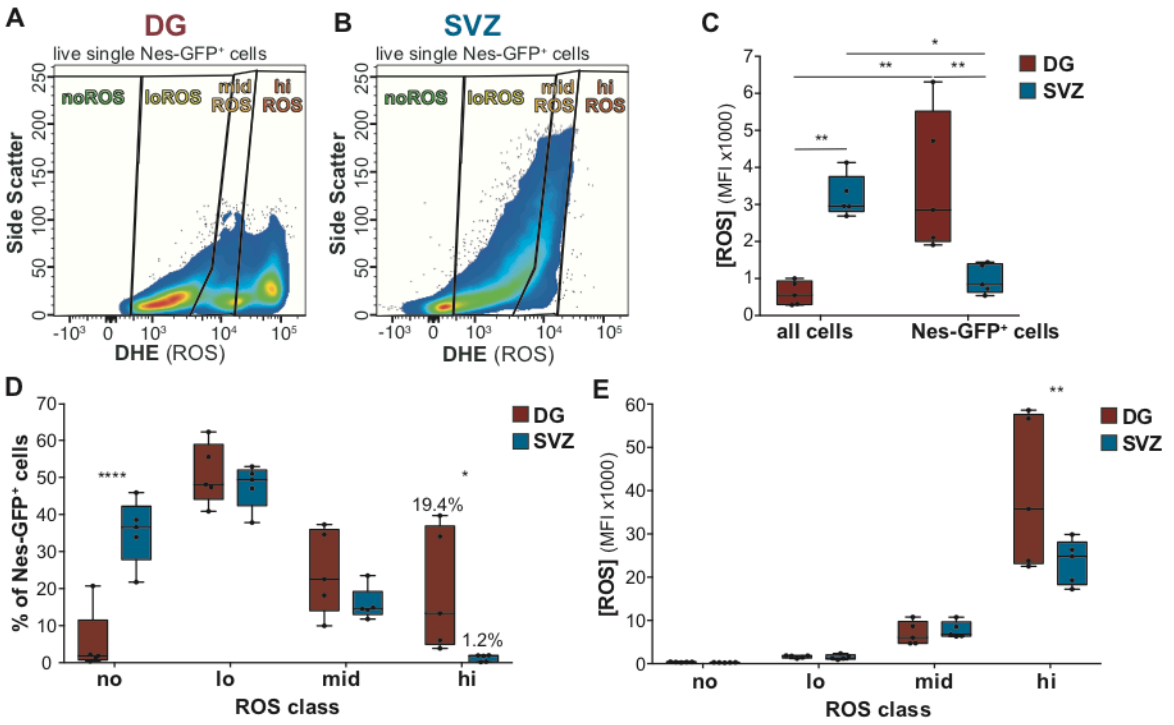

Figure 9: Nes-GFP cells within the ROS classes and comparison of distribution and median ROS content of Nes-GFP cells from DG and SVZ. FACS plots showing the Nes-GFP cells of the DG (A) and SVZ (B) within the ROS classes. (C) comparison of the ROS content in all single cells of DG and SVZ and all the Nes-GFP of DG and SVZ. (D) distribution of Nes-GFP cells of DG and SVZ into ROS classes and their median cellular ROS content (E). All data represent mean ± SEM. * $p < 0.05$, ** $p < 0.01$, **** $p < 0.0001$.

Neural precursors of the different ROS classes have distinct molecular profiles

To further characterize the precursor cells of the different ROS classes, I isolated and profiled the total RNA from 400 Nes-GFP$^+$ cells of the DG sorted into loROS, midROS and hiROS classes by means of next generation sequencing (NGS), together with the Dresden Genome Center (Dr. Andreas Dahl and Susanne Reinhart). Nes-GFP$^+$ cells within the noROS class (5.26 ± 3.87%) were omitted from this analysis as they represented only a negligible, and variable, proportion of precursor cells. The transcription profiles were analyzed in a collaborative effort with Dr. Rupert Overall. We could show that the Nes-GFP$^+$ cells in the different ROS classes have distinct transcription profiles, as evident from the principal component analysis (PCA; PC1: 41% and PC2: 13%; Fig. 10D). Further correlative analysis of the different biological samples showed a tight clustering of the expression profiles within a class (Fig. 10A-C). Of all the expressed transcripts within the precursor cells, 47.7% of the expressed transcripts segregated based on ROS content with 36.1% of transcripts being specific to cells of only one of the ROS classes. I could identify 1828

transcripts (12.1% of all expressed transcripts) specific for the hiROS class, 1043 transcripts (6.9%) for the midROS class and 2589 transcripts (17.1%) for the loROS class. Additionally, 684 transcripts (4.5%) were co-enriched between high and midROS class and 1050 transcripts (6.9%) among the mid and loROS classes. Only 25 transcripts (0.2%) were co-enriched in the Nes-GFP$^+$ cells of high and loROS, indicating that these ROS classes are the most distinct and cells with different ROS content essentially mark a trajectory of cellular states (Fig. 10E). A comparison of transcripts of Nes-GFP$^+$ cells that were unique to different ROS classes, to the signatures of all Nes-GFP$^+$ cells from the SVZ (Dr. Tara Walker, Fig. 3) showed that transcripts from Nes-GFP$^+$ cells with succeeding ROS classes had a higher degree of similarity to the SVZ precursors (Fig. 10F). Transcripts enriched within the Nes-GFP$^+$ cells of the hiROS class were more restricted to the DG than the SVZ, whereas transcripts exclusive to the Nes-GFP$^+$ cells with loROS were more likely to be expressed in the SVZ. To further characterize the functional states of the Nes-GFP$^+$ cells within each class, I first looked for the expression of transcripts that mark cellular processes such as neurogenesis (Table 4), cell cycle (Table 3) and, as control, ROS regulation (Table 2). As expected, I found a decline in the expression of transcripts considered to be essential for maintaining higher intracellular levels of ROS from hiROS to loROS class. This decline in ROS regulating genes is accompanied by an increase in active cell cycle markers' transcripts and the transcripts specific to neurogenic commitment (Fig. 10G).

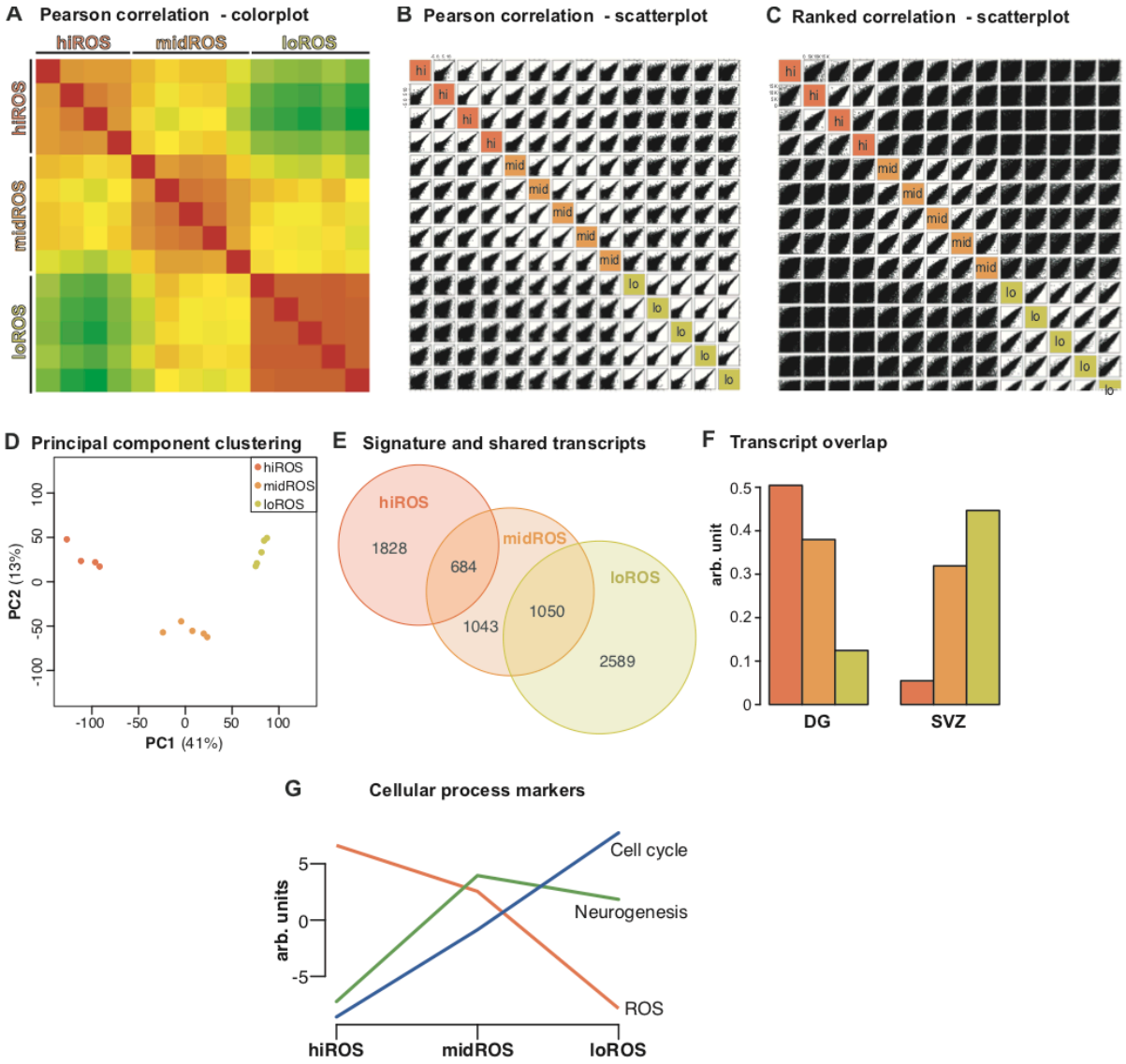

Figure 10: Nes-GFP$^+$ cells can be classified into distinct functional subsets based on their cellular ROS content. Correlation analysis between the expression profiles of the Nes-GFP$^+$ of the different ROS classes within the DG (hiROS class indicated in red, midROS in orange and loROS in green) (A) Pearson correlation color plot between the samples collected from separate experiments; (B) scatterplot of the Pearson correlation between the samples; (C) scatterplot of the Ranked correlation between samples; (D) Principal component (PC) analysis shows that samples from the different ROS groups have distinct transcriptional profiles. (E) Venn diagram showing the extent of differential gene expression between the Nes-GFP$^+$ cells of the different ROS classes. (F) Transcripts uniquely enriched in hiROS cells (signature) are more likely to be expressed in the DG than the SVZ, while loROS signature transcripts are more likely to be found in the SVZ. (G) Decreasing ROS is associated with an expected decrease in ROS marker transcript expression and an increase in cell cycle activity and neural differentiation.

As a next step I curated a list of 175 genes, which would reflect the functional status of the precursor cells and the enrichment of these genes would identify their proliferative potential

and neurogenic commitment. We performed a three-way enrichment analysis which would indicate the ROS classes, in which a gene is uniquely expressed or co-enriched compared to a third class (Fig. 11). General stem cell markers such as Nestin, Gfap, Notch2, Lpar1, Hes1, Id4, Lfng (Semerci et al., 2017), as well as Gli1 and Foxo1, which mark type-1 cells, the largely quiescent multipotent radial glial cells that represent a "start point" of adult neurogenesis, are significantly enriched within both, the Nes-GFP$^+$ of the hiROS and midROS class (compared to the loROS class). Furthermore, Nes-GFP$^+$ of the hiROS class lack expression of Eomes (Tbr2), a conventional marker of type-2 cells, E2f1, a potent G1/S promotor (Black et al., 2005; Cooper-Kuhn al., 2002) or various proliferation markers (Pcna, Mki67, Mcms and others). They have the highest expression levels for transcripts of cell cycle inhibitors Cdkn1a (Pechnick et al., 2008), Cdkn1b (p27, Hörster et al., 2017) and Pten (Bonaguidi et al., 2011; Hill and Wu, 2009), which are critical in controlling proliferation and cell cycle exit of stem cells. The hiROS cells also had comparatively high levels of the Notch ligand Jag1, as well as Notch1/ 4, and Sirt1, which might be seen as distinct cellular sensors of the microenvironment. This result suggests that the hiROS Nes-GFP$^+$ cells represent an early stage of multipotent stem cells, which transcriptionally have a high degree of quiescence. Nes-GFP$^+$ cells of the midROS class possess the highest levels of expression of proliferation markers such as Pcna, Mki67 and Mcm2/3/4/6; cyclins/CDKs required for G1/S transition such as E2f1, Ccnd2/3, Ccne1, Cdk2, Ccna2 and Ccnb1/2 as well as cell cycle promoters Bub1 and Aurka. The midROS Nes-GFP$^+$ cells had the highest levels of Sox1, 2 and 9 and expressed both pro-neural genes such as Ascl1 (Andersen et al., 2014; Kim et al., 2011), Hes5 (Lugert et al., 2010), Pax6, Fabp7 (BLBP) (Giachino et al., 2014) and genes of the astrocytic lineage such as Slc1a3 (GLAST). This result might suggest that, as the ROS content decreases from hiROS to midROS levels, active growth cycle is initiated.

However, this accretion is simplistic, as these midROS Nes-GFP$^+$ cells have similar levels of expression for various markers which are associated with quiescence, such as Hopx, Rest (Gao et al., 2011), Hes1 (Hatakeyama et al., 2004; Yan et al., 2018) and Aldoc (Shin et al., 2015), which negatively control cell cycle entry and maintenance (or mark quiescence). Furthermore, Thrsp (Spot14) and Cpt1a, genes essential for fatty acid oxidation (FAO), a critical pathway associated with precursor cell quiescence and a switch to active proliferation, were significantly co-enriched within the hiROS and the midROS class. These results suggest that cells with moderate ROS content represent two cellular

states – firstly, cells engaged in active growth cycle (based on proliferation markers) and secondly cells which are poised for, but not yet in active proliferation (based on FAO markers and negative regulators of neurogenesis).

Genes such as Dcx, Stmn1, Fasn (Knobloch et al., 2012), Eomes (Tbr2), Cdk4 and Ncam1, which indicate a high degree of neuronal commitment to proliferation, were co-enriched in Nes-GFP$^+$ cells of both the midROS and loROS classes. Additionally, SoxC (Sox4 and Sox11) were enriched only in the loROS class along with Nfib and Tcf4.

The Nes-GFP$^+$ cells of the loROS class were the only class of Nes-GFP$^+$ cells with expression of transcripts marking neuronal differentiation, such as Calb2 (calretinin), Rbfox3 (NeuN), Rbfox2, Prox1, Neurod1 and Gad1. The cells of the loROS class were also enriched for anti-apoptotic and DNA damage checkpoint markers such as Trp53 (p53), Casp3 and Apbb1, suggesting that, as the ROS content relatively decreases, cells become more committed, increasingly involved in repairing DNA damage and are unipotent.

The top GO pathways, which are enriched within each cluster of Nes-GFP$^+$ cells corroborate this hypothesis. The top 15 GO terms enriched within the significantly enriched transcripts (signatures) of the Nes-GFP$^+$ cells of the hiROS class reveal two important functions, first, regulation of cellular shape, migration, matrix organization and the responsiveness to microenvironment of the cell, reflected by enrichment of terms related to angiogenesis (Table 8). Secondly, these cells, which are enriched for genes negatively regulating transcription and cell proliferation, are also enriched for terms which potentially aid in responding to local and systemic cues. The midROS cells are enriched for terms which reflect the cell's preparedness to enter proliferation, with cell division, initiation of DNA replication and M phase progression are some of the most enriched GO terms (Table 9). As cells lower their ROS content and enter the loROS class, pathways which are essential for neuronal maturation, such as axonogenesis and axon guidance, positive regulation of synaptic assembly and increased transcription/ splicing become highly enriched (Table 10).

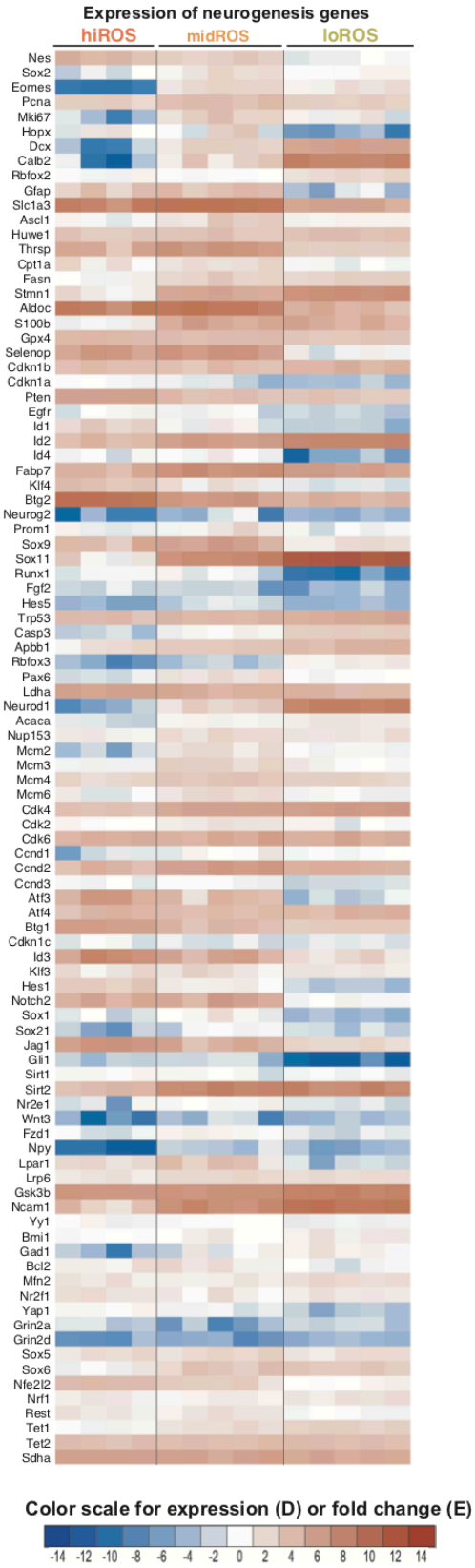
Expression of neurogenesis genes
hiROS
midROS
loROS
Nes
Sox2
Eomes
Pcna
Mki67
Hopx
Dcx
Calb2
Rbfox2
Gfap
Slc1a3
Ascl1
Huwe1
Thrsp
Cpt1a
Fasn
Stmn1
Aldoc
S100b
Gpx4
Selenop
Cdkn1b
Cdkn1a
Pten
Egfr
Id1
Id2
Id4
Fabp7
Klf4
Btg2
Neurog2
Prom1
Sox9
Sox11
Runx1
Fgf2
Hes5
Trp53
Casp3
Apbb1
Rbfox3
Pax6
Ldha
Neurod1
Acaca
Nup153
Mcm2
Mcm3
Mcm4
Mcm6
Cdk4
Cdk2
Cdk6
Ccnd1
Ccnd2
Ccnd3
Atf3
Atf4
Btg1
Cdkn1c
Id3
Klf3
Hes1
Notch2
Sox1
Sox21
Jag1
Gli1
Sirt1
Sirt2
Nr2e1
Wnt3
Fzd1
Npy
Lpar1
Lrp6
Gsk3b
Ncam1
Yy1
Bmi1
Gad1
Bcl2
Mfn2
Nr2f1
Yap1
Grin2a
Grin2d
Sox5
Sox6
Nfe2l2
Nrf1
Rest
Tet1
Tet2
Sdha
Color scale for expression (D) or fold change (E)
-14 -12 -10 -8 -6 -4 -2 0 2 4 6 8 10 12 14

Figure 11: Heatmap showing the expression of key genes within Nes-GFP$^+$ cells of the different ROS classes. 175 genes were curated and their expression in the different ROS classes is shown here as a heatmap. The lower color scheme shows the color assignment based on the degree of expression.

Table 8: Top 15 GO terms enriched within the signatures of the Nes-GFP$^+$ cells of hiROS class

GO.ID	Term	adjP
GO:0001525	angiogenesis	0.000015
GO:0008360	regulation of cell shape	0.000015
GO:0045944	positive regulation of transcription by RNA polymerase II	0.00035
GO:0030335	positive regulation of cell migration	0.00069
GO:0090090	negative regulation of canonical Wnt signaling pathway	0.001
GO:0016525	negative regulation of angiogenesis	0.0022
GO:0043406	positive regulation of MAP kinase activity	0.0059
GO:0071222	cellular response to lipopolysaccharide	0.0059
GO:0045766	positive regulation of angiogenesis	0.016
GO:0030838	positive regulation of actin filament polymerization	0.016
GO:0043536	positive regulation of blood vessel endothelial cell migration	0.016
GO:0032496	response to lipopolysaccharide	0.016
GO:0043066	negative regulation of apoptotic process	0.016
GO:0090316	positive regulation of intracellular protein transport	0.022
GO:1903779	regulation of cardiac conduction	0.023

Table 9: Top 15 GO terms enriched within the signatures of the Nes-GFP^{+} cells of midROS class

GO.ID	Term	adjP
GO:0051301	cell division	8E-28
GO:0051382	kinetochore assembly	0.000037
GO:0006270	DNA replication initiation	0.000037
GO:0034501	protein localization to kinetochore	0.000072
GO:0006284	base-excision repair	0.0002
GO:0090307	mitotic spindle assembly	0.00032
GO:0000070	mitotic sister chromatid segregation	0.00033
GO:0007094	mitotic spindle assembly checkpoint	0.00039
GO:0051383	kinetochore organization	0.00085
GO:0051345	positive regulation of hydrolase activity	0.0011
GO:0031297	replication fork processing	0.0021
GO:0045737	positive regulation of cyclin-dependent protein serine/threonine kinase activity	0.0028
GO:0032508	DNA duplex unwinding	0.0029
GO:0051315	attachment of mitotic spindle microtubules to kinetochore	0.0044
GO:0007143	female meiotic nuclear division	0.0047

Table 10: Top 15 GO terms enriched within the signatures of the Nes-GFP$^+$ cells of loROS class

GO.ID	Term	adjP
GO:0000381	regulation of alternative mRNA splicing, via spliceosome	0.0067
GO:0007413	axonal fasciculation	0.0067
GO:0007399	nervous system development	0.0067
GO:0021952	central nervous system projection neuron axonogenesis	0.0078
GO:0007411	axon guidance	0.0078
GO:0006355	regulation of transcription, DNA-templated	0.012
GO:0017148	negative regulation of translation	0.02
GO:0035249	synaptic transmission, glutamatergic	0.034
GO:0045773	positive regulation of axon extension	0.06
GO:0000122	negative regulation of transcription by RNA polymerase II	0.06
GO:0048488	synaptic vesicle endocytosis	0.06
GO:0022618	ribonucleoprotein complex assembly	0.06
GO:0021766	hippocampus development	0.067
GO:0007026	negative regulation of microtubule depolymerization	0.083
GO:1904851	positive regulation of establishment of protein localization to telomere	0.088

To corroborate our assertion that the segregation of Nes-GFP$^+$ cells into sub-classes based on decreasing cellular ROS content indeed represents a trajectory from quiescence to neuronal commitment, I compared our findings to previously published single cell

transcriptomic data of Nes-CFP^{nuc} cells within the adult DG (Shin et al., 2015), wherein the cells were aligned along a pseudotime trajectory ranging from quiescent to actively proliferating cells. The expression of genes associated with both the hiROS and midROS classes were more strongly expressed early in pseudotime, while the genes associated with the loROS class were expressed more strongly later in the reconstructed trajectory (Fig. 12A). I checked for the overlap of the signature genes of each ROS cluster that are among the Top 1000 UP and DOWN regulated ones along the developmental trajectory within Nes-GFP^{+} cells. Of the top 1000 DOWN genes (high in quiescent cells at the start of the pseudotime trajectory), 55.7% are picked up as enriched within one class or co-enriched between 2 ROS classes (Fig. 12C). Half of these genes, 227 (22.7%), are signatures for Nes-GFP^{+} cells of the hiROS class. 51.54**%** of these (117 genes) are unique signatures of the hiROS class, while the other half of genes are expressed in Nes-GFP^{+} cells of the hiROS class and midROS class (48.45%). 348 genes from the Shin et al. dataset show an overlap with midROS class, with 154 uniquely enriched in the midROS (44.25%) and 110 genes co-enriched between the mid and the hiROS class (31.61%) and 24.13% genes are co-enriched between the precursor cells of mid and loROS classes. 17.2% overlap is seen with genes in 1000 DOWN and the loROS signatures, of which 51.20% (88 genes) are unique to the cells in this class.

A stronger observation was that only 5.2% (52 genes) of the 1000 UP genes are expressed in the Nes-GFP^{+} cells of the hiROS class (Fig. 12D). These transcripts were shown to be associated with cell cycle entry and lineage specification. 23.0% of these 1000 upregulated genes of the trajectory are also expressed in cells of the midROS class (54.79% unique, 2.01% shared with the hiROS and 42.17% shared with loROS cells). The highest overlap of the 1000 UP genes is with loROS class, 32.7%, of which 70.34% are unique to the precursors to the lowest assayed cellular ROS content.

I next analyzed the expression of 82 transcription factors (TFs; Table 5), attributed by Shin et al. to the quiescent and active proliferative status of precursor cells, in the three ROS classes. Interestingly, TFs regulating quiescence had significantly higher expression in the hiROS cells, a relationship which inverts with the drop in ROS content. Conversely, TFs associated with active proliferation were almost absent in hiROS cells but their expression increased in cells with lower ROS content (Fig. 12B).

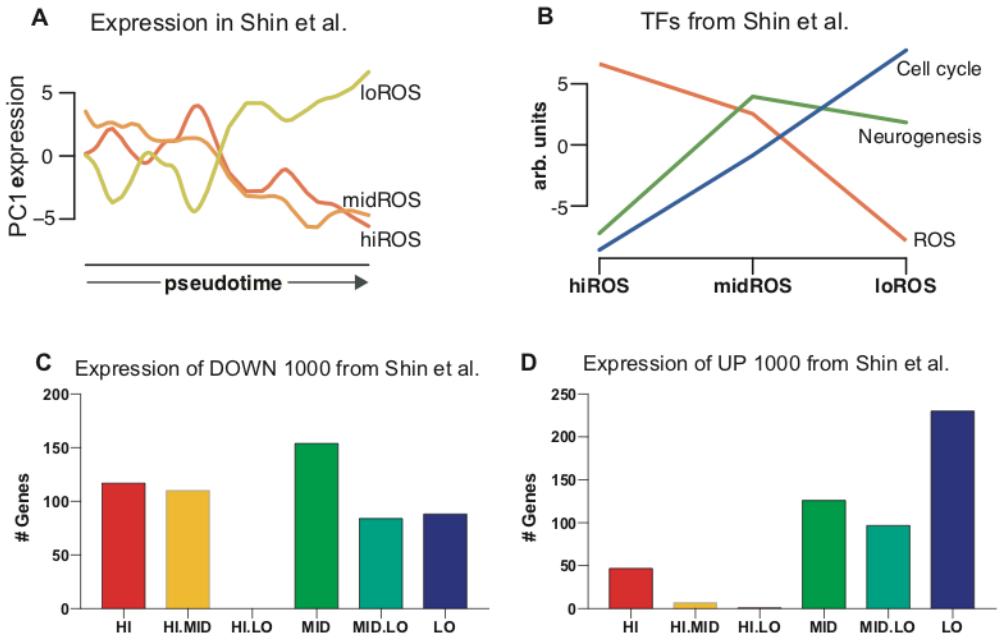

Figure 12: Alignment of expression of Nes-GFP$^+$ cells of the different ROS classes with data from Shin et al. (A) Plotting expression of the ROS groups along the pseudotime trajectory showed higher expression of hiROS transcripts in cells early in pseudotime, with later peaks in expression in the lower ROS groups. (B) Expression of transcription factors (TFs) associated with quiescence and activation identified in Shin et al. in the different ROS classes. (C) expression of the top 1000 DOWN genes (with decreased expression along the pseudotime trajectory) in the different ROS classes. (D) expression of the top UP 1000 genes (with decreased expression along the pseudotime trajectory) in the different enrichment groups.

Changes in intracellular ROS content precede cell fate changes

A substantial drop in cellular ROS content is observed between Nes-GFP$^+$ cells of the hiROS and midROS classes (~5-fold reduction in ROS content; see also Fig. 9D, E). To investigate expression changes at this transition points more closely, we performed a pairwise comparison of the expression profiles of the hiROS and midROS classes using a different statistical model. I found that between the hiROS and midROS cells, there is no significant change in the expression of some of the radial glial markers (Gfap, Egfr, Gli1) and quiescence markers such as Aldoc, Hopx, Thrsp, Cpt1a, Rest. However this ROS drop is marked by a downregulation of cell cycle inhibitors (Pten, Btg1/2, Hes1, Cdkn1a, Klf4, Ddx5) and an upregulation of markers for active proliferation (Sox2, Eomes, E2f1, Pcna, Fasn, Dcx, Stmn1, Hes5, Fabp7, Prox1, Ccnd1/2, Cdk4, Sirt2; Fig. 13).

Figure 13: Heatmap showing the change of curated transcripts with ROS drops. The curated list of 175 genes (cell cycle, neurogenic phase) were pair-wise analyzed for expression change along with the transition between hiROS-midROS and midROS and loROS classes. The panel on the left shows the division of the transcripts based on function and/or documented neurogenic phase of expression. The color scale shows the significance and directionality of change: transcripts with no significant change are shown in white, transcripts with significant downregulation

are shown in green, and the transcripts with significant upregulation are shown in red. The degree of change is correlated to the intensity of the color.

The second drop in ROS levels (~2 fold) between midROS and loROS classes was marked by a significant decrease in NSC markers (Gfap, Egfr, Nes, Slc1a3, Prom1, Notch2, Lpar1), markers for active proliferation (Sox2, Eomes, Pcna, Mki67, Mcm2/3/4/6, Hes5, Pax6). Quiescent markers (Hopx, Cpt1a, Thrsp, Aldoc) were also downregulated, while Stmn1 was upregulated together with redox sensors such as Foxo3 and Trp53. At the same time, this ROS drop is characterized by an increase in expression of transcripts underpinning the progression from transient amplification to a neuroblast-like identity (Rbfox2/3, Neurod1, Ncam1, Prox1, Calb2). Taken together these findings suggest that ROS content delineates functional states among NSCs and changes in ROS content precede changes in transcription profiles. This finding goes beyond previous characterizations and refines our model of the hippocampal NSC niche (Fig. 13).

A gene ontology analysis (GO) of the genes upregulated with the ROS drop from hiROS levels to midROS levels, shows an enrichment for genes involved in initiating DNA replication (transition into S phase of growth cycle) and progression through cell division. Furthermore, the enriched terms refer to a strong commitment to the neuronal lineage, including terms related to synapse assembly, axonal guidance and a decrease of genes negatively regulating neuron differentiation (Table 11). A GO analysis of downregulated transcripts shows that, as the cellular ROS levels decrease, the cells increase their transcriptional efficiency and translation of the mRNA (by reducing gene silencing through miRNAs). An important change that is observed as RGL/ type-1 cells divide is the differences in cell morphology of the daughter cells. Genes involved in the regulation of cell shape and the transition from an epithelial morphology are significantly enriched with ROS drop, which increases the confidence that reduction of cellular ROS content is indeed an important priming step for cells entering proliferation.

Table 11: Top 15 GO terms upregulated with the ROS drop from hiROS to midROS

GO.ID	Term	adjP
GO:0051301	cell division	5.9E-14
GO:0051965	positive regulation of synapse assembly	5.7E-11
GO:0006270	DNA replication initiation	0.00000017

GO:0007411	axon guidance	0.00000048
GO:0007399	nervous system development	0.00000048
GO:0045665	negative regulation of neuron differentiation	0.00011
GO:0009219	pyrimidine deoxyribonucleotide metabolic process	0.00011
GO:0099054	Pre-synapse assembly	0.00011
GO:0001764	neuron migration	0.00011
GO:0010976	positive regulation of neuron projection development	0.00011
GO:0021781	glial cell fate commitment	0.00012
GO:0051988	regulation of attachment of spindle microtubules to kinetochore	0.00012
GO:0071709	membrane assembly	0.0007
GO:0050808	synapse organization	0.00073
GO:0035418	protein localization to synapse	0.00073

Table 12: Top 15 GO terms downregulated with the ROS drop from hiROS to midROS

GO.ID	Term	adjP
GO:0030335	positive regulation of cell migration	5.4E-08
GO:0000122	negative regulation of transcription from RNA pol II promoter	0.000011
GO:0010718	positive regulation of epithelial to mesenchymal transition	0.000053
GO:0001525	angiogenesis	0.00018
GO:0008360	regulation of cell shape	0.00018
GO:0045944	positive regulation of transcription from RNA pol II promoter	0.00021
GO:0007097	nuclear migration	0.00036
GO:0002483	antigen processing and presentation of endogenous peptide antigen	0.00045
GO:0071277	cellular response to calcium ion	0.00045
GO:0007165	signal transduction	0.00061
GO:2000637	positive regulation of gene silencing by miRNA	0.00093
GO:0034446	substrate adhesion-dependent cell spreading	0.001
GO:0007179	transforming growth factor beta receptor signaling pathway	0.0018
GO:0007264	small GTPase mediated signal transduction	0.0018
GO:0001916	positive regulation of T cell mediated cytotoxicity	0.0021

GO analysis of genes differentially regulated at the second ROS drop from midROS to loROS levels show a significant enrichment of genes involved in neuronal differentiation, including axonal guidance and fasciculation, synaptic trafficking, and cytoskeletal organization. The enriched terms further indicate an increase in alternate splicing of expressed genes and a relation to transcription (Table 13). It has been shown that ERK signaling influences a cells ability to proliferate, a decrease in the GO term associated with ERK signaling is observed at this ROS drop, corroborating the hypothesis that the conversion of cells into a neuroblast-like state requires a decrease in ROS content from moderate to low levels (Table 14).

Table 13: Top 15 GO terms upregulated with the ROS drop from midROS to loROS

GO.ID	Term	adjP
GO:0006355	regulation of transcription, DNA-templated	6.1E-11
GO:0007411	axon guidance	0.000042
GO:0007413	axonal fasciculation	0.0001
GO:0007399	nervous system development	0.00052
GO:0021952	central nervous system projection neuron axonogenesis	0.0007
GO:0016569	covalent chromatin modification	0.0063
GO:0045773	positive regulation of axon extension	0.013
GO:0017148	negative regulation of translation	0.013
GO:0007026	negative regulation of microtubule depolymerization	0.014
GO:1904816	positive regulation of protein localization to telomeric region	0.015
GO:2000300	regulation of synaptic vesicle exocytosis	0.016
GO:0000381	regulation of alternative mRNA splicing, via spliceosome	0.016
GO:0035418	protein localization to synapse	0.027
GO:0001764	neuron migration	0.028
GO:0021987	cerebral cortex development	0.028

Table 14: Top 15 GO terms downregulated with the ROS drop from midROS to loROS

GO.ID	Term	adjP
GO:0070374	positive regulation of ERK1 and ERK2 cascade	1.3E-13
GO:0006954	inflammatory response	6.4E-12
GO:0008285	negative regulation of cell proliferation	3.2E-11
GO:0008360	regulation of cell shape	1.7E-08
GO:0006911	phagocytosis, engulfment	3.2E-08
GO:0045087	innate immune response	4.5E-08
GO:0032760	positive regulation of TNF production	4.5E-08
GO:0050766	positive regulation of phagocytosis	7.5E-08
GO:0045766	positive regulation of angiogenesis	0.00000021
GO:0030335	positive regulation of cell migration	0.0000003
GO:0007229	integrin-mediated signaling pathway	0.00000046
GO:0001525	angiogenesis	0.0000012
GO:0030593	neutrophil chemotaxis	0.0000025
GO:0006907	pinocytosis	0.0000045
GO:0043065	positive regulation of apoptotic process	0.0000067

ROS profiling of other cell types within the DG

As shown above, profiling the Nes-GFP expressing cells identified subsets of neurogenic cells with distinct functional and molecular states. However, it is important to note that Nestin has a broad range of expression. Hence, to corroborate the findings mentioned above and to further resolve the neurogenic niche with respect to intracellular ROS content, I next used different reporter mice to ascertain the ROS content of different cell types. Although this was done concomitantly for DG and SVZ, I am presenting only the data generated by profiling the DG which would enable an easier understanding of the answers to the central question.

ROS profiling of Astrocytes and type-1 cells

Gfap is a cytoskeletal protein which is well-documented, and routinely used, for its expression in wide range of astrocytes and multipotent type-1 cells (Nolte et al., 2001). The type-1 cells can be separated from the astrocytes by expression of plasma membrane

bound EGFR. Therefore, I used Gfap-GFP reporter animals, isolated the DG cells and stained them with the ROS dye DHE. By further staining the DG cells with fluorescently labeled EGF (EGF bound to Alexa fluor 647; EGF-647), it was possible to identify the EGFR expressing type-1 cells within the Gfap-GFP^{+} cell pool. This staining strategy allowed to cytometrically follow the intracellular ROS content, and the classification of identified genotypes into the manually gated ROS classes. As a first step, a comparison of the overall ROS content of all isolated DG cells from Gfap-GFP reporter line to Nes-GFP reporter line did not show any significant differences (Fig. 14A), suggesting that genotypic differences did not result in gross changes in the intracellular ROS content of the DG cells (unpaired t-test, p = 0.09). Further, manual classification of the entirety of DG cells from the Gfap-GFP reporter into the four ROS classes recapitulated the distribution pattern observed in the Nes-GFP reporter line (Fig. 14B), validating that the clustering of cells into ROS classes is independent of genotype of the reporter lines. Gating Gfap-GFP^{+} cells was done similar to the strategy described for Nes-GFP^{+} cells. It was possible to classify cells as follows: astrocytes (GFP^{+} cells) as events with significantly lower EGF median fluorescence (Gfap^{+} EGF^{-}); type-1 cells with high GFP and EGF fluorescence (Gfap^{+} EGF^{+}) and other neurogenic cells with low GFP and high EGF fluorescence (Gfap^{-} EGF^{+}; Fig. 14C). Within the Gfap^{+} pool 14 ± 3% of cells could be annotated as type-1 cells and 86 ±3% cells as astrocytes (Fig. 14D). Surprisingly, within the EGF^{+} pool only a small proportion of 7.4 ±1.4% showed GFP expression and could be classified as bonafide type-1 cells (Fig. 14E).

The most striking result is that type-1 cells have significantly higher overall intracellular ROS content compared to astrocytes and putative type-2 cells, which do not differ significantly for the overall ROS content (type-1 cells: 104.1 ± 35.7 A.U relative to total DG cells; astrocytes: 24 ±4.1 A.U relative to total DG cells; type-2 cells: 11.6 ± 0.95 A.U relative to total DG cells; one-way ANOVA , $p < 0.02$, $F_{(2,9)} = 6.2$; Tukey's, $p = 0.04$ for astrocyte to type-1 comparison; p = 0.02 for type-1 to type-2 comparison; Fig. 14F). Interestingly, the type-1 cells cluster equally into hiROS (37.7 ± 5.2%) and midROS (40.4 ± 4.3%), with significantly fewer cells clustering into the loROS (20.4 ± 7%) and a negligible proportion into noROS class (0.3 ± 0.3%) (FIG. 14G). These equal proportions of type-1 cells in hiROS and midROS classes, however, have significantly different intracellular ROS content (hiROS type-1 cells: 324.8 ± 14.6 A.U relative to total DG cells; midROS type-1 cells: 50.17 ± 5.7 A.U relative to total DG cells; one-way ANOVA , $p < 0.0001$, $F_{(3, 12)} = 386.8$; Tukey's,

$p < 0.0001$; Fig. 14H). This finding strongly supports the finding that multipotent NSCs show the highest enrichment within the higher ROS classes.

Astrocytes, which have lower overall ROS content, as expected show a significant lower enrichment in the hiROS class (20 ± 3.9%), but are equally distributed between midROS (38.5 ± 2.1%) and loROS class (39 ±3.1%) (Fig. 14I). The cells in these mid and loROS classes do not differ in their mean ROS content (Fig. 14J). $Gfap^{-}$ EGF^{+} neurogenic cells become more abundant as the ROS content decreases with the highest enrichment within the loROS class (52 ± 3.9%) and with the mean cellular ROS levels following a similar trajectory ((Fig. 14K; 14L).

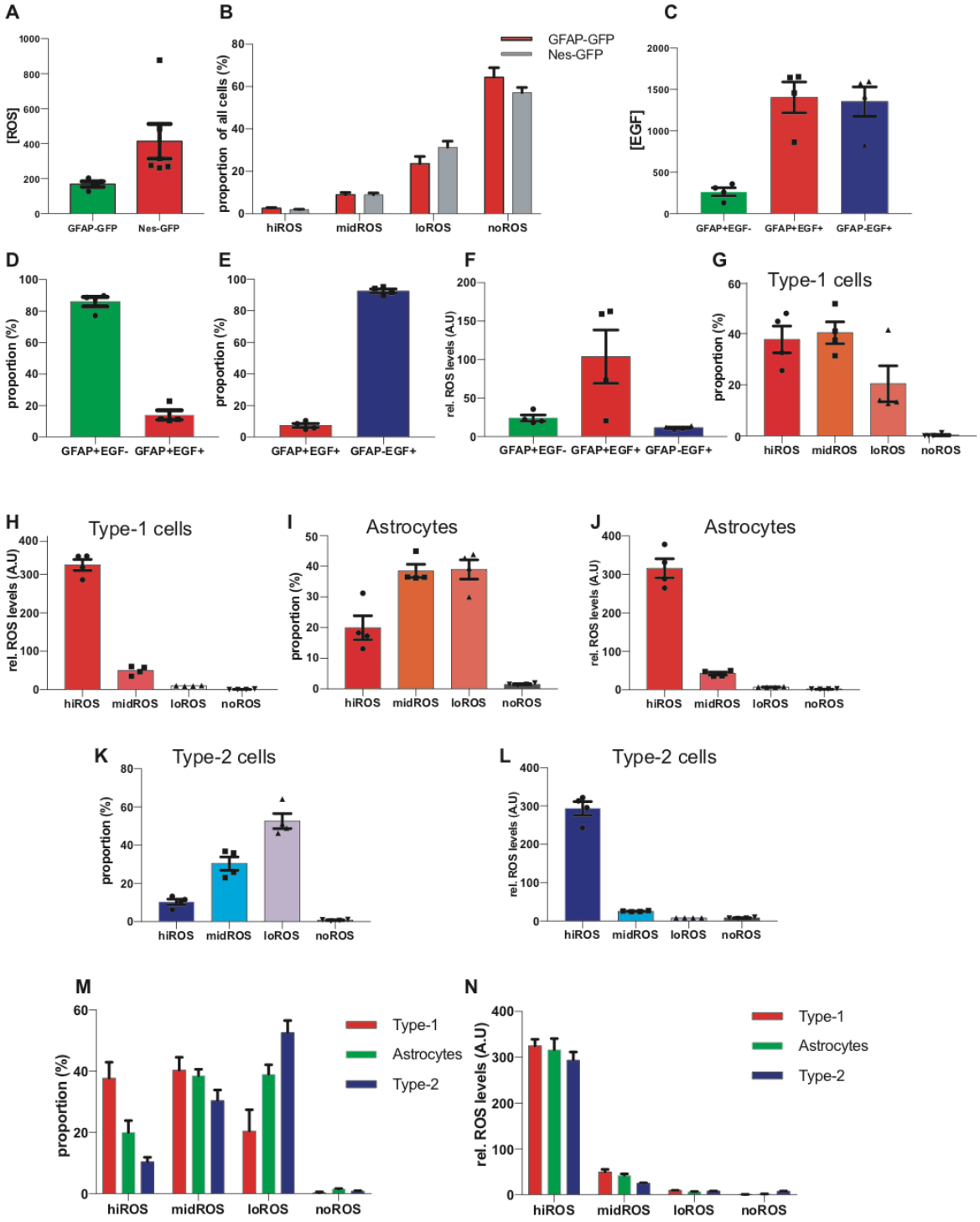

Figure 14: Classification of Gfap-GFP cells into different cell types and their ROS profiling. (A) Comparison of the ROS content of all single DG cells cytometrically analyzed from Nes-GFP and Gfap-GFP genotypes. (B) Comparison of the classification of all DG cells into the ROS classes from Nes-GFP and Gfap-GFP genotypes. (C) Classification of Gfap-GFP$^+$ cells into astrocytes (Gfap$^+$ EGF$^-$), type-1 cells (Gfap$^+$ EGF$^+$) and type-2 cells (Gfap$^-$ EGF$^+$) based on the cell autonomous EGF intensity. (D) Proportion of type-1 cells and astrocytes within the Gfap$^+$ population.

(E) Proportional distribution of type-1 and type-2 within the EGF^+ population. (F) Relative ROS content of the different cell types. (G) Proportional distribution of type-1 cells among the different ROS classes. (H) Relative ROS content within the type-1 cells of the different ROS classes. (I) Proportional distribution of astrocytes cells into the different ROS classes. (J) Relative ROS content within the astrocytes cells of different ROS classes. (K) Proportional distribution of type-2 cells into the different ROS classes. (L) Relative ROS content within the type-2 cells of the different ROS classes. (M) panel showing the proportional distribution of all cell types identified by using Gfap-GFP and labeled EGF. (N) Relative ROS levels in cell types identified by using Gfap-GFP and labeled EGF. All data represent mean ± SEM.

ROS profiling of Doublecortin (Dcx)-GFP positive cells of the neurogenic lineage

With progressive rounds of divisions, neurogenic precursors become lineage restricted, which is marked by expression changes of key pro-neuronal genes. These transient/ intermediate progenitor cells (Type-2b/ TAPs/ IPCs) have reduced expression of NSC markers, such as Gfap, Aldoc, Prom1, Nestin, and increased expression of Dcx, Rbfox3 (NeuN), Calb2, NeuroD1. Dcx is another cytoskeletal protein that can be detected starting in the type-2b IPC phase, which is concomitant with a lowered Nestin expression. Dcx expression is maintained as cells become more neuroblast-like type-3 cells and post-mitotic. These Calb2 expressing immature neurons maintain Dcx expression well past 2-3 weeks after their birth, with expression waning with increased neuronal maturation. This expression pattern makes Dcx promoter driven reporter mice an invaluable tool to study various cell biological and neurobiological properties of neurogenic cells and adult-born immature neurons. For this reason, I have used Dcx-GFP reporter mice to study the redox status of late-stage, neuronally restricted precursor cells and, by comparing their cellular ROS levels with $Nes\text{-}GFP^+$ cells, develop a more thorough understanding of the correlation between neurogenic progression and cellular oxidative stress.

For isolating all DG cells from young adult Dcx-GFP reporter mice (6-8 weeks old) and analyzing their cellular redox status, I employed the same strategy as describe above for Nes-GFP and Gfap-GFP. No significant differences were observed in the overall cellular ROS content or the proportional segregation of all DG cells into the four manually gated ROS classes between Nes-GFP and Dcx-GFP reporter lines, suggesting that genotypic differences of reporter lines did not result in gross changes in the intracellular ROS content (Fig. 15A, B). However, the segregation of $Dcx\text{-}GFP^+$ cells was significantly different from Nes-GFP positive cells. Only a minority of $Dcx\text{-}GFP^+$ cells were detected in the hiROS class (2.3 ± 0.88%), with 27.2 ± 5.7% in midROS class and the highest incidence in the loROS class (68.8 ± 5.1%; Fig. 15C).

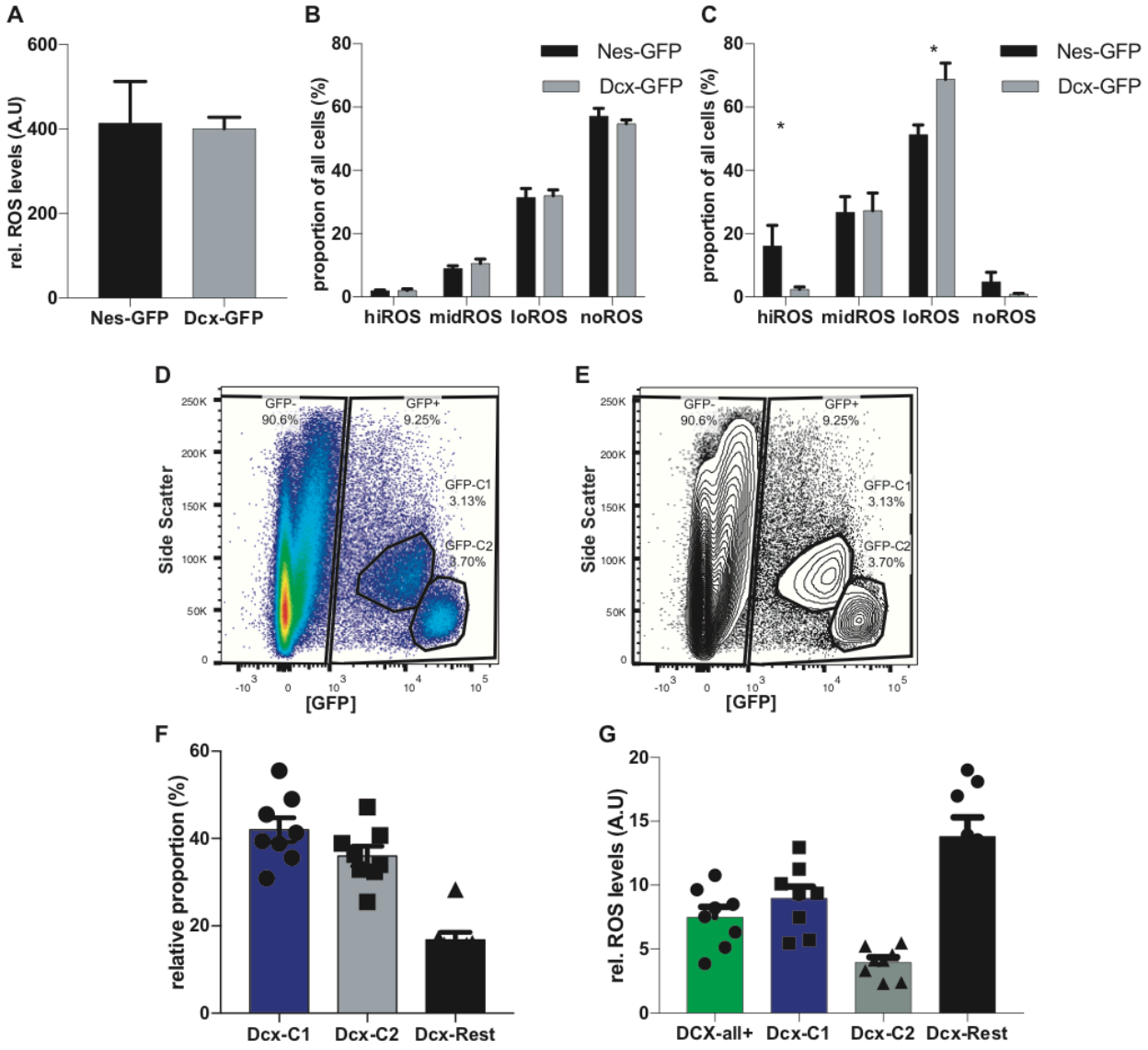

Figure 15: ROS profiling of all Dcx-GFP$^+$ cells and identification of subsets within Dcx-GFP$^+$ population. (A) Comparison of the ROS content of all single DG cells cytometrically analyzed from Nes-GFP and Dcx-GFP genotypes. (B) Comparison of the classification of all DG cells into the ROS classes from Nes-GFP and Dcx-GFP genotypes. (C) Proportional distribution of all Dcx-GFP$^+$ cells into the four ROS classes. (D) FACS plots showing the classification of all DG cells into GFP$^+$ and GFP$^-$ cells and the identification of the distinct subsets, Dcx-C1 and Dcx-C2, within the GFP$^+$ population based on the clustering (D- pseudocolor) and contour (E). All GFP$^+$ cells not in the two distinct subsets were classified as Dcx-rest. (F) Proportion of the 3 classified subsets within the Dcx-GFP$^+$ population. (G) Relative ROS content of the Dcx-GFP$^+$ cells and the 3 classified subsets within the Dcx-GFP$^+$ population. All data represent mean ± SEM.

When Dcx-GFP$^+$ are resolved for granularity (sideward scatter, SSC-A) and GFP content, two prominent clusters can be identified (Fig 15D, E). Hence, I divided the entirety of the Dcx-GFP$^+$ into cluster1 (Dcx-C1) with higher granularity, cluster2 (Dcx-C2) with lowest

granularity and grouped the cells outside these main clusters as Dcx-rest, which possess generally a wide range of cellular granularity. The subdivision of Dcx-GFP$^+$ cells was significant, 42 ± 2.8% of all Dcx-GFP$^+$ cells segregated into Dcx-C1, 36 ± 2.3% into Dcx-c2 and 16.8 ± 1.7% into Dcx-rest cluster (Fig. 15F). These sub-clusters had distinctly different overall ROS content: Dcx-C1 had similar average cellular ROS content compared to the entire Dcx-GFP pool (9 ± 0.92 relative to all the DG cells analyzed, compared to 7.5 ±0.8 fold observed in all Dcx-GFP$^+$ cells); Dcx-rest cluster had twice the average relative cellular ROS content compared to all Dcx-GFP$^+$ cells and Dcx-C1 (13.8 ± 1.5 fold relative to all the DG cells analyzed, compared to 7.5 ±0.8 fold observed in all Dcx-GFP$^+$ cells). Interestingly the Dcx-C2 cluster had significantly lower relative cellular ROS content compared to all Dcx-GFP$^+$ pool (4 ± 0.42-fold relative to all the DG cells analyzed, compared to 7.5 ±0.8 fold observed in all Dcx-GFP$^+$ cells; Fig. 15G).

These sub-clusters of Dcx-GFP$^+$ cells further differ in their distribution into the four ROS classes, Dcx-rest cells, which have significant higher ROS levels, have significantly more cells occupying the midROS class, compared to the total pool of Dcx-GFP$^+$ cells and significantly fewer cells in the loROS fraction. While cells within the Dcx-C1 cluster similar to the parent Dcx-GFP$^+$ population, Dcx-C2 shows a stark predominant segregation into lower ROS classes, with 88.2 ± 2.2% cells localizing to the loROS class (Fig. 16 A, B).

I further sorted the DCX clusters (C1, C2 and rest) for a qRT-PCR assay for key proneuronal genes. While Dcx-rest and Dcx-C1 have elevated levels of Ascl1, which indicates transient amplification and lineage restriction, Dcx-C2 cells have significantly higher expression of Calb2 (Calretinin) and Rbfox3 (NeuN), which indicates that these cells are post-mitotic immature neurons or late neuroblasts (Fig. 16 C- E; Kempermann et al., 2004). Taken together, it can be inferred that Dcx-GFP$^+$ cells within a young DG represent seemingly diverse types of cells along the neurogenic trajectory with a wide range of cellular ROS.

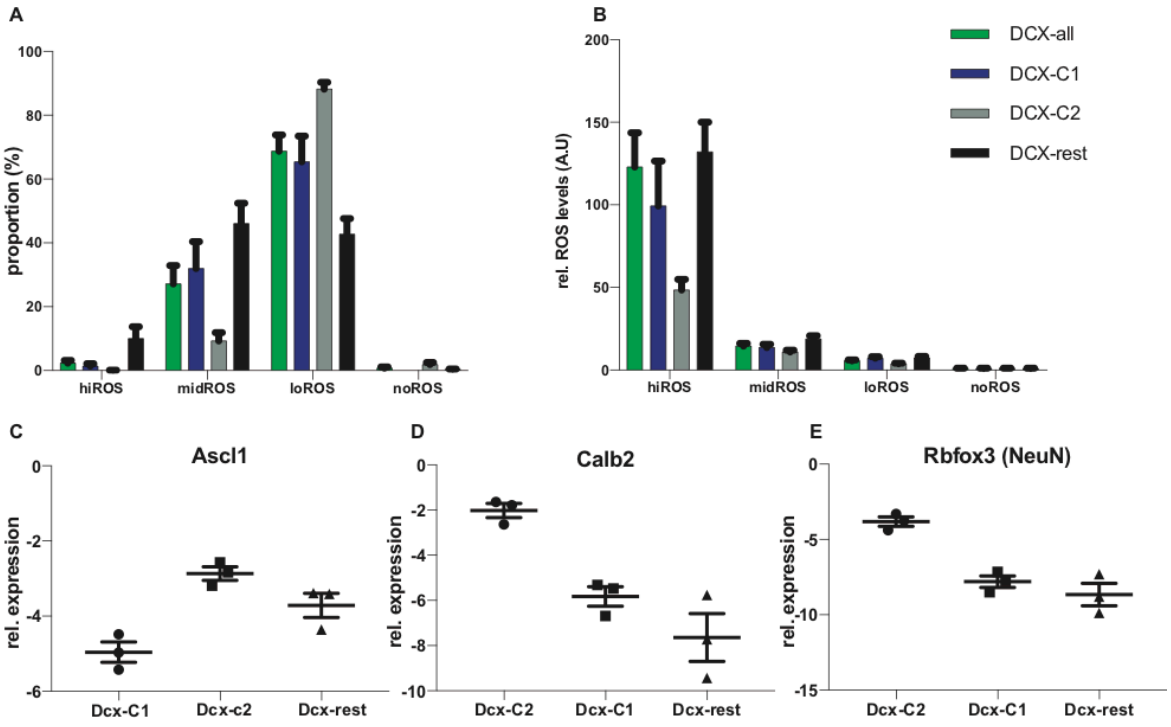

Figure 16: ROS profiling of Dcx-GFP$^+$ subsets and qRT-PCR for select genes from the Dcx- GFP$^+$ subsets. (A) Proportional distribution of Dcx-GFP$^+$ subsets into the different ROS classes. (B) Relative ROS content within the Dcx-GFP$^+$ subsets of the different ROS classes. Relative expression levels of Ascl1 (C), Calb2 (Calretinin; D) and Rbfox3 (NeuN; E) in the different Dcx-GFP$^+$ subsets normalized to the expression levels of Actb (beta-actin). All data represent mean ± SEM.

ROS profiling of microglial cells within the DG

Microglia are the resident immune cells of the brain and numerous reports suggest that they regulate the neurogenic homeostasis within the DG (Diaz-Aparicio et al., 2020; Sierra et al., 2015). Labelling with antibodies to surface proteins enables the identification of microglia, and Cd11b is a commonly targeted surface antigen (Sellgren et al., 2016). Using the same isolation strategy as for other genotypes, I isolated DG cells from wildtype C57Bl6/Rj mice (background strain of all the reporter lines employed), stained for ROS dyes and marked the microglia with a primary conjugated Cd11b-FITC antibody. Cytometric analysis showed that the mean cellular ROS content of DG cells in this experiment set is similar to the Nes-GFP reporter lines, as were the segregation of cells into the ROS classes. Analysis of Cd11b$^+$ cells' clustering into the ROS classes revealed that a minority of microglia (6.6 ± 0.8%) localize to hiROS class, and increasing proportion localize to lower ROS classes,

with almost half the pool localizing to the loROS class (32.4 ± 1.2% in midROS; 53.6 ± 0.7% into loROS; Fig. 17).

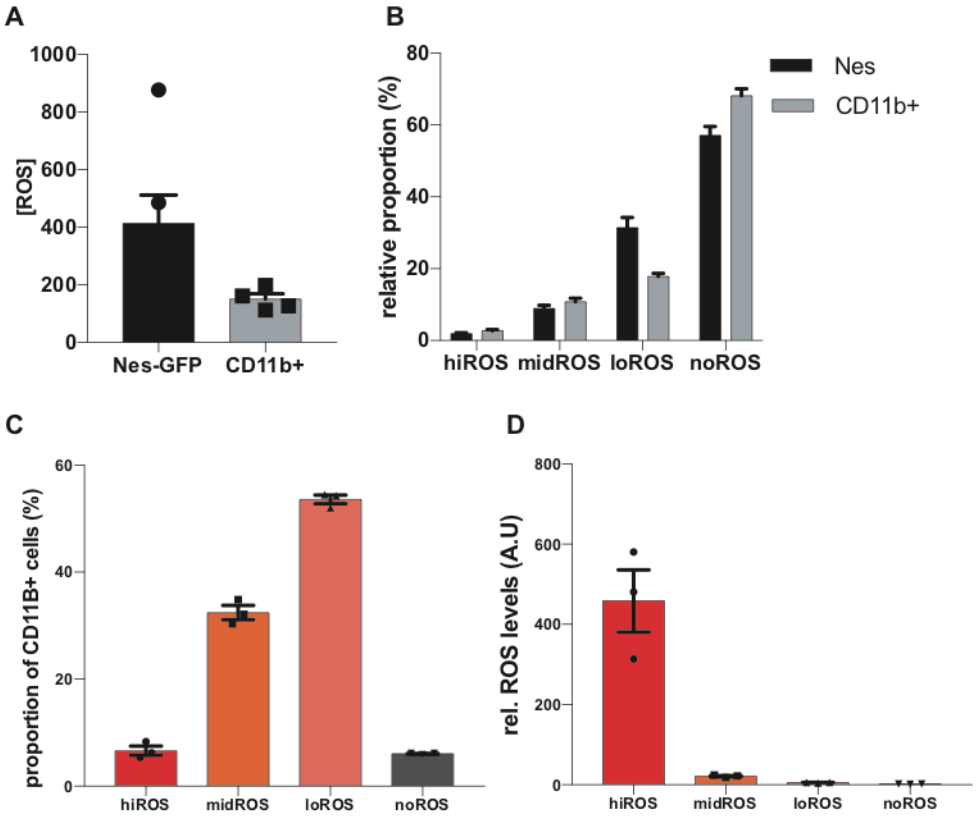

Figure 17: ROS profiling of microglial cells from DG. (A) Comparison of the ROS content of all Nes-GFP$^+$ cells and Cd11b$^+$ cells from DG cells. (B) Comparison of the classification of all DG cells into the ROS classes from Nes-GFP and wildtype cells used for identification of microglial cells (Cd11b$^+$). (C) Proportional distribution of microglia (Cd11b$^+$) into the different ROS classes. (D) Relative ROS content within the microglia (Cd11b$^+$) of the different ROS classes. All data represent mean ± SEM.

Resolving the response of Nes-GFP subpopulations to environmental stimulus

As shown above, different lines of evidence indicate that Nes-GFP$^+$ cells can be classified into different functional states or subpopulations based on their intracellular ROS content. I next focused on the functional relevance of these identified subpopulations of neural precursors in the niche's response to activity driven stimulations. To resolve the role/ responsiveness of these subpopulations when initiating the response to physical activity (arguably the most elementary known pro-neurogenic behavioral stimulus), I first temporally resolved the response to physical activity. To this end, based on the results from Fig. 3 and previous work from our lab (Brandt et al., 2010; 2012; Fischer et al., 2014), I used a dual

thymidine analog labelling strategy to deconvolve the effect of physical activity on cells with different proliferative status. The first analog (CldU) was injected 3 times, each injection separated by 9 hours, in young animals (6-8 weeks). This should mark all proliferating cells before the onset of a stimulus ($CldU^+$ cells would be referred to as baseline proliferators). I then separated these CldU injected animals into running/ control groups, which were singly housed for a period of 5 nights (5R - 5 nights with a running wheel; 5S - 5 nights without a wheel). To detect the effect of an acute bout of physical activity followed by an incubation period, a third group of mice had running wheel access only for 2 nights (2R) before returning to standard conditions for the remaining 3 nights. Injections of IdU were used to mark the proliferating cells at the end of the stimulation period (Fig. 18A).

As expected and a confirmation of the stimulus, compared to the 5S group (4517 ± 349) I found a strong pro-proliferative response, based on the number of IdU^+ cells, in the 5R group (6876 ± 474; plus 52%, Dunnett: p = 0.0005, Fig. 18B). Interestingly, a statistically significant increase in the number of IdU^+ cells was also seen in the 2R group (6217 ± 581, plus 38%, p = 0.0121), suggesting that physical activity is not required as a continued stimulation but rather represents an activating event. No significant differences were detected in the numbers of $CldU^+$ cells across the 3 groups (5S: 4496 ± 398; 2R: 4265 ± 319, p = 0.8961; 5R: 5052 ± 328, p = 0.5466), suggesting that cells already committed to active growth cycle do not respond to de novo physical activity. I noted that irrespective of the presence of the run stimulus, only a small proportion of $CldU^+$ cells were double positive for IdU (5S: 10.0 ± 0.9%; 2R: 8.7 ± 1.0%; 5R: 8.5 ± 0.4%; double positive in IdU+ cells: 5S: 8.9 ± 0.9%; 2R: 5.0 ± 0.6%; 5R: 5.1 ± 0.7%; percentage of all labeled cells; Fig 18C). Taken together, our results suggest that the increase in proliferation in response to exercise was due to an increased recruitment of previously non-proliferating cells and cells in active cycle are non-responsive to acute de novo stimulus.

To resolve if these quiescent cells, once activated by physical activity, would predominantly expand the NSC stage, or rather progress to subsequent stages of adult neurogenesis similar to cells that proliferate in the absence of a run stimulus (Kronenberg et al., 2003), I phenotyped IdU^+ cells using two different sets of antibodies: Sox2/Tbr2 to identify type-1 and type-2 cells (“early”, Fig. 18D, E) and Tbr2/Dcx to identify type-2b and type-3 cells (“late”, Fig. 18F, G), with the help of a brilliant masters student, Gesa Klatt. Under standard housing conditions, a majority of IdU^+ cells (84.5 ± 4.9%) was double positive for Sox2 and Tbr2, 9.6 ± 2.4% were exclusively positive for Sox2, whereas 3.6 ± 1.6% showed only Dcx

expression. Stimulation by physical activity (5R or 2R), did not significantly alter these proportions. This suggests that physical activity stimulates a population of quiescent, yet activatable, precursor cells to enter proliferation without otherwise affecting the distribution among neurogenic stages. Similar to the above described phenotyping of cells in proliferation at the end of the dual labelling experiment Gesa asked if physical activity altered the neurogenic progression of baseline progenitors marked by CldU. To this end, I performed a similar labelling strategy using Sox2/Tbr2 antibodies to identify $CldU^+$ cells still in the type-1 and type-2 neurogenic stage ("early") and Tbr2/DCX baseline progenitors which have progressed on to type-2b and type-3 "late" neurogenic stages. As mentioned above, it is important to reiterate that the minor population of double positive cells, whose proportional distribution does not alter with activity driven stimulation, was not analyzed any further.

Under standard housing conditions (5S) a majority of $CldU^+$ IdU^- cells (58.6 ± 2%) were positive only for DCX, a marker exclusive to type-3 stage and post-mitotic cells. This fraction did not change with cumulative running (5R, 56 ± 2.5%) or when running is used as an acute stimulus (2R, 56.3 ± 1.7%). One third of cells in 5S group seem to stop at the type-2 stage marked by the expression of Tbr2 and/or DCX (33.87 ± 2%) and this group too does not change in 5R (34.67 ± 2.18%) or in 2R (34.06 ± 1.81%). An interesting fraction is the CldU pool of cells, which exclusively express sox2. An unlikely explanation, given that gliogenesis at a young age is limited, is that this number could represent astrocytes which are a product of differentiation of type-2 cells, or cells which proliferated but remained in the earlier stages of neurogenic progression post the division marked by CldU incorporation. This fraction is also not subject to running mediated regulation, as evident by comparing the 5S group (7.3 ± 1.31%) to the 2R (7.5 ± 1.1%) or the 5R group (5.6 ± 1%) (Fig. 18D, F). This result suggests that once cell cycle is initiated, at any neurogenic phase (early/ late), the response to environmental stimulation through physical activity is lost. This result does contradict our lab's previous findings, but it has to be noted that different running wheels and thymidine injection paradigms were employed (Steiner et al., 2008).

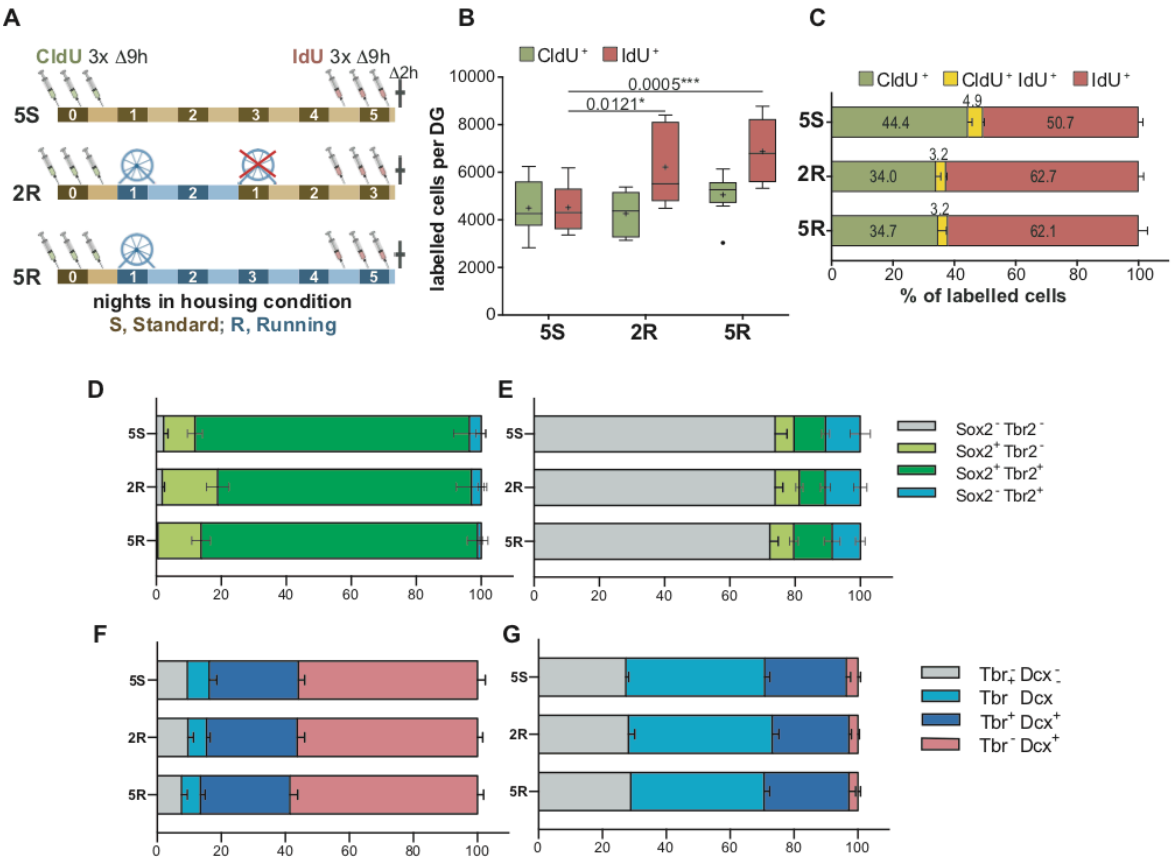

Figure 18: Dual-thymidine analog, 2 running group physical activity paradigm. (A) Experimental paradigm. (B) Plot showing the CldU and IdU numbers in the different groups. (C) proportions of single and double labelled cells within the different groups. Phenotyping of CldU$^+$ cells (D) and IdU$^+$ cells (E) for "early" neurogenic markers (Sox2 and Tbr2). Phenotyping of CldU$^+$ cells (F) and IdU$^+$ cells (G) for "late" neurogenic markers (Tbr2 and DCX). All data represent mean ± SEM.

Nes-GFP$^+$ cells of the hiROS class specifically respond to physical activity

As the Nes-GFP cells of the ROS class represent the putative non-proliferative pool specific to the DG, I reasoned that these are the cells which respond to de novo activity stimulus. My working hypothesis, therefore, was changes in cellular ROS levels and their redistribution should precede the overall increase in proliferative cells in response to a physical activity paradigm. To elucidate the effect of physical activity on Nes- GFP$^+$ cells of different ROS classes, I subjected Nes-GFP-reporter mice to two physical activity paradigms, first, an acute bout of one night of wheel access, which is not sufficient to elicit a measurable increase in proliferation, and the exposure to four nights of wheel access, which elicits the proliferative response. At the end of these paradigms, animals were sacrificed, DG was isolated, dissociated and the ROS profiles of controls and runners were analyzed.

Analyzing the ROS profiles under these conditions, I found that in response to one night of running, there is no redistribution of Nes-GFP$^+$ cells among ROS classes (Figure 19A). However, the Nes-GFP$^+$ cells of the hiROS class show a significant surge in cellular ROS content (increase to 152.6 ± 25.3%, two-way ANOVA, p = .0211, $F_{(6,64)}$ = 2.703; Tukey: hiROS Std vs. 1dRun p = .0013; Figure 19B). This surge was only observed post 1 night of stimulus as the ROS content in the Nes-GFP$^+$ cells of the hiROS class was similar in the 4 day runners and control animals (Tukey: Std vs. 4dRun p = .4424 ns; 1dRun vs. 4dRun p < 0.0001; Figure 19B). However, post the 4 day stimulus, the distribution of Nes-GFP$^+$ cells into ROS classes had distinctly changed compared to standard housed controls. An increase by a third (from 50.8 to 67.2% of all Nes-GFP$^+$ cells) in the proportion of Nes-GFP$^+$ cells in the proliferative and neuronally committed loROS class (Tukey, Std vs. 4dRun for loROS, p = .0338; Figure 19A) was observed. In the SVZ, the Nes-GFP$^+$ cells of the hiROS class showed a similar ROS spike, however this class of precursor cells represents a fraction of less than 1% of the Nes-GFP$^+$ cells, which is presumably far too small to translate into a meaningful neurogenic response (Fig. 19C, D; see also Fig. 9). Taken together, these results indicate that Nes-GFP$^+$ cells of the DG show distinct temporal responses to physical activity.

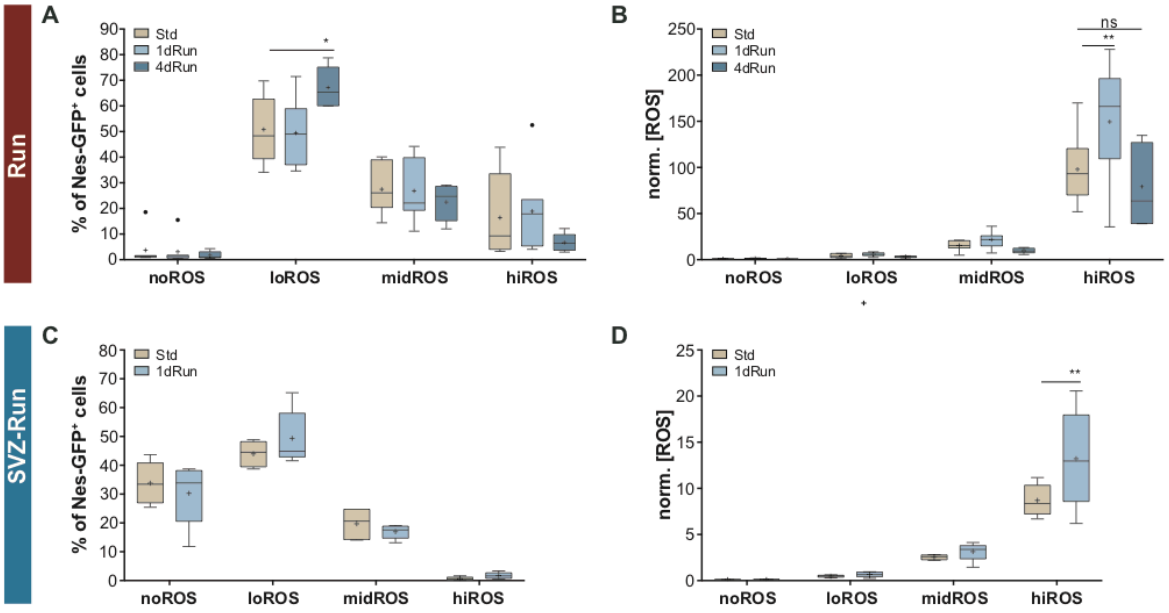

Figure 19: ROS profiling of Nes-GFP$^+$ cells post 1-day and 4-day physical activity. Above panel shows the experimental paradigm. Distribution of Nes-GFP cells of the DG into the four ROS classes (A) and their normalized ROS content (B) post 1 and 4 days of physical activity. Distribution of Nes-GFP cells of the SVZ into the four ROS classes (C) and their ROS content (D)

post 1 and 4 days of physical activity. All data represent mean ± SEM. * $p < 0.05$, ** $p < 0.01$, **** $p < 0.0001$.

Changes in ROS content are not driven by mitochondrial activity

Mitochondrial respiration is the major source for intracellular ROS (Jensen, 1966; Zorov et al., 2014). I therefore asked if mitochondria-generated ROS (mitoROS) is the reason for the ROS surge post 1 night of running. I used Mitosox red (Robinson et al., 2006), a mitochondria-targeting version of the DHE dye, in order to specifically analyze the distribution pattern of Nes-GFP$^+$ cells according to their mitoROS levels and to observe potential mitoROS fluctuations after one night of running. I classified the cells of the DG into four mitoROS classes by applying a similar gating strategy to that described for cellular ROS. I observed fewer Nes-GFP$^+$ cells in the hi-mitoROS class (1.15 ± 0.64%) than after staining for cellular ROS (16.40 ± 6.04%; two-way ANOVA, p = 0.0495, $F_{(3,32)} = 2.91$). Further, no significant changes were observed in the mitoROS levels within each mitoROS class post 1 night of running, suggesting alternate sources for the ROS surge after a run stimulus (Fig. 20).

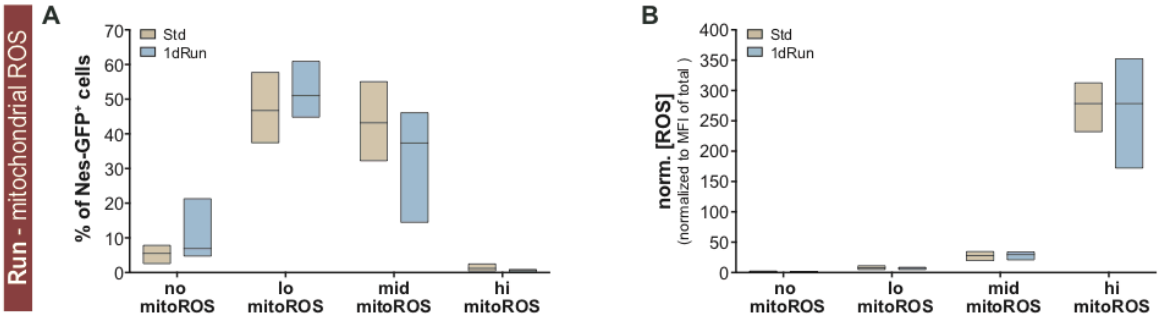

Figure 20: mitoROS profiling of Nes-GFP$^+$ cells post 1-day of physical activity. Distribution of Nes- GFP$^+$ cells into four mitoROS clusters in standard housed and 1-day runners. (B) Normalized mitoROS content in the Nes- GFP$^+$ cells of different mitoROS classes in standard housed and 1-day runners. All data points represent mean ± SEM.

NADPH oxidase enzyme complexes (NOX; Belle et al., 2011; Dickinson et al., 2011) are one such alternate, robust source of cellular ROS, which can be employed as a cell-autonomous secondary messenger. I therefore analyzed Nes-GFP$^+$ cells of the different ROS classes for their transcript expression of NOX isoforms, to find that the members of plasma membrane bound Nox2 complex, including Nox2 (Cybb) and p22phox (Cyba) and for the cytosolic P67phox (Ncf2) were the highest in Nes-GFP$^+$ cells of the hiROS class, while those of other subunits (Ncf4, Rac1/2) were maintained in Nes-GFP$^+$ cells of the

hiROS and midROS classes. Interestingly the transcript levels of Cyba, Cybb and Ncf2 decreased significantly at the ROS transition from hiROS to midROS, with even lower levels in cells of the loROS class. This strongly suggested to us that the Nox2 complex might, on demand, produce ROS in the Nes-GFP$^+$ cells of the hiROS class (Fig. 21).

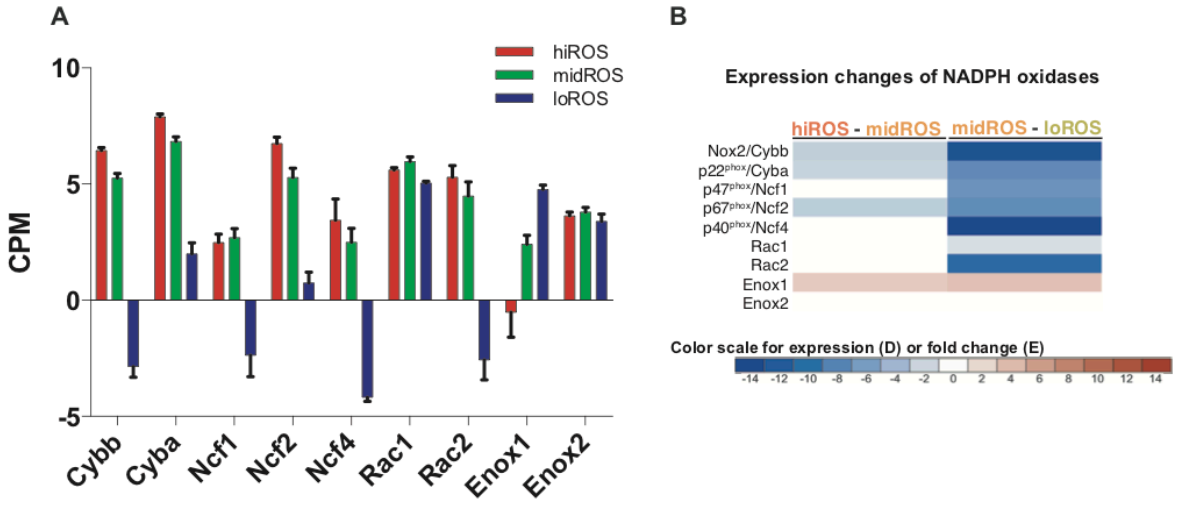

Figure 21: Expression of Nox2 complex genes in the Nes-GFP$^+$ cells of the different ROS classes. (A) Plot showing the levels of the different core and peripheral genes of the Nox2 complex in the Nes-GFP$^+$ cells of the different ROS classes. (B) Changes in the expression of Nox2 complex genes at the two ROS drops. Color scale shows the significance and directionality of change- white represents no significant change, blue and its intensity represents significant downregulation and red and color intensity represents significant upregulation.

I thus crossed Nes-GFP-reporter into Nox2-deficient mice (see methods for complete genotype; Nox2$^{-/y}$ males; Pollock et al., 1995) and analyzed the ROS profiles in this mouse model. Under baseline conditions, I detected similar distributions of Nes-GFP$^+$ cells among ROS classes (two-way ANOVA, $p = .3676$, $F_{(3,40)} = 1.08$, genotype variation $p = 0.9650$, $F_{(1,40)} < 0.01$) with similar ROS profiles (Fig. 22A, B; two-way ANOVA, $p = 0.9942$, $F_{(3,40)} = 0.03$, genotype variation $p = .8471$, $F_{(1,40)} = 0.04$) from reporter Nes-GFP and Nes-GFP::Nox2$^{-/y}$ mice. This suggested that Nox2 generated ROS was not essential to generate and maintain the redox status of NSCs and other cells of the DG. Further it also suggested that the decline in ROS content which is essential for transitioning cellular states is not achieved by regulating Nox2 activity.

Similar to the findings in Nes-GFP$^+$ animals (Fig. 18A), in the Nox2 mutants one night of physical activity did not change the distribution of Nes-GFP$^+$ cells into the different ROS classes (Fig. 22C). Nevertheless, instead of the ROS surge seen in the wildtype Nes-GFP$^+$ cells of the hiROS class, the ROS content in the Nox2 mutants decreased to 79.3 ± 16.8%

in response to the stimulus (two-way ANOVA, $p = 0.2031$, $F_{(6,44)} = 1.49$; housing variation $p = 0.1266$, $F_{(2,44)} = 2.17$; Fig. 22D). Furthermore, four nights of physical activity did not lead to a redistribution of Nes-GFP$^+$ cells among ROS classes (Figure 19A and 19B). These results suggest that the although the baseline kinetics of intracellular ROS regulation and cellular state transitions are Nox2 independent, ROS surge, and the subsequent change in distribution of Nes-GFP$^+$ cells into the ROS clusters elicited by acute physical activity, which is absent in Nox2 deficient mice and thus, must be driven by Nox2 activity.

I confirmed that the Nox2-mediated ROS surge is indeed essential for a pro-neurogenic response by quantifying Ki67$^+$ cells in the DG of wildtype and Nox2 mutants, under standard conditions and after 10 nights of physical activity. Comparing the controls of this experiment, Nox2-deficient animals had similar proliferation rates compared to wildtype littermates, as measured by Ki67$^+$ cell numbers (two-way ANOVA: $p = 0.01470$ ns, $F_{(1,46)} = 2.175$, genotype variation: $p = 0.0039$, $F_{(1,46)} = 9.235$, housing variation: $p = 0.0193$, $F_{(1,46)} = 5.879$; Tukey: wt-Std vs. Nox2$^{-/y}$-Std $p = 0.7007$; Fig. 22E). However, while physical activity increased Ki67+ cells in wild-type animals ($p = 0.0166$), no such increase was detected in Nox2 mutants ($p = 0.9073$; Fig. 22E). This result suggests that baseline neurogenesis and adaptive neurogenic responses are regulated by independent mechanisms with distinct key players.

Additionally, I performed a neurosphere from Nox2 mutants and littermates. While I got statically similar number under normal conditions, addition of KCl to the culture medium did not have any stimulatory effect on neurosphere formation from Nox2 mutant animals (two-way ANOVA, matched within genotypes: $p = 0.0019$, $F_{(1,19)} = 12.97$; Sidak: wt $p = 0.0009$, Nox2$^{-/y}$ $p = 0.6861$ ns; Fig. 22F). Taken together, these results show that Nox2-dependency is a distinguishing feature between baseline control of adult neurogenesis and the acute activation through the pro-proliferative stimulus of physical activity.

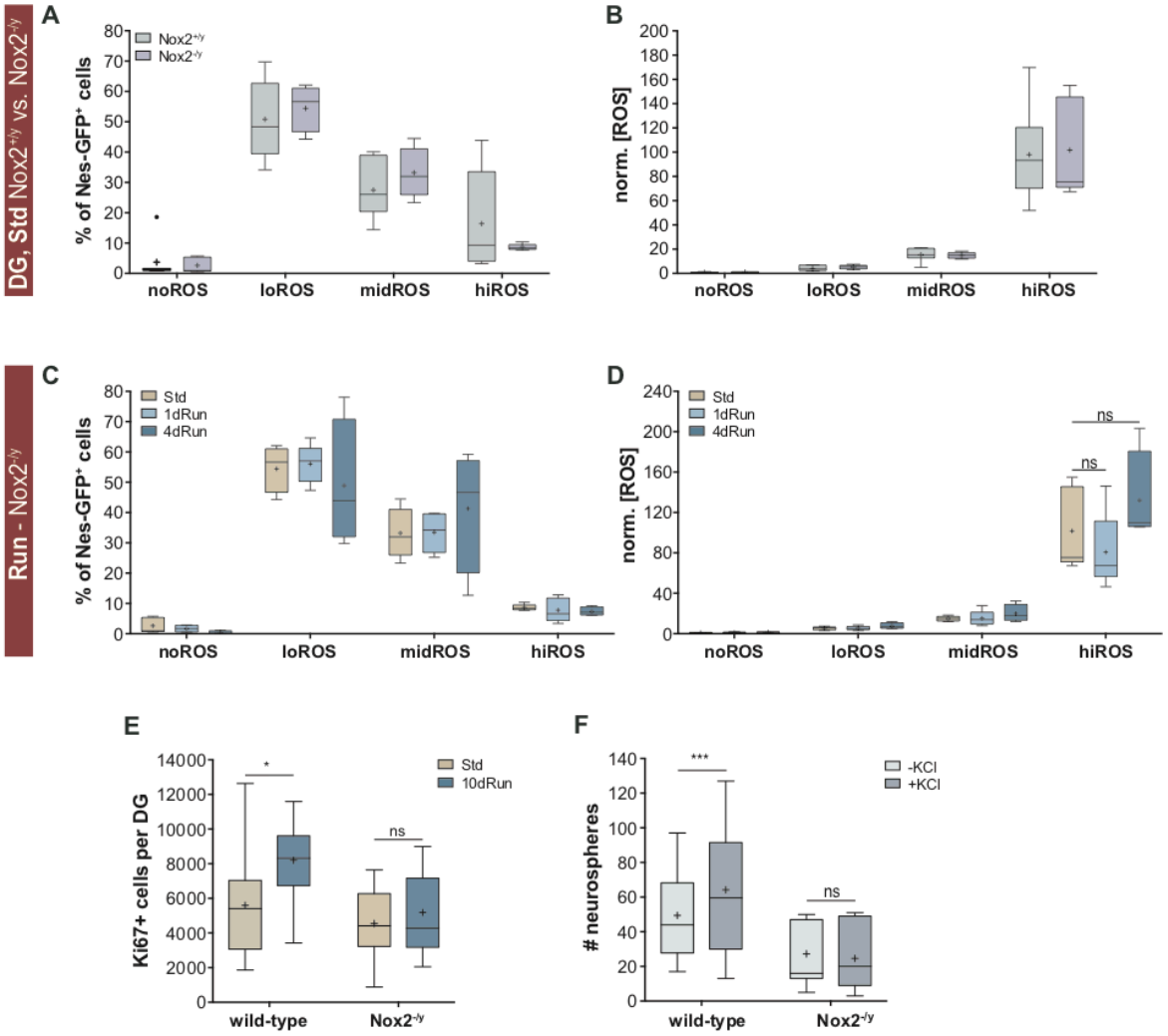

Figure 22: ROS profiling of Nes-GFP$^+$ cells of Nox2 mutants under standard housing and running conditions. Distribution of DG Nes-GFP$^+$ cells of the Nox2 mutants into the four ROS classes under standard housing conditions and the normalized ROS content (B) in Nes-GFP$^+$ cells of the different ROS classes. (C) Distribution of DG Nes-GFP$^+$ cells of the Nox2 mutants into the four ROS classes under standard housing conditions, 1 day and 4 day running paradigms. (D) The normalized ROS content in Nes-GFP$^+$ cells of the different ROS classes under standard housing conditions, 1 day and 4 day running paradigms. (E) Ki67 positive cells in the DG of wildtype and Nox2 mutants in standard housing conditions and post 10 days of running. (F) Neurosphere numbers from the DG of wildtype and Nox2 mutants with and without the addition of KCl. All data represent mean ± SEM. * $p < 0.05$, *** $p < 0.0005$.

In vitro monolayer culture of NPCs as an independent corroboration

When isolated adult DG cells are plated on surfaces coated with poly-d-lysine and Laminin, cells adhere as a monolayer. In the presence of exogenously added growth factors (FGF2 and EGF), only the precursors proliferate and self-renew. Withdrawal of EGF and adding BMP4 (in the presence of FGF2) has been previously shown to reduce proliferation and

push cells into a quiescent state. This quiescent state is stable; be maintained for protracted periods of time without terminal differentiation (even for 28 days) and is reversible by the splitting cells into proliferation medium (without BMP4 and with growth factors). I used this system as an independent assay to study the redox levels of proliferating, quiescent cells and the changes in redox potential as cells exit quiescence.

Precursor cells in monolayer culture, under proliferating conditions, have a narrow range of ROS content. I used EdU (2 hours incubation) to mark the cells in active S-phase, prior to fixation. As shown in the Fig. 23, 33.32 ± 1.45% cells were actively cycling. Upon the addition of BMP4 (20ng/ml), proliferation drastically decreases within a day and post 3 days of treatment there are no detectable proliferation events. This decrease in proliferation occurs with a marked change in morphology (Fig. 23), but does not induce a higher degree of cell death. This decrease in proliferation is concomitant with a progressive increase in cellular ROS content, which significantly increases by day 2 into BMP4 treatment and is ~4 fold, relative to the proliferating cells, on day 3 (day 1: 1.38 ± 0.31 fold relative to control; day 2: 2.77 ± 0.45 fold relative to control; day 3: 4.1 ± 1.21 fold relative to control; one-way ANOVA, $p < 0.0001$, $F_{(4, 26)} = 1.537$). In order to induce the return to proliferation, I found that it is not just enough to reintroduce EGF and withdraw BMP4, but it is paramount to split cells into proliferation medium in a new dish. Upon re-plating, I observed that the proliferation, as marked by EdU, was not initiated on day 1 (0.47 ± 0.21%; $p < 0.001$ relative to control cells) and, post this lag, begins to increase from day 2 (28.17 ± 6.36%; $p = 0.3186$ relative to control cells) onwards and by day 3 the levels are not significantly different from cells proliferating under control conditions (32.57 ± 6.06%; $p = 0.99$ relative to control cells; Fig. 23). The reversion to proliferation is progressively pro-oxidative, compared to the 3 day BMP4 treated cells. Cells on day 1 of reversion have 1.55 ± 0.61 fold levels of cellular ROS content ($p = 0.29$), cells on day 2 of reversion have 2.13 ± 0.63 fold levels of cellular ROS content, which is significantly higher than cells after 3 days of BMP4 ($p = 0.006$). Cellular ROS levels seemingly start to lower (could be considered as returning to normal levels) by day 3 (1.63 ± 0.17 fold compared to BMP4 treated cells; $p = 0.11$; Fig. 23). This pattern of ROS spiking in cultured, non-proliferating cells does resemble the response of quiescent hiROS precursors to acute physical activity. This result suggest that the monolayer culture could be a suitable system to decipher the molecular mechanism of cell cycle entry of quiescent cells.

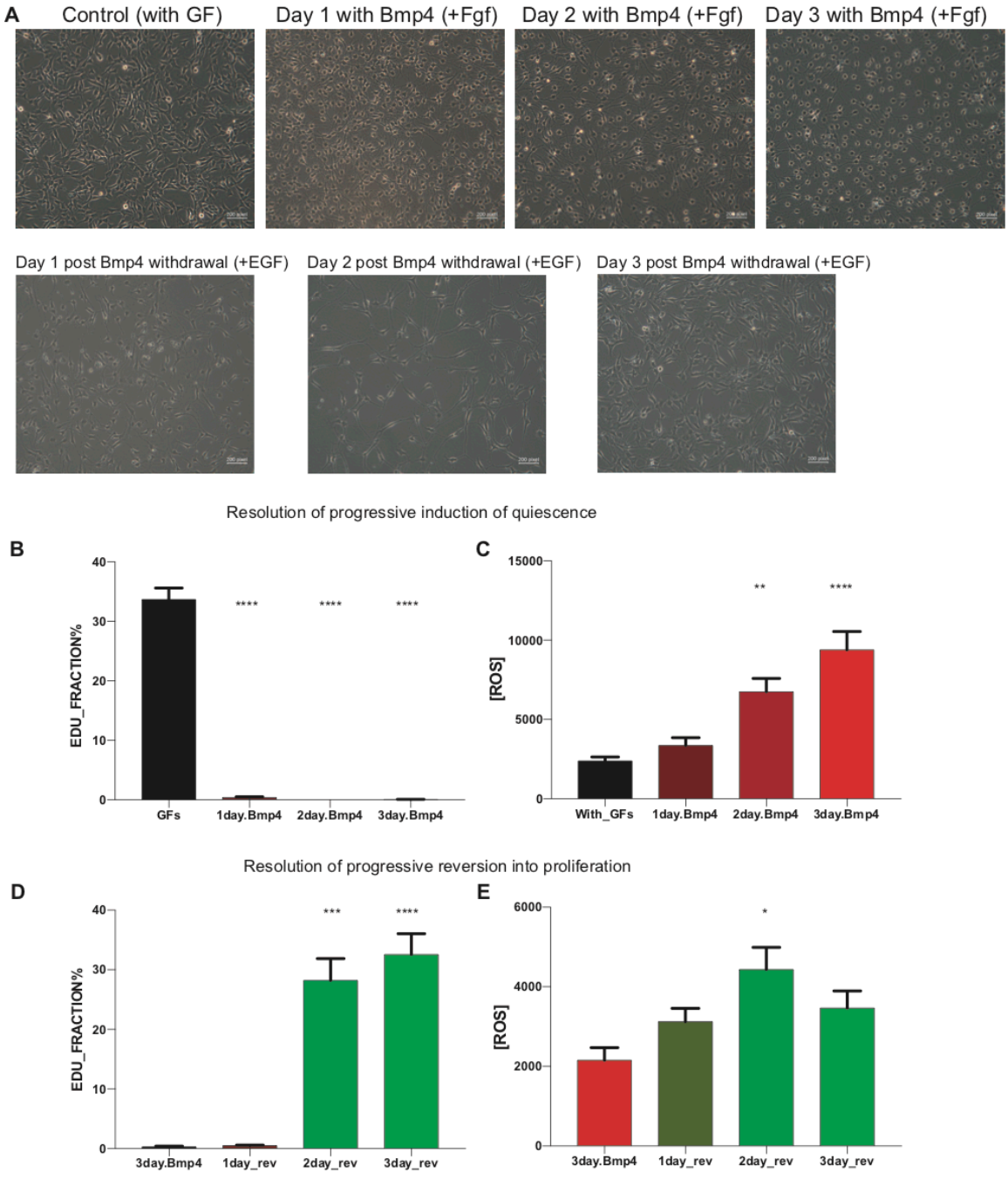

Figure 23: Monolayer culture to study cellular ROS levels in different cellular states. (A) Brightfield images of monolayer culture of NPCs under control, BMP4 treatment and reversion post BMP4 treatment. Scale bar represent 120 µm. (B) Proliferating cells in control conditions (with GFs) and progressive BMP4 treatment, marked by EdU incorporation. (C) Cellular ROS content in control conditions and progressive BMP4 treatment. (D) Proliferating cells in culture condition with BMP4 for 3 days and under temporally defined reversion conditions (withdrawal of BMP4 and re-addition of EGF), marked by the incorporation of EdU. (E) Cellular ROS content in cells cultured with BMP4 for 3 days and under temporally defined reversion conditions. All data represent mean ± SEM. * $p < 0.05$, ** $p < 0.01$, *** $p < 0.0005$, **** $p < 0.0001$.

Discussion

The work I pursued in my doctoral study shows that redox regulation plays a vital role in the biology of adult neural precursor cells and the progression through neurogenic phases. Using different methodologies and model systems, I have shown that functional subsets of neural precursors can be defined based on intracellular ROS content. Stemness and cellular redox regulation have been studied in other stem cell niches and, unlike these other niches including cardiac stem cells, MSCs, HSCs, ES, and iPSCs, wherein (all) reports suggest that quiescent cells are marked by a low ROS content and that the ROS trajectory via proliferation and lineage specification goes from low to high cellular ROS levels (Armstrong et al., 2010; Ludin et al., 2014). Unlike these models, the quiescent adult neural stem cells within the adult DG are uniquely characterized by the highest ROS content among all precursors and progenitors. Based on the ROS content, distinct cellular states can be identified, thereby providing a metabolic parameter for cytometric classification of the different stages of neurogenesis. Further, changes in these cellular states, at least on the transcriptomic scale are preceded by significant changes in cellular redox levels or oxidative stress. My work shows that the fraction of these highest ROS containing subset of neural precursors are highly enriched within the DG, compared to the SVZ. This subset of hiROS precursors specifically responds to acute de novo activity by a mechanism that is dependent on the activity of molecules not necessary to sustain the baseline process. The response involves a transient, further increase in cellular ROS levels to ~1.5 fold relative to the baseline levels, which is dependent on the plasma-membrane localizing Nox2 complex. In this section, I will present a model of the adult DG's neurogenic niche with regard to its organization, the baseline neurogenic process, and the differences between this 'hardwired' (or default) neurogenesis and adaptive neurogenesis.

The organization of an active neural stem cell niche of the adult DG with respect to cellular redox content

I have profiled the ROS content in different cell types within the DG of young adult mice (6-8 weeks old), using different reporter and markers. Considering the combined results for all assayed cell types resolves a bigger picture of the DG neurogenic niche. Cells which represent early phases of neurogenesis have significantly higher ROS content compared to their environment. Type -1 cells, which I defined as Gfap-GFP^{+} EGF^{+}, have the highest cellular ROS levels compared to all other cell types and a significantly decreasing ROS

gradient escorts the trajectory of neurogenesis. Post-mitotic DCX^+ cells with the highest levels of Calretinin (Calb2) and NeuN (Rbfox3) have the lowest ROS content among the assayed cell types. I did not directly mark neurons in the current study. However, neurons are the majority cell type within the DG and given that the majority of cells always cluster into classes with the lowest cellular ROS content, I make the (safe) assumption that neurons are the cell type with the least cellular ROS content. The plot below shows the different cell types within the DG resolved for their ROS content and it can be appreciated that multipotent type-1 cells have the highest and significantly higher ROS content than all other cell types.

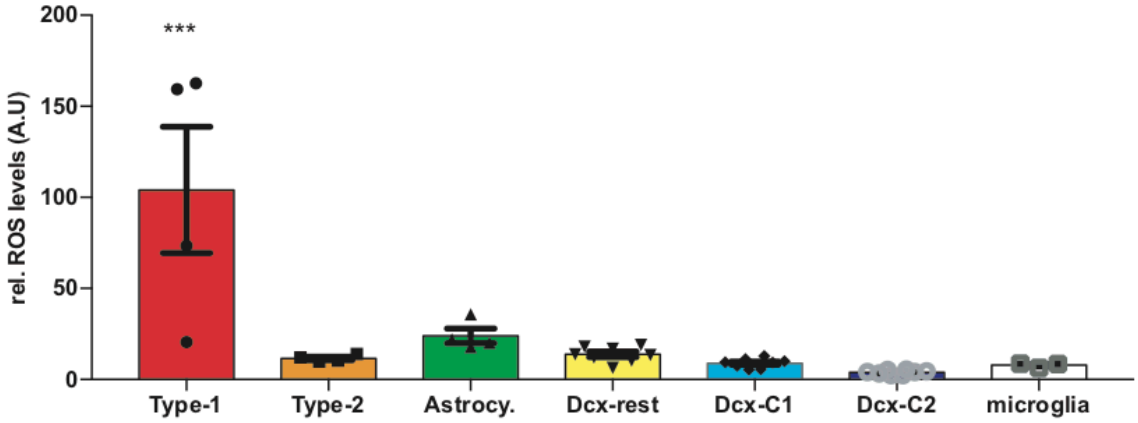

Figure 24: ROS profiling of all major cell types within the adult DG.

This result is corroborated to some extent by Walton and others (Walton et al., 2012), who show that the sub-granular zone within the DG is marked by increased cellular ROS products, oxidized lipids (4-Hydroxynoneonal staining) and oxidized DNA (8-hydroxy guanosine staining). This work does not, however, resolve the levels of these ROS readouts in different cell types. This caveat is not resolved by my work either, as repeated attempts to demonstrate oxidized lipids and DNA within Nestin- or Sox2-positive cells were not successful. The ROS gradient, as assayed by ex vivo dyes, is far more pronounced in the DG than in the SVZ, based on the cell types assayed. This raises the question, why is the cellular ROS gradient along the trajectory from quiescence to the differentiated end product flipped specifically in the DG? Although a speculation at this point, I postulate that an active stem cell niche requires a ROS gradient (either low-to-hi or vice versa). This gradient 'guides' or pushes the cells through cellular transitions, specifically into proliferation. The nature of the gradient depends on the lifespan of the longest surviving cell type within the

niche and, hence, the proximity of the terminally differentiated cell to the stem cell. In other systems, such as the HSC system, the terminal product (different blood cells) do not reside in close proximity to the stem cells. This would indicate that the longest surviving cell within the niche/ microenvironment has to be the quiescent, multipotent stem cell. This could be one reason why the long-term HSC can afford to have antioxidant defense to prevent macromolecular damage. Within the DG, neurons as the terminally differentiated end products reside in close proximity to the radial glial type-1 cells and are the longest surviving cell type within the niche, which might require an enrichment of antioxidative defenses. Thus, even with the trade-off of macromolecular damage (DNA, protein and lipid peroxidation) the precursors maintain high ROS levels. With an altered ROS gradient, the hypothesis to test is if quiescent cells are actively recruited into proliferation. Aging, wherein neuronal oxidative stress is widely reported (Castelli et al., 2019; Halliwell, 2001), would be one physiological setting to test this hypothesis. In support of this line of thinking, it has been recently shown, thorough mathematical modeling and in vivo studies, that the decrease in neurogenesis, which is observed in aging is not a consequence of stem cell exhaustion (Abdallah et al., 2010; Ziebell et al., 2017).

Cytometric classification of cells within the DG

As mentioned before, the current state of describing and investigating the cellular states within the neurogenic zone of the DG is heavily relied upon cellular morphology and marker expression. The ability to regularly and reliably identify cellular states using cytometric strategies and marker combinations is very much a work in progress, especially when compared to the published work on the neurogenic cells of the adult SVZ (Chaker et al., 2016; Codega et al., 2014). Hence it is plausible to envisage that multipotent type-1 cells, which are regularly marked by the expression of Gfap, EGFR, Hopx and lack of Ki67, Tbr2 (Eomes), or other neurogenic phases and even terminally differentiates cells such as neurons have distinct, functional subsets. Although transcriptomics provides a method to identify such subsets, each NGS approach has its limitations and there is particular need to combine this approach with other methods of profiling the metabolic status of cells.

The approach of assaying ex vivo primary cells with commercial redox dyes is a quick, reproducible, modifiable and reliable method. Alternately, there are genetically encoded sensors, such as Hyper; ro-GFP1 among others (Mishina et al., 2013; Nietzel et al., 2018; Sugiura et al., 2019; Zou et al., 2018), which can also detect global ROS levels/ specific

oxygen species and even ROS levels within a specified cellular compartment. Each of these approaches have distinct advantages and limitations. The major disadvantages include the lack of sensitivity of the genetically encoded sensors and the incompatibility of the fluorescence range of these sensors with reporter lines (such as Nes-GFP). For this reason, I chose to use commercial dyes. Most of these fluorescent dyes are cell permeable in their reduced form and, upon oxidation become trapped within the cell. Hence the cellular ROS content is proportional to the fluorescent intensity cytometrically observed. Another consideration pertains to the visualization method. Although visualization in acute slices is possible, it is a highly stress-inducing process and thus could generate highly variable results. As the dyes are not reliably retained within the cell post permeabilization, I could not employ classical histochemical approaches. Further, acute slices of adult hippocampus are short-lived, which precludes long-term assays for stemness and progression of cellular states. Hence, I chose to employ an ex vivo cytometry-based methodology to determine the ROS content as this approach is quantitative and as an added advantage, it allows further bioassays.

A seminal result from my work is that, by marking and classifying classes of cells based on their intracellular ROS status (cellular oxidative stress), seemingly homogenous populations can be further segregated into distinct subsets within the DG. This result could lay the ground work for further resolving cells according to their biological properties by complementary *-omics* approaches, such as transcriptomic profiling (which was employed in this study). Based on our results, it is possible to curate a list of surface markers which can be used as cytometric identifiers of cell types in isolation (or coupled with ROS dyes), at least within the pool of early precursors of the DG. The following three tables are a preliminary effort in that direction, wherein I list signature transcripts of Nes- GFP^+ within the different ROS classes, with restricted, yet high expression to one class (> 2 CPM). I have annotated the sub-cellular location of their putative translated product. The listed genes are not necessarily translated in vivo (and are not based on a cellular function), but based on our data, their expression could serve as putative discrimination features to develop reporter lines (either in isolation or as a bar code) and cytometric tools. In conjugation to this, the further development of genetic sensors, with a robust dynamic fluorescence range, and longitudinal imaging methodologies could make in vivo classification a reality in the near future.

Table 15: Signature transcripts with unique expression in Nes-GFP$^+$ of the hiROS class

Symbol	sub-cellular location	avg. hi	avg. mid	avg. lo
Serpine1	secreted	5.09215	-1.77308	-2.12064
Clec4e	plasma membrane	4.13605	-0.03864	-3.67662
Apoc2	secreted	3.361225	-0.84886	-3.79314
Cd300lb	plasma membrane	3.359525	-1.33822	-3.70998
Padi6	nucleus	2.9373	-1.28014	-3.68242
Gpr141	plasma membrane	2.91655	-0.47218	-4.16188
Cfap45	nucleus	2.8978	-1.39342	-3.59522
Pilrb1	plasma membrane	2.761575	-1.3425	-4.04996
Irs3	cytoplasm	2.72865	-1.83132	-3.37146
Wfdc6a	secreted	2.707925	-0.90108	-4.16516
Tfap2a	nucleus	2.653675	-0.45606	-3.4888
Tdgf1	secreted	2.618	-0.05058	-3.67654
Clec4d	plasma membrane	2.4581	-0.01798	-3.59558
Rassf6	cytoplasm	2.43575	-1.02872	-3.6159
Fzd10	plasma membrane	2.135125	-0.22952	-3.16604
Orm3	secreted	2.03485	-1.88616	-4.04996

Table 16: Signature transcripts with unique expression in Nes-GFP$^+$ of the midROS class

Symbol	sub-cellular location	avg. hi	avg. mid	avg. lo
Pimreg	nucleus	-2.297	5.5866	3.17938
Ska1	cytoplasm	-3.0854	4.28886	1.91414
Tspan18	plasma membrane	1.886075	4.1007	1.90174
Cd209g	plasma membrane	-1.661125	3.92174	-3.90022
Inhba	secreted	-1.3592	3.22476	0.66386
Hist1h1b	nucleus	-1.02945	2.99906	0.6264
Ccl8	secreted	-1.64475	2.88874	-4.3598
Cfap54	cytoplasm	0.32085	2.42958	-0.32846

Table 17: Signature transcripts with unique expression in Nes-GFP^{+} of the loROS class

Symbol	sub-cellular location	avg. hi	avg. mid	avg. lo
Zfp385b	nucleus	-0.64795	-0.63992	5.65508
Adamts18	secreted	-1.756175	-1.1348	5.64078
Sphkap	cytoplasm	-1.03455	-0.1818	5.43666
Cpne9	plasma membrane	-0.60865	-0.88632	5.19966
Cnih3	plasma membrane	-2.986825	-1.43328	4.95008
Neurod2	nucleus	-1.960525	-1.3233	4.70822
Syt2	cytoplasm	-1.00745	-1.39202	4.6919
Golga7b	cytoplasm	-1.01045	-0.96306	4.54258
Abcc8	plasma membrane	-2.6935	-0.20476	4.48346
Nell1	secreted	-2.48075	-0.1375	4.25926
Amer3	plasma membrane	-2.214475	-0.76376	4.24076
Prdm8	nucleus	-1.968975	-1.46946	4.01466
Smim18	plasma membrane	-3.766975	-0.38692	3.95438
Ablim3	cytoplasm	-2.0426	-0.19146	3.87114
Nhlh2	cytoplasm	-0.659475	-0.5376	3.82236
Gpr68	plasma membrane	-0.187725	-2.19772	3.72798
Tbata	cytoplasm	-2.048225	-1.69524	3.70642
Cntnap5a	plasma membrane	-2.04315	-2.23882	3.68488
Cdh8	plasma membrane	-3.127075	-1.97528	3.64604
Ltbp2	secreted	-1.032825	-1.56778	3.576
Galr1	plasma membrane	-2.5844	-2.41752	3.42094
Islr2	plasma membrane	-2.411925	-1.43708	3.28688
Hydin	plasma membrane	-0.541025	-1.36194	3.25286
Cacng2	plasma membrane	-1.11145	-1.55142	3.23738
Zbtb8b	nucleus	-0.444825	-0.59272	3.15074
Unc5d	plasma membrane	-1.525425	-0.79366	3.12862
Stk32b	cytoplasm	-2.643075	-0.55522	3.12744
Cldn3	cytoplasm	-4.113425	-3.9421	3.09548

Establishing the cellular states of redox defined subsets of Nes-GFP$^+$ adult precursors within the DG

As mentioned in the introduction, Berg and coworkers have shown that the adult neural stem cell is a product of gradual transitions of embryonic neural stem cells, and quiescence, as marked by loss of proliferative markers, is first observed at postnatal day P3. Between P3 and P45 (6 weeks), there is a further loss of active proliferation markers and the cellular metabolism strongly shifts towards fatty acid oxidation. One of the key pathways that is upregulated between these time points is redox regulation. This corroborates our finding that, as a whole, Nestin-expressing neural precursors are significantly enriched of core redox regulating genes (Fig. 1). As opposed to Berg et al., we chose to use Nestin reporter mice, as it is the broadest single marker for early precursor phases in the adult animal (type-1, type-2a and some expression in type-2b). This system thus enables us to query the ROS levels within different subsets and follow their expression profiles.

We first showed that segregating the total pool of DG cells into non-overlapping, distinct ROS classes is a very potent classifier for neurosphere forming cells. The neurosphere bioassay, in its very nature, is a “black box”. It is hard to predict if the primary cells, which form neurospheres ex vivo, are had been actively proliferating in vivo. However, this assay does reflect the total stemness of the stem and progenitor cells, with more committed cells forming fewer (and smaller) neurospheres. I could show that 50% of Nes-GFP$^+$ cells fall into a ROS class that does not form any neurospheres, under baseline or stimulated conditions (KCl). The 50% that do fall in hiROS and midROS classes have significantly distinct median cellular ROS content. Based on the transcriptomic profiling, we further show that Nes-GFP$^+$ of the hiROS and loROS classes have a negligible overlap of expressed transcripts, which indicates that the trajectory of neurogenic progression involves a ROS gradient. Nes-GFP$^+$ cells within the hiROS class can be defined by three hallmark features at the RNA level: 1. They express characterized markers of radial glial cells, including Gfap, Nestin, Lpar, Sox2, Hopx, among others; 2. They have high expression of quiescence markers such as Btg1/2 (Farioli-Vecchioli et al., 2014), REST, Hes1, Id 1/ 4, P21 (Cdkn1a; Epp et al., 2013; Li and Wong, 2018) and Pten (among others). They have no detectable expression of type-2 markers, such as Tbr2 (Eomes) or Mcm family members (Mcm 2-6), and 3-fold lower expression of Mki67; 3. These cells have high expression of markers involved in fatty acid oxidation, such as Cpt1a and Spot14, which have been shown as critical inhibitors of proliferation. These features justify our assertion that Nes-GFP$^+$ cells of the hiROS class

are quiescent. It also has to be noted that a tight clustering of the expression profiles from biological replicates exists, which suggests that this result is not incidental and based on experimental conditions on that given day. I used pair-wise comparison to clarify that a decrease in cellular ROS content (from hi- to midROS) does not immediately equals the entry into cell cycle. There are no significant changes in genes involved in FAO or reduction of quiescent markers such as Hopx and REST in Nes-GFP$^+$ of the midROS class. I propose that the shift to midROS results in multipotent stem cells, which are primed to enter cell division, a state distinct from long-term quiescence. This ROS content does facilitate proliferation, as marked by the expression of key promoting factors of G1/S transition, proliferation genes such as MKi67, PCNA, or Aurka(/b). It could be argued that cells maintain moderate ROS levels as they shift their metabolic programs from FAO dependency to de novo lipogenesis, as indicated by the expression of Fasn. The next ROS drop to create Nes-GFP$^+$ of the loROS class is characterized by strong lineage specification as marked by the incidence of Ncam1, Dcx and Rbfox3 transcripts. We strongly propose that, based on the expression profiles, Nes-GFP$^+$ cells of the loROS class are neuroblasts, with reduced proliferative potential and increased neuronal commitment. We have also shown that a strong shift in the mode cellular respiration occurs between mid- and loROS classes, namely from a glycolytic to a mitochondrial oxidative phosphorylation (oxphos) paradigm. It has been previously shown that adult NSCs shift their paradigm for energy production and this marks a strong shift towards lineage restriction (Beckervordersandforth, 2017a; Beckervordersandforth et al., 2017b; Zheng et al., 2016). Another possible interpretation could be that Nes-GFP$^+$ cells of the hiROS class could be a distinct subset, which does not enter proliferation under standard housing conditions. All baseline neurogenesis happens by recruitment of primed Nes-GFP$^+$ cells of the midROS class into active growth cycle. This interpretation argues that midROS cells essentially generate neurogenic cells as well as non-proliferative hiROS cells and a disequilibrium might underlie decreasing neurogenesis observed with aging. This argument needs further investigation, specifically with single cell transcriptomic profiling to investigate whether cells exclusively transit from a higher to a lower ROS content or also in the other direction (from moderate to higher ROS levels).

Despite all the above results, it has proved rather difficult to identify a strong candidate as the pioneering redox sensing transcription factor, which regulates the changes in cellular ROS content from high to moderate or moderate to low. It is plausible that a multitude of

factors might synergistically alter physiological levels of cellular ROS content. Further work, with acute labeling of cells and a time course based transcriptomic profiling of precursors could shed further insights into the timeline of quiescence to proliferation commitment. It can be argued that Nes-GFP$^+$ cells of the hiROS class represent a distinctive subtype, which never enter active growth cycle under baseline (unstimulated) conditions or represent a near-exhausted pool of stem cells, which are created by increasing ROS levels in Nes-GFP$^+$ cells of the midROS class. My work does not alleviate this caveat as I based it on bulk sequencing of Nes-GFP$^+$ cells in the different ROS classes. Single-cell sequencing of Nes-GFP$^+$ post sorting based on cellular ROS content can address this question. Furthermore, especially following the proportional abundance of Nes-GFP$^+$ among ROS class in the course of aging could be a good starting point for a follow up study.

Timeline of baseline proliferation within precursors and identifying the subset of precursors responsive to de novo physical activity

I used a dual thymidine analog paradigm to follow cell cycle kinetics of precursor cells at the population level. I injected animals with each thymidine analog in a window of 18 hours by using a 3-injection strategy, each separated by 9 hours. Post the last injection, I ensured a 2 hour "washout period" before either changing the housing condition or perfusing the animals. I chose this injection strategy based on results from our lab (Fischer et al., 2014) and different mathematical models (Pfeuty, 2015; Podgorny et al., 2018), which show that the total cell cycle length is around 20 hours and the S-phase is close to 10 hours. Even assuming that cells enter asynchronously into active cell cycle, the 3 injections paradigm spanning 20 hours (18 + 2-hour washout) would cover the largest cohort of cells which enter or are engaged in active S-phase. CldU was the first thymidine analog injected and IdU was injected starting 20 hours before perfusion. Cells which incorporated CldU had a window of 90 hours before perfusion. A few inferences can be made by focusing on the CldU numbers. First, a majority of CldU labeled cells (> 90%) did not incorporate IdU suggesting that the window of active proliferation, at the population level, was less than 90 hours (thus less than 4-5 rounds of division). This is corroborated by the fact that 83.77 ± 4.77% of cells were positive for DCX, a late stage proliferation mark, before neurogenic cells become post-mitotic. Interestingly, about 14% of CldU$^+$ cells exited cell cycle, while continuing to express Sox2 and/ or Tbr2, which mark the early phases of neurogenic progression. Secondly, irrespective of cumulative stimulus of running (5R) or an acute bout of running (2R), CldU

numbers do not change, relative to the control. All these results taken together highlight one novel finding, cells which were in active cycling before the running stimulus ($CldU^+$), irrespective of continued proliferation or "resting" in particular neurogenic stages (Urbán et al., 2016), do not respond to a de novo activity-driven stimulus. Thirdly, CldU cells had a longer time window to undergo more rounds of proliferation than IdU incorporating cells. However, at day 5 (perfusion time point) the number of $CldU^+$ cells and IdU^+ cells did not show any significant differences. These results suggest that in the window of 90 hours proliferating cells undergo a high degree of cell death. Longitudinal imaging of sparsely labeled cells shows that the average time for a type-1 radial glial cell to complete its proliferation cycle is 9.6 ± 1.4 days, during which cells divide an average of 2.3 ± 0.1 times (Pilz et al., 2018). Another feature observed using this model was that cells do not actively return to long-term quiescence. This stands out as a strong caveat for the study as other reports have shown long term quiescence of activated cells (Podgorny et al., 2018a). Our results show a shorter window of proliferation at the population level (3.75 days).

As two different thymidine analogs were employed along with 2 running paradigms, a set of results could be anticipated, which would indicate dominant mechanism resulting in increased proliferation events post stimulation. First, an increase in the number of IdU+ cells in the 5R group, compared to the 5S group, would serve as a proof of principle for the effect of the running paradigms. A similar increase in the 2R group, would indicate that physical activity acts as an activation cue and is not required as a continuous stimulus to result in a pro-proliferative response. An increase, or any change, in the CldU numbers would indicate that baseline progenitors respond to physical activity and alter their cell cycle kinetics. An increase in $CldU^+IdU^-$ without a concomitant increase in the double positive fraction would indicate an effect on baseline proliferators' survival without triggering increased rounds of division. An increase in $CldU^+IdU^+$ (double positive cells) would indicate increased rounds of divisions of baseline progenitors when stimulated by physical activity. An increase in both $CldU^+IdU^-$ and double positive cells would likely result from a synergistic rescue from cell death and increased proliferative cycles. Finally, an exclusive increase in $CldU^-IdU^+$ numbers indicates that baseline proliferators are non-responsive to physical activity and previously non-dividing/ quiescent cells are recruited into active cycling by physiological stimuli. Comparing 2R and 5R enquires if the stimulation works as a gradient. Our results strongly show that the increase in proliferating cells (IdU^+) post running results from an activation of previously non-dividing cells, for which a continuous running stimulus is not

required. These activated cells quickly resort to a similar neurogenic progression paradigm by day 4 of running as no phenotypic differences can be observed between runners and non-runners. This observation that non-dividing cells respond to physical activity has been recently corroborated by the work of Berg and others. A further result shows that this recruitment of quiescent cells is an activation event, as the response observed in 2R group is statistically similar to the 5R runners.

I showed that it is the Nes-GFP$^+$ cells of the hiROS class, the quiescent precursors, which respond to acute voluntary running and this response, to the best of our knowledge, is the first line of work showing the responsive subset of precursor cells to physical activity. The Nes-GFP$^+$ cells of the hiROS class exhibit a ROS surge, which is temporally followed by a delineated lowering of the ROS content and a significant increase in the proliferation fractions of the Nes-GFP$^+$ cells of the loROS class. This group of cells both in proportion and expression profile are specific to the DG and are near-absent from the SVZ. Taken together, an increased ROS level of hiROS Nes-GFP$^+$ cells, which constitute about 15-20% of all Nes-GFP$^+$ cells in the DG, is the “first response” to acute physical activity, which is followed by their redistribution among ROS classes over the ensuing 4 days. Given the similarity in the response to a 2 day or a 4-day bout of activity, the acute response should be followed by a period of refraction wherein no further response is observed. The niche recalibrates to replenish the hiROS subset of precursors before the system responds to continued activity-driven stimulation, explaining why a continued stimulus, even 4 weeks, does not further enhance the pro-proliferative response observed post an acute bout (Fig 1; compare also Akers et al., Science 2014). These results also suggest that cells along the neurogenic trajectory may shuttle between early developmental phases or between high and moderate ROS classes.

Upon sustained stimulation, the acute response may give way to an effect on maintenance of the precursor cell pool, in line with the observation that upon prolonged exposure to the running wheel pro-proliferation relatively recedes, cell cycle length shortens and net neurogenesis (adult born neuronal abundance) continues to increase significantly which indicates a pro-survival effect on the post-mitotic pool of immature neurons (Farioli-Vecchioli and Tirone, 2015; Farioli-Vecchioli et al., 2014). In other words: a novel stimulus of exercise would exert a stronger effect on a naïve population of Nestin expressing precursors than a pool of cells that has already been primed. The neurogenic niche would acquire a memory of activation which is reflected in the functional features of the stem cells and other cells of

the neurogenic trajectory (including but not limited to proliferation rounds, cell cycle length, cell cycle exit and cell survival).

Monolayer culture to study cellular states and redox regulation

As mentioned above, the monolayer system has certain caveats in studying in vivo cellular states. However, I could show that cells in culture have a very narrow and reproducible range of cellular ROS levels and proliferation levels. Although I used this system to try various different treatments, in the thesis, I wanted to highlight the treatment of these seemingly homogenous cells with bone morphogenic protein 4 (BMP4). It has been repeatedly shown that treating proliferating cells with BMP4 in the presence of FGF2 pushes them into a non-proliferative state with distinct changes in the expression profile, criteria for considering this as a quiescent stage. BMPs are the largest class of the Transforming growth factor beta (TGF-β) superfamily. Their binding to surface receptors BMPRIA or BMPRII in NPCs leads to phosphorylation of receptor associated R-Smads (Smad 1/5/8), which heterodimerize with co-Smad4 and localize to the nucleus to function as transcription factors. The main targets of BMP4 include genes of inhibitor of differentiation family (IDs, specifically Id1, Id3/4), which, by antagonizing bHLH transcription factors, contribute to the quiescent state and arrest EGF induced proliferation of neural precursor cells (Cole et al., 2016). BMP4 further regulates Hes1 (notch signaling) and can induce changes in gene regulation by inducing the expression of nuclear factor one family members, specifically NFIX (Martynoga et al., 2013). BMP4 treatment also strongly enhances fatty acid oxidation (Knobloch et al., 2017). It has been further shown that antagonizing BMP4 alters neurogenesis kinetics in vivo (Armenteros et al., 2018; Bond et al., 2014; Meyers et al., 2016). These results argue that treating monolayer culture with BMP4 could be a suitable model to study the induction of and the reversion from quiescence. As I have shown, cells leave proliferation paradigm rather quickly with BMP4 (one day), at this time point the ROS content only marginally increases from the levels observed in proliferating cells. But along with changes in the expression, ROS levels continue to increase and plateau around day 3-4. The induced quiescence is stable and long-term redox regulation in this system has to be further studied. The other important result I have shown is that the reversion into proliferation upon BMP4 withdrawal is also pro-oxidative and cellular ROS peaks significantly at the point when cells transition from G1 to S-phase of the cell cycle. Again, this result, in the light of the Nox2 results, might be invaluable to understand the role of

redox regulation in the activation of NPC's proliferation. I would like to stress that my work, thus far, should only be considered as a foundation for this hypothesis and further work is necessary to understand if the process of reversion is similar to baseline regulation of the quiescent state in vivo.

Nox2 dependency as a discriminatory feature of adaptive neurogenesis

Mitochondrial maturation is critically linked to proliferation and progression through the developmental stages of neurogenesis (Beckervordersandforth et al., 2017). My work with Mitosox, a variant of DHE with orders of magnitude higher preferential localization to mitochondria, enables following mitoROS production, which in itself is a proxy for mitochondrial activity. Some of the work I pursued showed that Nes-GFP^{+} cells in the hiROS fraction have moderate to low mitochondrial ROS production (mitoROS levels), which has to be revisited and verified. However, the finding that under running conditions no mitoROS surge occurred, strongly argues for a role of other means for pan-cellular ROS generation as a putative signaling messenger, which is temporally delineated from a metabolic shift in energy production. To this end, ROS surge post running has to be a directed response to running. Nox homologs (Nox1-5, Duox 1,2) form membrane bound complexes, which localize to different cellular compartments. Nox1 has been shown to associate with caveolae, Nox4 to the endoplasmic reticulum and mitochondria; Nox3, Nox5 and Duox enzymes have low cellular expression and localize to the plasma and internal membranes. Nox2, dependent on the cell type, can be found in various cellular compartments, including the plasma membrane, "redoxisomes" (endosomes) and the leading edge of lamellipodia. Gp91 ^{phox} (Nox2 or Cybb) and p22^{phox} (Cyba) are integral membrane proteins which form a dimeric complex. Activation of the heterodimer leads to the localization of other membrane partners to the membrane, including the multidomain regulatory subunits, p40^{phox}, p47^{phox} and p67^{phox}. This active complex transfers electrons from the substrate to oxygen through a prosthetic group, flavin, and a heme group(s), which carries electrons. This is a Rac2 and Rap1A dependent process. Subsequently, superoxide radicals are generated through the enzyme complex, which leads to proximal protein oxidation and/ or conversion to other ROS species (Brown and Griendling, 2009; Lambeth, 2004; Lambeth and Neish, 2014). I could not detect any expression of Nox1, 3, 5 or Duox 1,2 in any of Nes-GFP^{+} cells. I could however show that the entirety of the core and activated Nox2 complex, including

Nox2 (Cybb), p22^{phox} (Cyba), p40^{phox} (Ncf-4), p47^{phox} (Ncf-1), p67^{phox} (Ncf-2), Rac1, and Rac2, are expressed and enriched in Nes- GFP^{+} cells of the hiROS and midROS classes, with almost no expression for any of these genes in the loROS class. Rap1A is exclusively enriched in the Nes-GFP^{+} cells of the hiROS class. Based on these expression profiles, I chose Nox2 as a strong candidate involved in causing the ROS surge after one night of running. My results show that the baseline distribution of Nes-GFP^{+} cells among ROS classes and the mean ROS content of precursors within each ROS class is not affected in Nox2 mutants. Furthermore, baseline proliferation of cells, as measured by the numbers of Ki67 expressing cells, was unaffected in Nox2-deficient mice. We thus propose that under standard housing conditions, the mechanisms by which a cell generates, maintains and regulates ROS is independent from Nox2 activity. It still remains elusive if the hiROS cells generate more cellular ROS or express negligible levels of antioxidants. Nevertheless, I could show that Nox2-mediated ROS fluctuations in Nes-GFP^{+} cells of the hiROS class are vital for the subsequent increase of Nes-GFP^{+} cells of the loROS class post 4 days of running. It has been previously speculated that certain strains could have a delayed response to physical activity (Overall et al., 2013). To address if Nox2-deficiency indeed leads to a decreased response to physical activity, I used a robust running paradigm of 10 days. Herein I observe that while the wildtype littermates have a pro-proliferative response, the Nox2-deficient mice do not show this response. Previous work, employing neurospheres from SVZ and other in vivo models, have demonstrated that Pten, a well-established tumor suppressor, is a downstream target of Nox2 (Belle et al., 2011; Hervera et al., 2018). Nox2 generated ROS leads to the oxidation and inactivation of Pten, which augments phosphatidylinositol 3,4,5-triphosphate (PI3K) production and Akt activation, which further phosphorylates a number of downstream factors that regulate cellular responses including cellular growth and proliferation (Luo et al., 2003). This scenario is a possible mechanism how NSCs, in an independent mode and dependent on Nox2 function, enter cell cycle when triggered by environmental or activity cues. This finding goes a way into redefining the baseline characteristics of cellular sates and mechanism by which different modes of neurogenic responses occur.

Conclusion

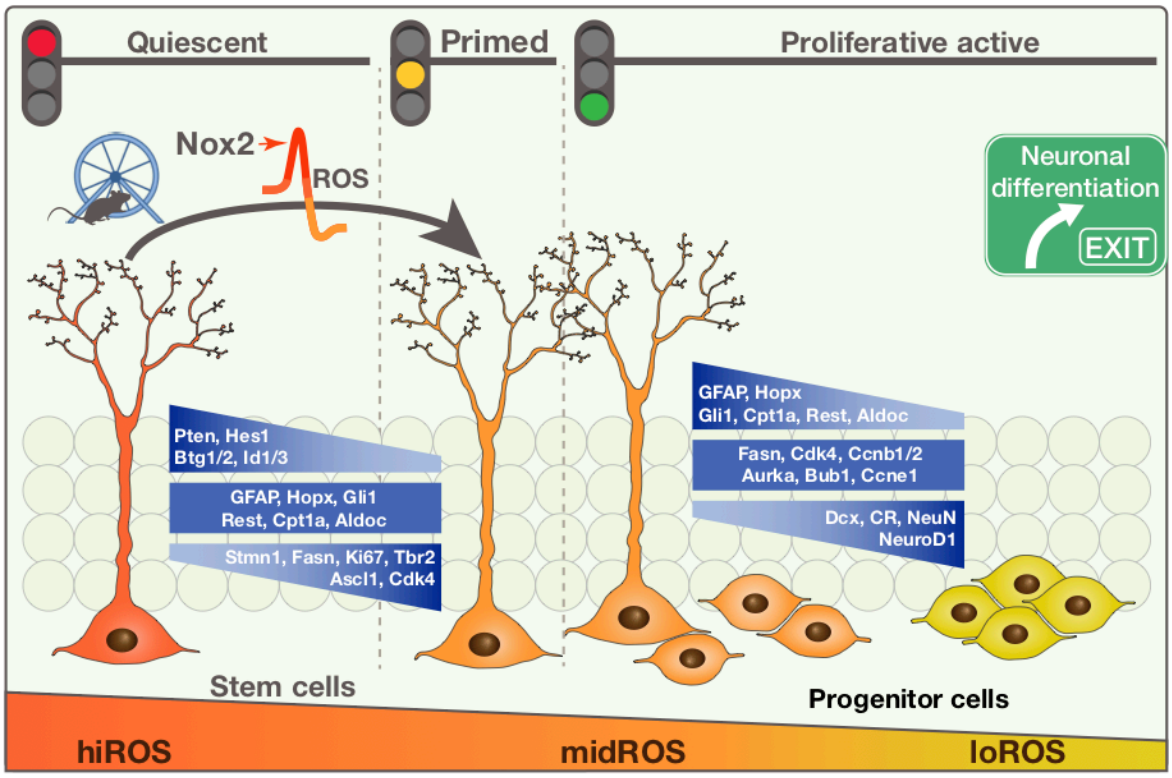

Based on the results presented, my doctoral work has identified an unique role for redox regulation and intracellular ROS for neural precursor cells of the adult dentate gyrus. Using optimized cytometric methodologies, I have shown that Nes-GFP^{+} cells of the DG have significantly higher cellular ROS content, compared to the precursors in the SVZ. A classification of the DG's neurogenic cells, based on intracellular ROS levels, into non-overlapping ROS classes unraveled a functional heterogeneity marked by differential stem cell potential and unique expression profiles. I characterized the expression profiles of the ROS classes, which show that, unlike other in vivo and in vitro stem cell models, quiescent NPCs possess the highest cellular oxidative stress and, as cells enter proliferation and progress through the neurogenic trajectory, the cellular ROS levels significantly decrease. These results were compared to previously published data to show a high degree of concurrence. Using different statistical models, my results argue that the observed change in cellular redox content is temporally upstream to incremental transcriptional changes and other metabolic processes that characterize the progression to successive cellular states, specifically the transition from quiescence to active proliferation. Based on these findings, I

conclude that distinct subsets of high-ROS quiescent and moderate-ROS quiescent-primed states can be distinguished among the otherwise homogenous, non-proliferating type-1 precursor cells.

To understand the responsiveness of these ROS-defined subsets to environmental stimulation, we temporally outlined the events following acute de novo physical activity. I utilized a dual-thymidine analog paradigm to show that previously non-proliferating cells are activated by physical activity. This activation is a process that involves a cellular ROS spike in the hiROS class of Nes-GFP^{+} cells, which leads to a redistribution of precursor cells among the ROS classes at a timepoint, where a significant increase in proliferation can be detected. This spike in cellular ROS content is not driven by fluctuations in mitochondrial activity, but is contingent on the function of the Nox2 enzyme complex. The ROS-surge-mediated recruitment of quiescent cells represents an independent mode of cell cycle entry, as in the absence of Nox2 expression baseline neurogenesis remains unaffected with no adaptive response to physical activity.

The findings presented here, thus, resolve the neurogenic niche and adult neural precursor pool to the highest degree yet.

References

Abbas, H.A., Maccio, D.R., Coskun, S., Jackson, J.G., Hazen, A.L., Sills, T.M., You, J.M., Hirschi, K.K., and Lozano, G. (2010). Mdm2 Is Required for Survival of Hematopoietic Stem Cells/Progenitors via Dampening of ROS-Induced p53 Activity. Cell Stem Cell *7*, 606–617.

Abdallah, N.M., Slomianka, L., Vyssotski, A.L., and Lipp, H.-P. (2010). Early age-related changes in adult hippocampal neurogenesis in C57 mice. Neurobiol Aging *31*, 151–161.

Adrian Alexa and Jorg Rahnenfuhrer (2018). topGO: Enrichment Analysis for Gene Ontology. R package version 2.34.0.

Aimone, J., Li, Y., Lee, S.W., Clemenson, G.D., Deng, W., and Gage, F.H. (2014). Regulation and function of adult neurogenesis: from genes to cognition. Physiol Rev *94*, 991–1026.

Akers, K.G., Martinez-Canabal, A., Restivo, L., Yiu, A.P., Cristofaro, A., Hsiang, H.-L., Wheeler, A.L., Guskjolen, A., Niibori, Y., Shoji, H., et al. (2014). Hippocampal Neurogenesis Regulates Forgetting During Adulthood and Infancy. Science *344*, 598–602.

Altman, J., and Das, G. (1965). Autoradiographic and histological evidence of postnatal hippocampal neurogenesis in rats. J Comp Neurology *124*, 319–335.

Alvarez, D.D., Giacomini, D., Yang, S., Trinchero, M.F., Temprana, S.G., Büttner, K.A., Beltramone, N., and Schinder, A.F. (2016). A disynaptic feedback network activated by experience promotes the integration of new granule cells. Science *354*, 459–465.

Alvarez-Buylla, A., Theelen, M., and Nottebohm, F. (1990). Proliferation “hot spots” in adult avian ventricular zone reveal radial cell division. Neuron *5*, 101–109.

Andersen, J., Urbán, N., Achimastou, A., Ito, A., Simic, M., Ullom, K., Martynoga, B., Lebel, M., Göritz, C., Frisén, J., et al. (2014). A Transcriptional Mechanism Integrating Inputs from Extracellular Signals to Activate Hippocampal Stem Cells. Neuron *83*, 1085–1097.

Armenteros, T., Andreu, Z., Hortigüela, R., Lie, C.D., and Mira, H. (2018). BMP and WNT signalling cooperate through LEF1 in the neuronal specification of adult hippocampal neural stem and progenitor cells. Sci Rep-Uk *8*, 9241.

Armstrong, L., Tilgner, K., Saretzki, G., Atkinson, S.P., Stojkovic, M., Moreno, R., Przyborski, S., and Lako, M. (2010). Human Induced Pluripotent Stem Cell Lines Show Stress Defense Mechanisms and Mitochondrial Regulation Similar to Those of Human Embryonic Stem Cells. Stem Cells *28*, 661–673.

Babu, H., Cheung, G., Kettenmann, H., Palmer, T.D., and Kempermann, G. (2007). Enriched monolayer precursor cell cultures from micro-dissected adult mouse dentate gyrus

yield functional granule cell-like neurons. Plos One *2*, e388.

Babu, H., Claasen, J.-H., Kannan, S., Rünker, A.E., Palmer, T., and Kempermann, G. (2011). A Protocol for Isolation and Enriched Monolayer Cultivation of Neural Precursor Cells from Mouse Dentate Gyrus. Front Neurosci-Switz *5*, 89.

Barnea, A., and Nottebohm, F. (1994). Seasonal recruitment of hippocampal neurons in adult free-ranging black-capped chickadees. Proc National Acad Sci *91*, 11217–11221.

Beccari, S., Valero, J., Maletic-Savatic, M., and Sierra, A. (2017). A simulation model of neuroprogenitor proliferation dynamics predicts age-related loss of hippocampal neurogenesis but not astrogenesis. Sci Rep-Uk *7*, 16528.

Beckervordersandforth, R. (2017). Mitochondrial Metabolism-Mediated Regulation of Adult Neurogenesis. Adv Neurol *Preprint*, 1–15.

Beckervordersandforth, R., Ebert, B., Schäffner, I., Moss, J., Fiebig, C., Shin, J., Moore, D.L., Ghosh, L., Trinchero, M.F., Stockburger, C., et al. (2017). Role of Mitochondrial Metabolism in the Control of Early Lineage Progression and Aging Phenotypes in Adult Hippocampal Neurogenesis. Neuron *93*, 1518.

Belle, J.E., Orozco, N.M., Paucar, A.A., Saxe, J.P., Mottahedeh, J., Pyle, A.D., Wu, H., and Kornblum, H.I. (2011). Proliferative Neural Stem Cells Have High Endogenous ROS Levels that Regulate Self-Renewal and Neurogenesis in a PI3K/Akt-Dependant Manner. Cell Stem Cell *8*, 59–71.

Berdugo-Vega, G., Arias-Gil, G., López-Fernández, A., Artegiani, B., Wasielewska, J.M., Lee, C.-C., Lippert, M.T., Kempermann, G., Takagaki, K., and Calegari, F. (2020). Increasing neurogenesis refines hippocampal activity rejuvenating navigational learning strategies and contextual memory throughout life. Nat Commun *11*, 135.

Berg, D.A., Su, Y., Jimenez-Cyrus, D., Patel, A., Huang, N., Morizet, D., Lee, S., Shah, R., Ringeling, F., Jain, R., et al. (2019). A Common Embryonic Origin of Stem Cells Drives

Developmental and Adult Neurogenesis. Cell *177*, 654-668.e15.

Bergami, M., Masserdotti, G., Temprana, S.G., Motori, E., Eriksson, T.M., Göbel, J., Yang, S., Conzelmann, K.-K., Schinder, A.F., Götz, M., et al. (2015). A Critical Period for Experience-Dependent Remodeling of Adult-Born Neuron Connectivity. Neuron *85*, 710–717.

Besnard, A., and Sahay, A. (2015). Adult Hippocampal Neurogenesis, Fear Generalization, and Stress. Neuropsychopharmacol Official Publ Am Coll Neuropsychopharmacol *41*, 24–44.

Bigarella, C.L., Liang, R., and Ghaffari, S. (2014). Stem cells and the impact of ROS signaling. Development *141*, 4206–4218.

Black, E.P., Hallstrom, T., Dressman, H.K., West, M., and Nevins, J.R. (2005). Distinctions in the specificity of E2F function revealed by gene expression signatures. P Natl Acad Sci Usa *102*, 15948–15953.

Boareto, M., Iber, D., and Taylor, V. (2017). Differential interactions between Notch and ID factors control neurogenesis by modulating Hes factor autoregulation. Development *144*, 3465–3474.

Bonaguidi, M.A., Wheeler, M.A., Shapiro, J.S., Stadel, R.P., Sun, G.J., Ming, G., and Song, H. (2011). In Vivo Clonal Analysis Reveals Self-Renewing and Multipotent Adult Neural Stem Cell Characteristics. Cell *145*, 1142–1155.

Bond, A.M., Peng, C.-Y., Meyers, E.A., McGuire, T., Ewaleifoh, O., and Kessler, J.A. (2014). BMP signaling regulates the tempo of adult hippocampal progenitor maturation at multiple stages of the lineage. Stem Cells Dayt Ohio *32*, 2201–2214.

Bovetti, S., Veyrac, A., Peretto, P., Fasolo, A., and Marchis, S. (2009). Olfactory enrichment influences adult neurogenesis modulating GAD67 and plasticity-related molecules expression in newborn cells of the olfactory bulb. Plos One *4*, e6359.

Brandt, M.D., Maass, A., Kempermann, G., and Storch, A. (2010). Physical exercise increases Notch activity, proliferation and cell cycle exit of type-3 progenitor cells in adult hippocampal neurogenesis. Eur J Neurosci *32*, 1256–1264.

Brandt, M.D., Hübner, M., and Storch, A. (2012). Brief Report: Adult Hippocampal Precursor Cells Shorten S-Phase and Total Cell Cycle Length During Neuronal Differentiation. Stem Cells *30*, 2843–2847.

Brown, J., Cooper-Kuhn, C.M., Kempermann, G., Praag, H., Winkler, J., Gage, F.H., and Kuhn, G.H. (2003). Enriched environment and physical activity stimulate hippocampal but not olfactory bulb neurogenesis. Eur J Neurosci *17*, 2042–2046.

Castelli, V., Benedetti, E., Antonosante, A., Catanesi, M., Pitari, G., Ippoliti, R., Cimini, A., and d'Angelo, M. (2019). Neuronal Cells Rearrangement During Aging and Neurodegenerative Disease: Metabolism, Oxidative Stress and Organelles Dynamic. Front Mol Neurosci *12*, 132.

Chaker, Z., Codega, P., and Doetsch, F. (2016). A mosaic world: puzzles revealed by adult neural stem cell heterogeneity. Wiley Interdiscip Rev Dev Biology *5*, 640–658.

Codega, P., Silva-Vargas, V., Paul, A., Maldonado-Soto, A.R., DeLeo, A.M., Pastrana, E., and Doetsch, F. (2014). Prospective Identification and Purification of Quiescent Adult Neural Stem Cells from Their In Vivo Niche. Neuron *82*, 545–559.

Cooper-Kuhn, C., Vromen, M., Brown, J., H., Y., Thon, M., Winkler, J., and Kuhn, H. (2002) Impaired Adult Neurogenesis in Mice Lacking the Transcription Factor E2F1. Mol Cell Neurosci *21*, 312–323.

Davide de Peitri Tonelli, (2017), *Essentials of non-coding RNAs in Neuroscience*, Academic Press. ISBN: 978-0-12-804402-5

DeCarolis, N.A., and Eisch, A.J. (2010). Hippocampal neurogenesis as a target for the treatment of mental illness: a critical evaluation. Neuropharmacology *58*, 884–893.

Deng, W., mone, J., and Gage, F.H. (2010). New neurons and new memories: how does adult hippocampal neurogenesis affect learning and memory? Nat Rev Neurosci *11*, 339–350.

Dengler, C., and Coulter, D. (2016). Normal and epilepsy-associated pathologic function of the dentate gyrus. Prog Brain Res *226*, 155–178.

Deshpande, A., Bergami, M., Ghanem, A., Conzelmann, K.-K., Lepier, A., Götz, M., and Berninger, B. (2013). Retrograde monosynaptic tracing reveals the temporal evolution of inputs onto new neurons in the adult dentate gyrus and olfactory bulb. P Natl Acad Sci Usa *110*, E1152-61.

Diaz-Aparicio, I., Paris, I., Sierra-Torre, V., Plaza-Zabala, A., Rodríguez-Iglesias, N., Márquez-Ropero, M., Beccari, S., Huguet, P., Abiega, O., Alberdi, E., et al. (2020). Microglia actively remodel adult hippocampal neurogenesis through the phagocytosis secretome. J Neurosci Official J Soc Neurosci 0993–19.

Dickinson, B.C., Peltier, J., Stone, D., Schaffer, D.V., and Chang, C.J. (2011). Nox2 redox signaling maintains essential cell populations in the brain. Nat Chem Biol *7*, 106.

Dikalov, S.I., and Harrison, D.G. (2012). Methods for Detection of Mitochondrial and Cellular Reactive Oxygen Species. Antioxidants Amp Redox Signal *20*, 372–382.

Dobin, A., Davis, C.A., Schlesinger, F., Drenkow, J., Zaleski, C., Jha, S., Batut, P., Chaisson, M., and Gingeras, T.R. (2013). STAR: ultrafast universal RNA-seq aligner. Bioinformatics *29*, 15–21.

Doetsch, F., García-Verdugo, J., and Alvarez-Buylla, A. (1997). Cellular composition and three-dimensional organization of the subventricular germinal zone in the adult mammalian brain. J Neurosci Official J Soc Neurosci *17*, 5046–5061.

Doetsch, F., García-Verdugo, J., and Alvarez-Buylla, A. (1999). Regeneration of a germinal layer in the adult mammalian brain. P Natl Acad Sci Usa *96*, 11619–11624.

Dranovsky, A., Picchini, A.M., Moadel, T., Sisti, A.C., Yamada, A., Kimura, S., Leonardo, D.E., and Hen, R. (2011). Experience dictates stem cell fate in the adult hippocampus. Neuron *70*, 908–923.

Encinas, J.M., Michurina, T.V., Peunova, N., Park, J.-H., Tordo, J., Peterson, D.A., Fishell, G., Koulakov, A., and Enikolopov, G. (2011). Division-Coupled Astrocytic Differentiation and Age-Related Depletion of Neural Stem Cells in the Adult Hippocampus. Cell Stem Cell *8*, 566–579.

Enikolopov, G., Overstreet-Wadiche, L., and Ge, S. (2015). Viral and Transgenic Reporters and Genetic Analysis of Adult Neurogenesis. Csh Perspect Biol *7*, a018804.

Epp, J.R., Beasley, C.L., and Galea, L. (2013). Increased hippocampal neurogenesis and p21 expression in depression: dependent on antidepressants, sex, age, and antipsychotic

exposure. Neuropsychopharmacol Official Publ Am Coll Neuropsychopharmacol *38*, 2297–2306.

Fabel, K., Fabel, K., Tam, B., Kaufer, D., Baiker, A., Simmons, N., Kuo, C.J., and Palmer, T.D. (2003). VEGF is necessary for exercise-induced adult hippocampal neurogenesis. Eur J Neurosci *18*, 2803–2812.

Fabel, K., Wolf, S.A., Ehninger, D., Babu, H., Leal-Galicia, P., and Kempermann, G. (2009). Additive effects of physical exercise and environmental enrichment on adult hippocampal neurogenesis in mice. Front Neurosci-Switz *3*, 50.

Farioli-Vecchioli, S., Ceccarelli, M., Saraulli, D., Micheli, L., Cannas, S., D'Alessandro, F., Scardigli, R., Leonardi, L., Cinà, I., Costanzi, M., et al. (2014). Tis21 is required for adult neurogenesis in the subventricular zone and for olfactory behavior regulating cyclins, BMP4, Hes1/5 and Ids. Front Cell Neurosci *8*, 98.

Ferber, E., Peck, B., Delpuech, O., Bell, G., East, P., and Schulze, A. (2011). FOXO3a regulates reactive oxygen metabolism by inhibiting mitochondrial gene expression. Cell Death Differ *19*, cdd2011179.

Fischer, T.J., Walker, T.L., Overall, R.W., Brandt, M.D., and Kempermann, G. (2014). Acute effects of wheel running on adult hippocampal precursor cells in mice are not caused by changes in cell cycle length or S phase length. Front Neurosci-Switz *8*, 314.

Fuentealba, L.C., Rompani, S.B., Parraguez, J.I., Obernier, K., Romero, R., Cepko, C.L., and Alvarez-Buylla, A. (2015). Embryonic Origin of Postnatal Neural Stem Cells. Cell *161*, 1644–1655.

Furutachi, S., Miya, H., Watanabe, T., Kawai, H., Yamasaki, N., Harada, Y., Imayoshi, I., Nelson, M., Nakayama, K.I., Hirabayashi, Y., et al. (2015). Slowly dividing neural progenitors are an embryonic origin of adult neural stem cells. Nat Neurosci *18*, 657–665.

Gage, F., Coates, P., Palmer, T., Kuhn, H., Fisher, L., Suhonen, J., Peterson, D., Suhr, S., and Ray, J. (1995). Survival and differentiation of adult neuronal progenitor cells transplanted to the adult brain. P Natl Acad Sci Usa *92*, 11879–11883.

Gao, Z., Ure, K., Ding, P., Nashaat, M., Yuan, L., Ma, J., Hammer, R.E., and Hsieh, J. (2011). The Master Negative Regulator REST/NRSF Controls Adult Neurogenesis by Restraining the Neurogenic Program in Quiescent Stem Cells. J Neurosci *31*, 9772–9786.

Garthe, A., Behr, J., and Kempermann, G. (2009). Adult-Generated Hippocampal Neurons Allow the Flexible Use of Spatially Precise Learning Strategies. Plos One *4*, e5464.

Garthe, A., Huang, Z., Kaczmarek, L., Filipkowski, R., and Kempermann, G. (2014). Not all water mazes are created equal: cyclin D2 knockout mice with constitutively suppressed adult hippocampal neurogenesis do show specific spatial learning deficits. Genes Brain Behav *13*, 357–364.

Garthe, A., Roeder, I., and Kempermann, G. (2016). Mice in an enriched environment learn

more flexibly because of adult hippocampal neurogenesis. Hippocampus *26*, 261–271.

Giachino, C., Basak, O., Lugert, S., Knuckles, P., Obernier, K., Fiorelli, R., Frank, S., Raineteau, O., Alvarez-Buylla, A., and Taylor, V. (2014). Molecular Diversity Subdivides the Adult Forebrain Neural Stem Cell Population. Stem Cells *32*, 70–84.

Gilbert, Scott F. Developmental Biology. Sunderland, Mass: Sinauer Associates, 2000. Print.

Gong, S., Zheng, C., Doughty, M.L., Losos, K., Didkovsky, N., Schambra, U.B., Nowak, N.J., Joyner, A., Leblanc, G., Hatten, M.E., et al. (2003). A gene expression atlas of the central nervous system based on bacterial artificial chromosomes. Nature *425*, 917.

Götz, M., Nakafuku, M., and Petrik, D. (2016). Neurogenesis in the Developing and Adult Brain—Similarities and Key Differences. Csh Perspect Biol *8*, a018853.

Gould, E., Beylin, A., Tanapat, P., Reeves, A., and Shors, T. (1999). Learning enhances adult neurogenesis in the hippocampal formation. Nat Neurosci *2*, 260–265.

Gurusamy, N., Mukherjee, S., Lekli, I., Bearzi, C., Bardelli, S., and Das, D.K. (2009). Inhibition of Ref-1 Stimulates the Production of Reactive Oxygen Species and Induces Differentiation in Adult Cardiac Stem Cells. Antioxid Redox Sign *11*, 589–599.

Hagihara, H., Toyama, K., Yamasaki, N., and Miyakawa, T. (2009). Dissection of Hippocampal Dentate Gyrus from Adult Mouse. J Vis Exp Jove 1543.

Halliwell, B. (2001). Role of free radicals in the neurodegenerative diseases: therapeutic implications for antioxidant treatment. Drug Aging *18*, 685–716.

Hatakeyama, J., Bessho, Y., Katoh, K., Ookawara, S., Fujioka, M., Guillemot, F., and Kageyama, R. (2004). Hes genes regulate size, shape and histogenesis of the nervous system by control of the timing of neural stem cell differentiation. Development *131*, 5539–5550.

Hill, R., and Wu, H. (2009). PTEN, Stem Cells, and Cancer Stem Cells. J Biol Chem *284*, 11755–11759.

Hill, M.N., Titterness, A.K., Morrish, A.C., Carrier, E.J., Lee, T., Gil-Mohapel, J., Gorzalka, B.B., Hillard, C.J., and Christie, B.R. (2010). Endogenous cannabinoid signaling is required for voluntary exercise-induced enhancement of progenitor cell proliferation in the hippocampus. Hippocampus *20*, 513–523.

Hochmuth, C.E., Biteau, B., Bohmann, D., and Jasper, H. (2011). Redox Regulation by Keap1 and Nrf2 Controls Intestinal Stem Cell Proliferation in Drosophila. Cell Stem Cell *8*, 188–199.

Hodge, R.D., Kowalczyk, T.D., Wolf, S.A., Encinas, J.M., Rippey, C., Enikolopov, G., Kempermann, G., and Hevner, R.F. (2008). Intermediate Progenitors in Adult Hippocampal

Neurogenesis: Tbr2 Expression and Coordinate Regulation of Neuronal Output. J Neurosci *28*, 3707–3717.

Hodge, R.D., Nelson, B.R., Kahoud, R.J., Yang, R., Mussar, K.E., Reiner, S.L., and Hevner, R.F. (2012). Tbr2 Is Essential for Hippocampal Lineage Progression from Neural Stem Cells to Intermediate Progenitors and Neurons. J Neurosci *32*, 6275–6287.

Holmström, K.M., and Finkel, T. (2014). Cellular mechanisms and physiological consequences of redox-dependent signalling. Nat Rev Mol Cell Bio *15*, 411–421.

Hörster, H., Garthe, A., Walker, T.L., Ichwan, M., Steiner, B., Khan, M., Iie, D., Nicola, Z., Ramirez-Rodriguez, G., and Kempermann, G. (2017). p27kip1 Is Required for Functionally Relevant Adult Hippocampal Neurogenesis in Mice. Stem Cells *35*, 787–799.

Jensen, P.K. (1966). Antimycin-insensitive oxidation of succinate and reduced nicotinamide-adenine dinucleotide in electron-transport particles II. Steroid effects. Biochimica Et Biophysica Acta Bba - Enzym Biological Oxid *122*, 167–174.

Jhaveri, D.J., Mackay, E.W., Hamlin, A.S., Marathe, S.V., Nandam, S.L., Vaidya, V.A., and Bartlett, P.F. (2010). Norepinephrine Directly Activates Adult Hippocampal Precursors via β3-Adrenergic Receptors. J Neurosci *30*, 2795–2806.

Kalamakis, G., Brüne, D., kanth Ravichandran, Bolz, J., Fan, W., Ziebell, F., Stiehl, T., Catalá-Martinez, F., Kupke, J., Zhao, S., et al. (2019). Quiescence Modulates Stem Cell Maintenance and Regenerative Capacity in the Aging Brain. Cell *176*, 1407-1419.e14.

Katsimpardi, L., and Lledo, P.-M. (2018). Regulation of neurogenesis in the adult and aging brain. Curr Opin Neurobiol *53*, 131–138.

Kempermann, G. (2011a). Seven principles in the regulation of adult neurogenesis. Eur J Neurosci *33*, 1018–1024.

Kempermann, G. (2011b). The Pessimist's and Optimist's Views of Adult Neurogenesis. Cell *145*, 1009–1011.

Kempermann, G. (2012). New neurons for "survival of the fittest." Nat Rev Neurosci *13*, 727.

Kempermann, G. (2015). Adult Neurogenesis: An Evolutionary Perspective. Csh Perspect Biol *8*, a018986.

Kempermann, G., Kuhn, G.H., and Gage, F.H. (1997). More hippocampal neurons in adult mice living in an enriched environment. Nature *386*, 386493a0.

Kempermann, G., Jessberger, S., Steiner, B., and Kronenberg, G. (2004). Milestones of neuronal development in the adult hippocampus. Trends Neurosci *27*, 447–452.

Kempermann, G., Song, H., and Gage, F.H. (2015). Neurogenesis in the Adult Hippocampus. Csh Perspect Biol *7*, a018812.

Kheirbek, M.A., Klemenhagen, K.C., Sahay, A., and Hen, R. (2012). Neurogenesis and generalization: a new approach to stratify and treat anxiety disorders. Nat Neurosci *15*, 1613–1620.

Kim, E.J., Ables, J.L., Dickel, L.K., Eisch, A.J., and Johnson, J.E. (2011). Ascl1 (Mash1) Defines Cells with Long-Term Neurogenic Potential in Subgranular and Subventricular Zones in Adult Mouse Brain. Plos One *6*, e18472.

Klempin, F., Beis, D., Mosienko, V., Kempermann, G., Bader, M., and Alenina, N. (2013). Serotonin Is Required for Exercise-Induced Adult Hippocampal Neurogenesis. J Neurosci *33*, 8270–8275.

Knobloch, M., Braun, S.M., Zurkirchen, L., von Schoultz, C., Zamboni, N., Araúzo-Bravo, M.J., Kovacs, W.J., Karalay, Ö., Suter, U., Machado, R.A., et al. (2012). Metabolic control of adult neural stem cell activity by Fasn-dependent lipogenesis. Nature *493*, 226.

Knobloch, M., von Schoultz, C., Zurkirchen, L., Braun, S., Vidmar, M., and Jessberger, S. (2014). SPOT14-Positive Neural Stem/Progenitor Cells in the Hippocampus Respond Dynamically to Neurogenic Regulators. Stem Cell Rep *3*, 735–742.

Knobloch, M., Pilz, G.-A., Ghesquière, B., Kovacs, W.J., Wegleiter, T., Moore, D.L., Hruzova, M., Zamboni, N., Carmeliet, P., and Jessberger, S. (2017). A Fatty Acid Oxidation-Dependent Metabolic Shift Regulates Adult Neural Stem Cell Activity. Cell Reports *20*, 2144–2155.

Kronenberg, G., Reuter, K., Steiner, B., Brandt, M.D., Jessberger, S., Yamaguchi, M., and Kempermann, G. (2003). Subpopulations of proliferating cells of the adult hippocampus respond differently to physiologic neurogenic stimuli. J Comp Neurol *467*, 455–463.

Kuhn, G.H., Toda, T., and Gage, F.H. (2018). Adult hippocampal neurogenesis: a coming-of-age story. J Neurosci Official J Soc Neurosci *38*, 10401–10410.

Kuhn, H., Dickinson-Anson, H., and Gage, F. (1996). Neurogenesis in the dentate gyrus of the adult rat: age-related decrease of neuronal progenitor proliferation. J Neurosci *16*, 2027–2033.

Li, Y.-Q., and Wong, C. (2018). Effects of p21 on adult hippocampal neuronal development after irradiation. Cell Death Discov *4*, 15.

Li, D., Takeda, N., Jain, R., Manderfield, L.J., Liu, F., Li, L., Anderson, S.A., and Epstein, J.A. (2015). Hopx distinguishes hippocampal from lateral ventricle neural stem cells. Stem Cell Res *15*, 522–529.

Liao, Y., Smyth, G.K., and Shi, W. (2013). The Subread aligner: fast, accurate and scalable read mapping by seed-and-vote. Nucleic Acids Res *41*, e108–e108.

Lim, D.A., and Alvarez-Buylla, A. (2016). The Adult Ventricular–Subventricular Zone (V-SVZ) and Olfactory Bulb (OB) Neurogenesis. Csh Perspect Biol *8*, a018820.

Linnarsson, S. (2015). Sequencing Single Cells Reveals Sequential Stem Cell States. Cell Stem Cell *17*, 251–252.

Llorens-Bobadilla, E., Zhao, S., Baser, A., Saiz-Castro, G., Zwadlo, K., and Martin-Villalba, A. (2015). Single-Cell Transcriptomics Reveals a Population of Dormant Neural Stem Cells that Become Activated upon Brain Injury. Cell Stem Cell *17*, 329–340.

Lois, C., and Alvarez-Buylla, A. (1994). Long-distance neuronal migration in the adult mammalian brain. Science *264*, 1145–1148.

Ludin, A., Gur-Cohen, S., Golan, K., Kaufmann, K.B., Itkin, T., Medaglia, C., Lu, X.-J., Ledergor, G., Kollet, O., and Lapidot, T. (2014). Reactive oxygen species regulate hematopoietic stem cell self-renewal, migration and development, as well as their bone marrow microenvironment. Antioxid Redox Sign *21*, 1605–1619.

Lugert, S., Basak, O., Knuckles, P., Haussler, U., Fabel, K., Götz, M., Haas, C.A., Kempermann, G., Taylor, V., and Giachino, C. (2010). Quiescent and Active Hippocampal Neural Stem Cells with Distinct Morphologies Respond Selectively to Physiological and Pathological Stimuli and Aging. Cell Stem Cell *6*, 445–456.

Luna, V.M., Anacker, C., Burghardt, N.S., Khandaker, H., Andreu, V., Millette, A., Leary, P., Ravenelle, R., Jimenez, J.C., Mastrodonato, A., et al. (2019). Adult-born hippocampal neurons bidirectionally modulate entorhinal inputs into the dentate gyrus. Science *364*, 578–583.

Martynoga, B., Mateo, J., Zhou, B., Andersen, J., Achimastou, A., Urban, N., van den Berg, D., Georgopoulou, D., Hadjur, S., Wittbrodt, J., et al. (2013). Epigenomic enhancer annotation reveals a key role for NFIX in neural stem cell quiescence. Gene Dev *27*, 1769–1786.

Menn, B., Garcia-Verdugo, J., Yaschine, C., Gonzalez-Perez, O., Rowitch, D., and Alvarez-Buylla, A. (2006). Origin of Oligodendrocytes in the Subventricular Zone of the Adult Brain. J Neurosci *26*, 7907–7918.

Meyers, E.A., Gobeske, K.T., Bond, A.M., Jarrett, J.C., Peng, C.-Y., and Kessler, J.A. (2016). Increased bone morphogenetic protein signaling contributes to age-related declines in neurogenesis and cognition. Neurobiol Aging *38*, 164–175.

Mishina, N.M., Markvicheva, K.N., Bilan, D.S., Matlashov, M.E., Shirmanova, M.V., Liebl, D., Schultz, C., Lukyanov, S., and Belousov, V.V. (2013). Visualization of intracellular hydrogen peroxide with HyPer, a genetically encoded fluorescent probe. Methods Enzymol *526*, 45–59.

Mizrak, D., Levitin, H., Delgado, A.C., Crotet, V., Yuan, J., Chaker, Z., Silva-Vargas, V., Sims, P.A., and Doetsch, F. (2019). Single-Cell Analysis of Regional Differences in Adult V-SVZ Neural Stem Cell Lineages. Cell Reports *26*, 394-406.e5.
Moon, B.-S., Bai, J., Cai, M., Liu, C., Shi, J., and Lu, W. (2018). Kruppel-like factor 4-dependent Staufen1-mediated mRNA decay regulates cortical neurogenesis. Nat Commun *9*, 401.

Morshead, C., Reynolds, Craig, C., McBurney, M., Staines, W., Morassutti, D., Weiss, S., and van der Kooy, D. (1994). Neural stem cells in the adult mammalian forebrain: a relatively quiescent subpopulation of subependymal cells. Neuron *13*, 1071–1082.

Murata, H., Ihara, Y., Nakamura, H., Yodoi, J., Sumikawa, K., and Kondo, T. (2003). Glutaredoxin Exerts an Antiapoptotic Effect by Regulating the Redox State of Akt. J Biol Chem *278*, 50226–50233.

Nicola, Z., Fabel, K., and Kempermann, G. (2015). Development of the adult neurogenic niche in the hippocampus of mice. Front Neuroanat *9*, 53.

Nietzel, T., Elsässer, M., Ruberti, C., Steinbeck, J., Ugalde, J., Fuchs, P., Wagner, S., Ostermann, L., Moseler, A., Lemke, P., et al. (2018). The fluorescent protein sensor ro GFP 2-Orp1 monitors in vivo H 2 O 2 and thiol redox integration and elucidates intracellular H 2 O 2 dynamics during elicitor-induced oxidative burst in Arabidopsis. New Phytol *221*, 1649–1664.

Nobel, M., Ith, J., and Mayer-Pröschel, M., (2003) Redox State as a Central Modulator of Precursor Cell Function. Ann Ny Acad Sci *991*, 251–271.

Noble, M., Mayer-Pröschel, M., and Pröschel, C. (2005). Redox regulation of precursor cell function: insights and paradoxes. Antioxid Redox Sign *7*, 1456–1467.

Nolte, C., Matyash, M., Pivneva, T., Schipke, C., Ohlemeyer, C., Hanisch, U., Kirchhoff, F., and Kettenmann, H. (2001). GFAP promoter-controlled EGFP-expressing transgenic mice: a tool to visualize astrocytes and astrogliosis in living brain tissue. Glia *33*, 72–86.

Nottebohm, F. (1985). Neuronal Replacement in Adulthood. Ann Ny Acad Sci *457*, 143–161.

Overall, R.W., Walker, T.L., Leiter, O., Lenke, S., Ruhwald, S., and Kempermann, G. (2013). Delayed and Transient Increase of Adult Hippocampal Neurogenesis by Physical Exercise in DBA/2 Mice. Plos One *8*, e83797.

Overall, R.W., Walker, T.L., Fischer, T.J., Brandt, M.D., and Kempermann, G. (2016). Different Mechanisms Must Be Considered to Explain the Increase in Hippocampal Neural Precursor Cell Proliferation by Physical Activity. Front Neurosci-Switz *10*, 362.

Palmer, T., Schwartz, P., Taupin, P., Kaspar, B., Stein, S., and Gage, F. (2001). Cell culture. Progenitor cells from human brain after death. Nature *411*, 42–43.

Pechnick, R.N., Zonis, S., Wawrowsky, K., Pourmorady, J., and Chesnokova, V. (2008). p21Cip1 restricts neuronal proliferation in the subgranular zone of the dentate gyrus of the hippocampus. Proc National Acad Sci *105*, 1358–1363.

Phaniendra, A., Jestadi, D., and Periyasamy, L. (2015). Free Radicals: Properties, Sources, Targets, and Their Implication in Various Diseases. Indian J Clin Biochem *30*, 11–26.

Pilz, G.-A., Bottes, S., Betizeau, M., Jörg, D.J., Carta, S., Simons, B.D., Helmchen, F., and Jessberger, S. (2018). Live imaging of neurogenesis in the adult mouse hippocampus. Science *359*, 658–662.

Podgorny, O., Peunova, N., Park, J.-H., and Enikolopov, G. (2018a). Triple S-Phase Labeling of Dividing Stem Cells. Stem Cell Rep *10*, 615–626.

Podgorny, O., Peunova, N., and Enikolopov, G. (2018b). Tracing dividing stem cells. Aging Albany Ny *10*, 1534–1535.

Pollock, J.D., Williams, D.A., Gifford, M., Li, L., Du, X., Fisherman, J., Orkin, S.H., Doerschuk, C.M., and Dinauer, M.C. (1995). Mouse model of X–linked chronic granulomatous disease, an inherited defect in phagocyte superoxide production. Nat Genet *9*, ng0295-202.

Ponti, G., Obernier, K., and Alvarez-Buylla, A. (2013). Lineage progression from stem cells to new neurons in the adult brain ventricular-subventricular zone. Cell Cycle Georget Tex *12*, 1649–1650.

van Praag, H., Kempermann, G., and Gage, F.H. (1999). Running increases cell proliferation and neurogenesis in the adult mouse dentate gyrus. Nat Neurosci *2*, 266–270.

Rakic, P. (2009). Evolution of the neocortex: a perspective from developmental biology. Nat Rev Neurosci *10*, 724–735.

Rangel, L.M., Quinn, L.K., Chiba, A.A., Gage, F.H., and mone, J. (2013). A hypothesis for temporal coding of young and mature granule cells. Front Neurosci-Switz *7*, 75.

Raposo, A., Vasconcelos, F.F., Drechsel, D., Marie, C., Johnston, C., Dolle, D., Bithell, A., Gillotin, S., van den Berg, D., Ettwiller, L., et al. (2015). Ascl1 Coordinately Regulates Gene Expression and the Chromatin Landscape during Neurogenesis. Cell Reports *10*, 1544–1556.

Reynolds, and Weiss, S. (1992). Generation of neurons and astrocytes from isolated cells of the adult mammalian central nervous system. Science *255*, 1707–1710.

Rietze, R.L., and Reynolds, B.A. (2006). Methods in Enzymology. Sect Ectoderm *419*, 3–23.

Robinson, M.D., McCarthy, D.J., and Smyth, G.K. (2010). edgeR: a Bioconductor package for differential expression analysis of digital gene expression data. Bioinformatics *26*, 139–140.

Ryu, J., Hong, C., Kim, J., Kim, E.-K., Sun, W., and Yu, S.-W. (2016). Control of adult neurogenesis by programmed cell death in the mammalian brain. Mol Brain *9*, 43.

Sahay, A., Scobie, K.N., Hill, A.S., O'Carroll, C.M., Kheirbek, M.A., Burghardt, N.S., Fenton, A.A., Dranovsky, A., and Hen, R. (2011a). Increasing adult hippocampal neurogenesis is sufficient to improve pattern separation. Nature *472*, 466.

Sahay, A., Wilson, D.A., and Hen, R. (2011b). Pattern Separation: A Common Function for New Neurons in Hippocampus and Olfactory Bulb. Neuron *70*, 582–588.

Salminen, A., Kaarniranta, K., and Kauppinen, A. (2013). Crosstalk between Oxidative Stress and SIRT1: Impact on the Aging Process. Int J Mol Sci *14*, 3834–3859.

Sellgren, C., Sheridan, S., Gracias, J., Xuan, D., Fu, T., and Perlis, R. (2016). Patient-specific models of microglia-mediated engulfment of synapses and neural progenitors. Mol Psychiatr *22*, 170–177.

Semerci, F., and Maletic-Savatic, M. (2016). Transgenic mouse models for studying adult neurogenesis. Frontiers Biology *11*, 151–167.

Semerci, F., Choi, W., Bajic, A., Thakkar, A., Encinas, J., Depreux, F., Segil, N., Groves, A.K., and Maletic-Savatic, M. (2017). Lunatic fringe-mediated Notch signaling regulates adult hippocampal neural stem cell maintenance. Elife *6*, e24660.

Shin, J., Berg, D.A., Zhu, Y., Shin, J.Y., Song, J., Bonaguidi, M.A., Enikolopov, G., Nauen, D.W., Christian, K.M., Ming, G., et al. (2015). Single-Cell RNA-Seq with Waterfall Reveals Molecular Cascades underlying Adult Neurogenesis. Cell Stem Cell *17*, 360–372.

Sierra, A., Martín-Suárez, S., Valcárcel-Martín, R., Pascual-Brazo, J., Aelvoet, S.-A., Abiega, O., Deudero, J.J., Brewster, A.L., Bernales, I., Anderson, A.E., et al. (2015). Neuronal Hyperactivity Accelerates Depletion of Neural Stem Cells and Impairs Hippocampal Neurogenesis. Cell Stem Cell *16*, 488–503.

Silva-Vargas, V., Crouch, E.E., and Doetsch, F. (2013). Adult neural stem cells and their niche: a dynamic duo during homeostasis, regeneration, and aging. Curr Opin Neurobiol *23*, 935–942.

Simsek, T., Kocabas, F., Zheng, J., DeBerardinis, R.J., Mahmoud, A.I., Olson, E.N., Schneider, J.W., Zhang, C., and Sadek, H.A. (2010). The Distinct Metabolic Profile of Hematopoietic Stem Cells Reflects Their Location in a Hypoxic Niche. Cell Stem Cell *7*, 380–390.

Smith, J., Ladi, E., Mayer-Pröschel, M., and Noble, M. (2000). Redox state is a central modulator of the balance between self-renewal and differentiation in a dividing glial precursor cell. Proc National Acad Sci *97*, 10032–10037.

Snyder, J.S., Glover, L.R., nzone, K., Kamhi, F.J., and Cameron, H.A. (2009). The effects of exercise and stress on the survival and maturation of adult-generated granule cells. Hippocampus *19*, 898–906.

Song, J., Olsen, R., Sun, J., Ming, G., and Song, H. (2016). Neuronal Circuitry Mechanisms Regulating Adult Mammalian Neurogenesis. Csh Perspect Biol *8*, a018937.

Spalding, K.L., Bergmann, O., Alkass, K., Bernard, S., Salehpour, M., Huttner, H.B., Boström, E., Westerlund, I., Vial, C., Buchholz, B.A., et al. (2013). Dynamics of Hippocampal Neurogenesis in Adult Humans. Cell *153*, 1219–1227.

Steiner, B., Klempin, F., Wang, L., Kott, M., Kettenmann, H., and Kempermann, G. (2006). Type-2 cells as link between glial and neuronal lineage in adult hippocampal neurogenesis. Glia *54*, 805–814.

Steiner, B., Zurborg, S., Hörster, H., Fabel, K., and Kempermann, G. (2008). Differential 24 h responsiveness of Prox1–expressing precursor cells in adult hippocampal neurogenesis to physical activity, environmental enrichment, and kainic acid–induced seizures. Neuroscience *154*, 521–529.

Sugiura, K., Tanaka, H., Kurisu, G., Wakabayashi, K.-I., and Hisabori, T. (2019). Multicolor redox sensor proteins can visualize redox changes in various compartments of the living cell. Biochimica Et Biophysica Acta Gen Subj *1863*, 1098–1107.

Suh, H., Consiglio, A., Ray, J., Sawai, T., D'Amour, K.A., and Gage, F.H. (2007). In vivo fate analysis reveals the multipotent and self-renewal capacities of Sox2+ neural stem cells in the adult hippocampus. Cell Stem Cell *1*, 515–528.

Toni, N., and Schinder, A.F. (2016). Maturation and Functional Integration of New Granule Cells into the Adult Hippocampus. Csh Perspect Biol *8*, a018903.

Torres-Pérez, M., Tellez-Ballesteros, R., Ortiz-López, L., Ichwan, M., Vega-Rivera, N., Castro-García, M., Gómez-Sánchez, A., Kempermann, G., and Ramirez-Rodriguez, G. (2015). Resveratrol Enhances Neuroplastic Changes, Including Hippocampal Neurogenesis, and Memory in Balb/C Mice at Six Months of Age. Plos One *10*, e0145687.

Trejo, J., Carro, E., and Torres-Alemán, I. (2001). Circulating Insulin-Like Growth Factor I Mediates Exercise-Induced Increases in the Number of New Neurons in the Adult Hippocampus. J Neurosci *21*, 1628–1634.

Trinchero, M.F., Buttner, K.A., Cuevas, J.N., Temprana, S.G., Fontanet, P.A., Monzón-Salinas, C.M., Ledda, F., Paratcha, G., and Schinder, A.F. (2017). High Plasticity of New Granule Cells in the Aging Hippocampus. Cell Reports *21*, 1129–1139.

Vivar, C., and van Praag, H. (2017). Running Changes the Brain: the Long and the Short of It. Physiology *32*, 410–424.

Walker, T.L., and Kempermann, G. (2014). One Mouse, Two Cultures: Isolation and Culture of Adult Neural Stem Cells from the Two Neurogenic Zones of Individual Mice. J Vis Exp Jove 51225.

Walker, T.L., Yasuda, T., Adams, D.J., and Bartlett, P.F. (2007). The doublecortin-expressing population in the developing and adult brain contains multipotential precursors in addition to neuronal-lineage cells. J Neurosci Official J Soc Neurosci *27*, 3734–3742.

Walker, T.L., White, A., Black, D.M., Wallace, R.H., Sah, P., and Bartlett, P.F. (2008). Latent Stem and Progenitor Cells in the Hippocampus Are Activated by Neural Excitation. J Neurosci *28*, 5240–5247.

Walker, T.L., Overall, R.W., Vogler, S., Sykes, A.M., Ruhwald, S., Lasse, D., Ichwan, M., Fabel, K., and Kempermann, G. (2016). Lysophosphatidic Acid Receptor Is a Functional

Marker of Adult Hippocampal Precursor Cells. Stem Cell Rep *6*, 552–565.

Walker, T.L., Schallenberg, S., Rund, N., Grönnert, L., Rust, R., Kretschmer, K., and Kempermann, G. (2018). T Lymphocytes Contribute to the Control of Baseline Neural Precursor Cell Proliferation but Not the Exercise-Induced Up-Regulation of Adult Hippocampal Neurogenesis. Front Immunol *9*, 2856.

Walton, N.M., Shin, R., Tajinda, K., Heusner, C.L., Kogan, J.H., Miyake, S., Chen, Q., Tamura, K., and Matsumoto, M. (2012). Adult neurogenesis transiently generates oxidative stress. Plos One *7*, e35264.

Wiskott, L., Rasch, M.J., and Kempermann, G. (2006). A functional hypothesis for adult hippocampal neurogenesis: Avoidance of catastrophic interference in the dentate gyrus. Hippocampus *16*, 329–343.

Yamaguchi, M., Saito, H., Suzuki, M., and Mori, K. (2000). Visualization of neurogenesis in the central nervous system using nestin promoter-GFP transgenic mice. Neuroreport *11*, 1991.

Yan, R., Zhang, L., Li, M., Liu, X., Yang, X., and Chen, L. (2018). Hes1 negatively regulates neurogenesis in the adult mouse dentate gyrus following traumatic brain injury. Exp Ther Med *16*, 2267–2274.

Yao, P.J., Petralia, R.S., and Mattson, M.P. (2016). Sonic Hedgehog Signaling and Hippocampal Neuroplasticity. Trends Neurosci *39*, 840–850.

Ye, Z.-W., Zhang, J., Townsend, D.M., and Tew, K.D. (2015). Oxidative stress, redox regulation and diseases of cellular differentiation. Biochimica Et Biophysica Acta Bba - Gen Subj *1850*, 1607–1621.

Yoshida, S., Hong, S., Suzuki, T., Nada, S., Mannan, A.M., Wang, J., Okada, M., Guan, K.-L., and Inoki, K. (2011). Redox Regulates Mammalian Target of Rapamycin Complex 1 (mTORC1) Activity by Modulating the TSC1/TSC2-Rheb GTPase Pathway. J Biol Chem

286, 32651–32660.

Zhang, J., and Jiao, J. (2015). Molecular Biomarkers for Embryonic and Adult Neural Stem Cell and Neurogenesis. Biomed Res Int *2015*, 727542.

Zhao, C., Deng, W., and Gage, F.H. (2008). Mechanisms and functional implications of adult neurogenesis. Cell *132*, 645–660.

Zheng, X., Boyer, L., Jin, M., Mertens, J., Kim, Y., Ma, L., Ma, L., Hamm, M., Gage, F.H., and Hunter, T. (2016). Metabolic reprogramming during neuronal differentiation from aerobic glycolysis to neuronal oxidative phosphorylation. Elife *5*, e13374.

Zhou, G., Meng, S., Li, Y., Ghebre, Y.T., and Cooke, J.P. (2016). Optimal ROS Signaling Is Critical for Nuclear Reprogramming. Cell Reports *15*, 919–925.

Ziebell, F., Dehler, S., Martin-Villalba, A., and Marciniak-Czochra, A. (2017). Revealing age-related changes of adult hippocampal neurogenesis using mathematical models. Development *145*, dev153544.

Zielonka, J., Vasquez-Vivar, J., and Kalyanaraman, B. (2008). Detection of 2-hydroxyethidium in cellular systems: a unique marker product of superoxide and hydroethidine. Nat Protoc *3*, nprot.2007.473.

Zorov, D.B., Juhaszova, M., and Sollott, S.J. (2014). Mitochondrial reactive oxygen species (ROS) and ROS-induced ROS release. Physiol Rev *94*, 909–950.

Zou, Y., Wang, A., Shi, M., Chen, X., Liu, R., Li, T., Zhang, C., Zhang, Z., Zhu, L., Ju, Z., et al. (2018). Analysis of redox landscapes and dynamics in living cells and in vivo using genetically encoded fluorescent sensors. Nat Protoc *13*, 2362–2386.

Declarations

Anlage 1

Erklärungen zur Eröffnung des Promotionsverfahrens

1. Hiermit versichere ich, dass ich die vorliegende Arbeit ohne unzulässige Hilfe Dritter und ohne Benutzung anderer als der angegebenen Hilfsmittel angefertigt habe; die aus fremden Quellen direkt oder indirekt übernommenen Gedanken sind als solche kenntlich gemacht.

2. Bei der Auswahl und Auswertung des Materials sowie bei der Herstellung des Manuskripts habe ich ausschließlich die im Manuskript angegebenen Unterstützungsleistungen erhalten.

3. Weitere Personen waren an der geistigen Herstellung der vorliegenden Arbeit nicht beteiligt. Insbesondere habe ich nicht die Hilfe eines kommerziellen Promotionsberaters in Anspruch genommen. Dritte haben von mir weder unmittelbar noch mittelbar geldwerte Leistungen für Arbeiten erhalten, die im Zusammenhang mit dem Inhalt der vorgelegten Dissertation stehen.

4. Die Arbeit wurde bisher weder im Inland noch im Ausland in gleicher oder ähnlicher Form einer anderen Prüfungsbehörde vorgelegt.

5. Die Inhalte dieser Dissertation wurden in folgender Form veröffentlicht:

bioRxiv preprint doi: https://doi.org/10.1101/606186

GSE124095 (GEO superseries)

6. Ich bestätige, dass ich die Promotionsordnung der Medizinischen Fakultät der Technischen Universität Dresden anerkenne.

Ort, Datum

Unterschrift des Doktoranden

Anlage 2

Hiermit bestätige ich die Einhaltung der folgenden aktuellen gesetzlichen Vorgaben im Rahmen meiner Dissertation

◊ das zustimmende Votum der Ethikkommission bei Klinischen Studien, epidemiologischen Untersuchungen mit Personenbezug oder Sachverhalten, die das Medizinproduktegesetz betreffen Aktenzeichen der zuständigen Ethikkommission

◊ die Einhaltung der Bestimmungen des Tierschutzgesetzes Aktenzeichen der Genehmigungsbehörde zum Vorhaben/zur Mitwirkung:

Tierversuchsantrag:
TVT 7/2016 – 25-1531/365/8
TVT8/2016 – 25-5131/365/9
TVA 28/2016 – 25-5131/367/30
TVA 16/2018 – 25-5131/450/17

◊ die Einhaltung des Gentechnikgesetzes Projektnummer

Az.: 54-8451/251

◊ die Einhaltung von Datenschutzbestimmungen der Medizinischen Fakultät und des Universitätsklinikums Carl Gustav Carus.

Ort, Datum

Unterschrift des Doktoranden